SEISMIC RATCHETING OF RC COLUMNS WITH ECCENTRIC GRAVITY LOADINGS AND NON-SYMMETRIC LATERAL STIFFNESS AND STRENGTH

KHALED ZUHAIR M. SAIF

A thesis submitted in partial fulfillment of the requirements for the degree of Master of Engineering endorsed in Earthquake Engineering

Supervised by:

Senior Lecturer Chin-Long Lee (Main supervisor)

Associate Professor Gregory A. MacRae (Co-supervisor)

Dr. Trevor Yeow (Associate supervisor)

Department of Civil and Natural Resources Engineering

University of Canterbury

Christchurch

New Zealand

November 2017

ABSTRACT

Structures with different lateral force resistance or different stiffness in both directions due to eccentric gravity loading and/or strength differences may have a tendency to displace more in once direction than the other during strong earthquake shaking. This effect is known as “ratcheting”.

This thesis examines current provisions to consider ratcheting, provides methods to estimate the displacement demands for single-degree-of-freedom reinforced concrete (RC) and steel structures that have eccentric gravity loading and subjected to strong ground motion shaking by performing inelastic time history analyses using a fibre section model with different force reduction factors, periods, eccentric moments, and axial load ratios. Methods to mitigate ratcheting were developed and a number of approaches to best consider ratcheting effects are also evaluated.

It was found that the wording used to define some parameters in NZS1170.5 (2016) is confusing and can be interpreted in different ways, and new definitions to clarify these complexities were proposed. It was also found that the new provisions are conservative in estimating the maximum displacement for RC structures with eccentric gravity loading for different eccentric moments and periods. However, it needs to be modified to account for higher values of force reduction factor (R>5) and lower axial load ratios (P/P_o<0.1). The results have shown that when there is no mitigation of ratcheting, the steel structures had significantly higher ratcheting displacements than those modelled as reinforced concrete. Graphs and empirical equations were developed to estimate these displacements for a set of earthquake records. Increasing the strength in the weak side of the column by 3.4 times the eccentric moment was required to mitigate maximum displacement ratcheting for RC columns. Furthermore, it was shown that of the methods evaluated to account for ratcheting, the best one was the period ratio, which is based on calculating the period in each direction, when the eccentric moment was less than 0.4.

ACKNOWLEDGMENTS

I would like to thank my parents, Hiyam Al-Najjar and Zuhair Saif, and my brother, Waleed Saif, for their support throughout the development of this thesis.

I also would like to thank my supervisors, Chin-Long Lee, Greg MacRae, and Trevor Yeow. I am grateful for their guidance, time and support.

I would also like to thank the king of Jordan, king Abdullah II, for paving the way for Jordanian students to pursue higher education in New Zealand, The Ministry of Foreign Affairs in New Zealand for awarding me the NZAID scholarship, and Omrania & Associates company in Jordan for recommending me for this scholarship.

TABLE OF CONTENTS

LIST OF TABLES

LIST OF FIGURES

1. INTRODUCTION

1.1 Background

Some structures have different lateral yield forces in forward and reverse directions as a result of eccentric gravity loading on the structure, such as C-bent columns as shown in **Figure 1.1b,** or structural form, such as T-shaped walls. This effect may cause the structure to yield more in one direction than the other when subjected to strong earthquake ground shaking. This behaviour is called "ratcheting". A ratcheting structure is likely to have larger permanent and peak displacements in one direction than the other compared with a regular structure. Such a structure, therefore, has an increased likelihood of collapse during earthquake shaking or due to an aftershock.

Structures about which concerns of ratcheting have been expressed include the Hotel Grand Chancellor and C-bent bridge columns. The Hotel Grand Chancellor is a 22-storey building with a cantilevered bay on the east side of the building, as shown in **Figure 1.1a**. It was damaged during the 22 February 2011 earthquake shaking in Christchurch. C-bent bridge piers are bridge columns that support cantilever beams, as shown in **Figure 1.1b**. They are used when concentric columns cannot be constructed. It can be seen that the line of gravity load is located away from the centreline of the column causing an eccentric moment that can cause ratcheting. Other examples include concentrically braced frames where the orientation of the braces are in one direction and cause different storey strengths in different directions, and T-section reinforced concrete walls.

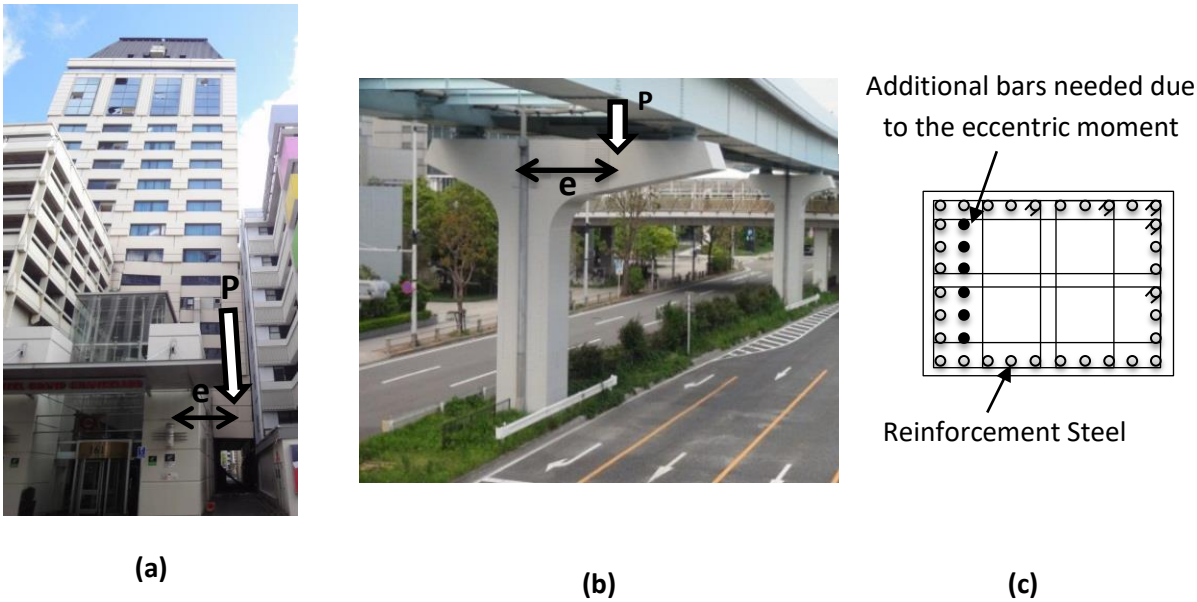

Figure 1.1: Some different configurations that lead to ratcheting: a) The Southern elevation of the Hotel Grand Chancellor (Royal Commission Report, 2011), b) Photograph of C-bent Column (courtesy of Yeow), and c) Typical Cross Section of Cantilever Bridge Column

The amount of increase in displacement due to seismic ratcheting is not well understood, and current methods to mitigate the ratcheting effect are generally not based on robust science. For example, the Japanese Road Association Code (1990) provides a specific clause for ratcheting of C-bent bridge piers, requiring additional reinforcing on the tension side of the pier, as shown in **Figure 1.1c**, to increase the strength of the column in that direction by the eccentric moment.

More recent studies (e.g., Yeow et al. 2013) have shown that the strength should be increased by more than this. However, these studies also have limitations, particularly in the assumptions made. First, the possible change in stiffness associated with the strength change has been ignored. In many cases structural strength may be proportional to structural stiffness (Priestley, 2003), which would have likely affected the findings from their study. Second, the concrete section flexural strength was modelled assuming Takeda hysteretic behaviour (Takeda et al., 1970) in these studies, which did not explicitly consider the actual reinforcement effects. Third, the study did not investigate whether the proposed strength increases are physically realistic.

As a result of the poor performance of the Hotel Grand Chancellor, the New Zealand Standard (NZS1170.5, 2016) has included new provisions to account for ratcheting. However, the background work of these provisions has not been published and needs to be investigated. Furthermore, some discrepancies have been found in the new provisions which can be interpreted in different ways. Feedback from practising engineers is that this approach is complex and it is not clear how these should be implemented.

1.2 Objectives and Scope

Based on the discussion above it may be seen that the new ratcheting provisions in NZS1170.5 (2016) need to be evaluated to assess their clarity and adequacy. In addition, there is a need for robust design methods to estimate the displacement demands of structures with a ratcheting tendency and to mitigate this effect. These should use realistic models of the structures considering stiffness changes in addition to strength changes.

This work seeks to address the needs described above by considering reinforced concrete C-bent columns with a ratcheting tendency, as the C-bent model represents single-degree-of-freedom structures and may be applied to structures where the first mode of vibration governs, by seeking answers to the following questions:

1. What are the issues with the new NZS1170.5 ratcheting provisions and are they adequate to estimate maximum displacements when ratcheting is considered?
2. How can the maximum and residual displacements of C-bent columns with eccentric gravity loads be estimated, and can ratcheting be mitigated?
3. Can simple design/assessment methods be developed for engineers to estimate displacement demands in practice and mitigate ratcheting effects for single-storey structures?

1.3 Outline

The questions raised above will be answered in this thesis to provide a better understanding of ratcheting and how to mitigate it. First, a literature review will be presented in Chapter 2 to report the work that has been done in the past and to point out the areas that need more investigation, followed by the methodology that was adapted in this thesis. Chapter 4 will discuss the issues in the current ratcheting provisions in NZS1170.5 (2016), and will propose suggestions to overcome these issues. Chapter 5 will focus on ratcheting in C-bent columns and how to mitigate it, and simple alternatives to account for ratcheting will be presented in Chapter6. Finally, conclusions and recommendations for future work will be presented in Chapter 7.

2. LITERATURE REVIEW

To review and understand the previous research on ratcheting of C-bent bridge piers, the following literature review was conducted. Current standards that consider the ratcheting effect have also been reviewed to validate the current methods accounting for ratcheting.

2.1 Past Experimental and Field Observations of Seismic Ratcheting

2.1.1 C-Bent Bridge Piers

C-bent bridge piers are columns that have cantilever beams on only one side. This configuration is used where there is a space limitation, such as when having to accommodate a turning lane, as shown in **Figure 2.1a**. Due to this configuration, the centroid of gravity loading is located away from the centreline of the supporting column, which creates a static eccentric moment. This eccentric moment increases the lateral flexural strength of the column in the direction opposite to the eccentricity, M^-, and decreases it in the other direction, M^+, as shown in **Figure 2.1b**. If the column has the same reinforcement on both sides, the column would tend to predominantly deform in the direction of eccentricity. This effect is referred to as ratcheting. This response can lead to excessive damage at the compression face of the column as observed in experimental tests by Kawashima et al. (2010), shown in **Figure 2.2**.

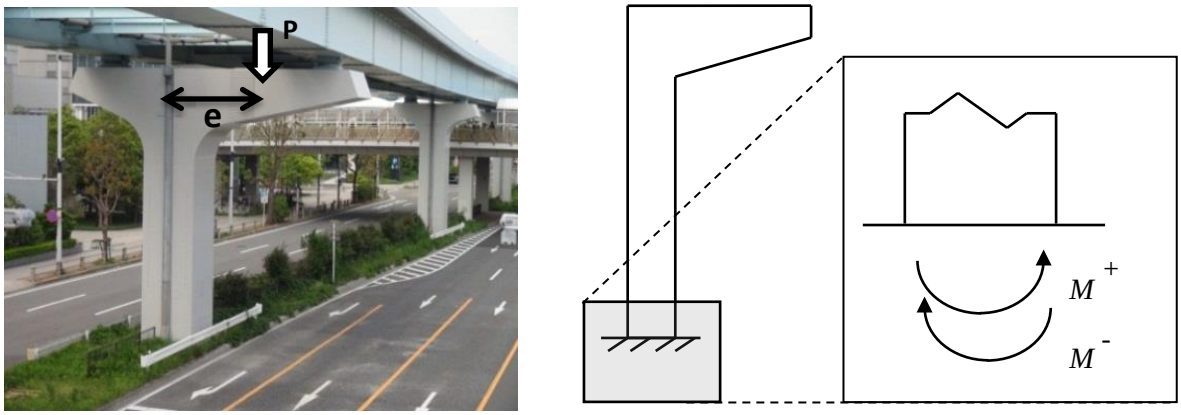

(a) Photograph of C-bent pier, where *P* is the axial load and *e* is the eccentricity

(b) Moment capacities

Figure 2.1: C-bent bridge pier

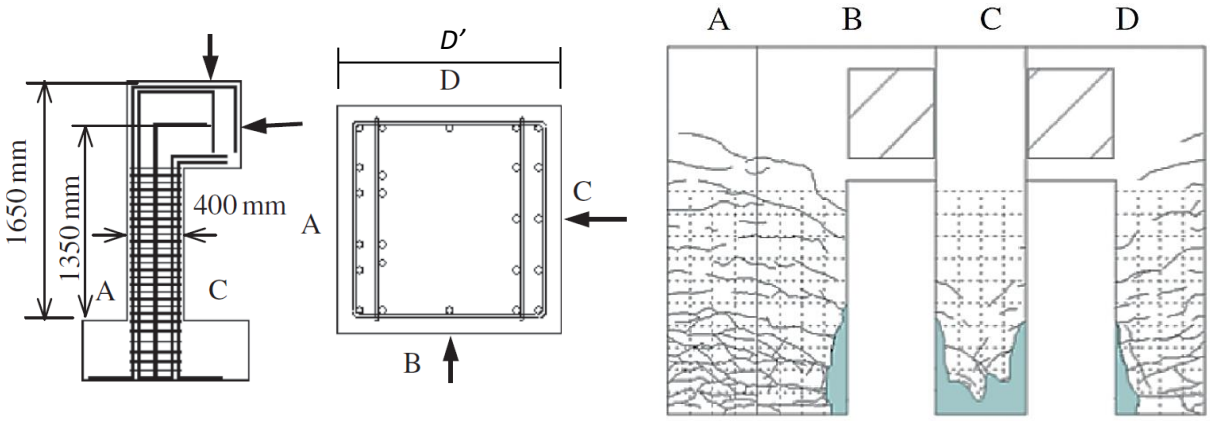

(a) Pier model **(b) Damage under cyclic loading for *e*=*D'*, coloured area represents cover spalling**

Figure 2.2: Damage at the compression face of the C-bent pier (Kawashima et al., 2010)

The existing literature examining methods of mitigating the ratcheting effect have suggested that M^+ should be increased by adding more reinforcing bars according to **Equation 2-1**. The Japanese Road Association Code (1990) suggested increasing M^+ by the eccentric moment, M_E. However, MacRae and Kawashima (1993) highlighted that the flexural strengths relative to static loading conditions are still unbalanced, and that M^+ should instead be increased by twice the eccentric moment when the P-delta effect is not included. Yeow et al. (2013) found that even larger amount is required when including the P-delta effect for piers exhibiting bilinear hysteretic response, and proposed an equation to estimate the amount required:

$$M^+ = M^- + M_E \quad (2\text{-}1)$$

Yeow et al. (2013) also analysed the performance of piers exhibiting hysteretic response characterized by Takeda et al. (1970), referred to hereafter as the Takeda hysteretic model. They suggested that the ratio should be increased by 2.3, which is generally higher than the range of β examined in their bilinear case. Their explanation behind the higher ratio using the Takeda hysteretic model was that more energy was needed to cause yielding in the opposite direction compared with the bilinear case. This is illustrated in **Figure 2.3**, where the potential energy at point A under the Takeda hysteretic model is smaller than that required to yield in the reverse direction, while the energy required for the bilinear case is about the same or smaller. Therefore, piers with the Takeda hysteretic model require higher amounts of reinforcement.

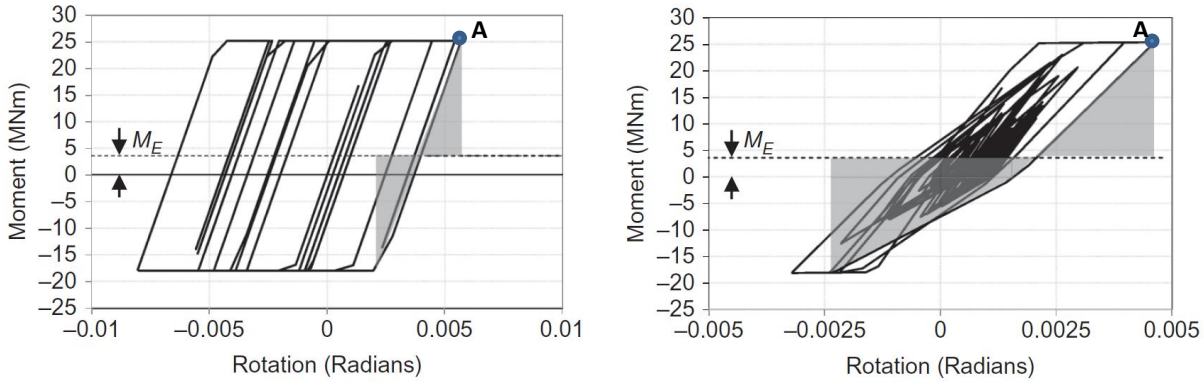

(a) Bilinear hysteresis loop **(b) Takeda et al. (1970) hysteresis loop**

Figure 2.3: Comparison of hysteretic behaviour (Yeow et al., 2013)

A key limitation in the previous studies is that stiffness was assumed to be independent of strength, as shown in **Figure 2.4a**. In reality, experiments and detailed studies (Priestley, 2003; Priestley and Grant, 2005; Priestley, 2006) showed that if the dimensions of the pier are kept the same but more reinforcement is added, the strength and stiffness would be effectively proportional for reinforced concrete sections, as shown in **Figure 2.4b**. Another drawback in the previous studies is that the actual reinforcement layout was not considered, which does not give a clear indication about how practical it is to achieve the optimum strength ratio. Finally, axial–moment interaction of the section was not considered.

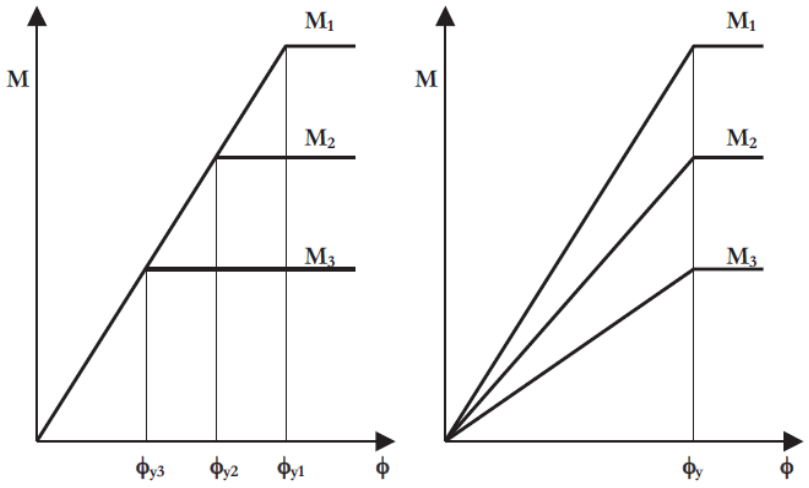

(a) Design assumptions (constant stiffness) **(b) Realistic conditions (constant yield curvature)**

Figure 2.4: Influence of Flexural Strength on Moment–Curvature Relationship (Priestley, 2003)

2.1.2 Hotel Grand Chancellor (HGC)

One of the most famous examples of buildings which exhibited seismic ratcheting behaviour was the Hotel Grand Chancellor building. The need to consider ratcheting effects in design was highlighted by the performance of the Hotel Grand Chancellor building during the 22 February 2011 Canterbury earthquake event. This building was designed such that the eastern-most bay was cantilevered, as shown in **Figure 2.5a**. It was reported that this building ratcheted severely in the eastern direction; the effect of which was captured in a numerical study conducted for The Royal Commission (2011) and shown in **Figure 2.5b**. The threat of further ratcheting, which was considered to lead to an increased probability of building collapse in an aftershock, meant that even neighbouring structures that had behaved well, but were in the proximity of the Hotel Grand Chancellor, were not permitted to be accessed until the building was demolished. This affected the recovery of Christchurch's central business district.

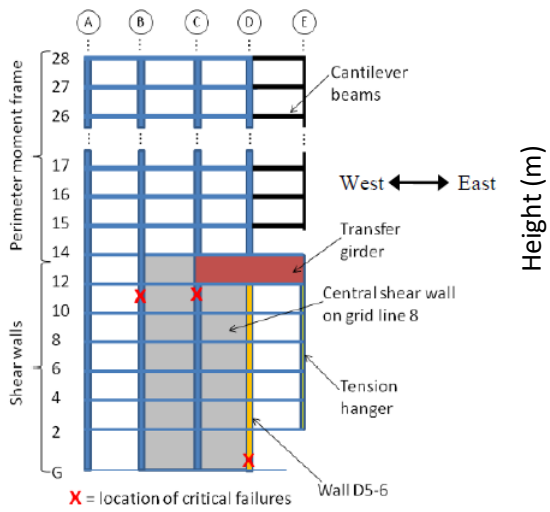

(a) Schematic plan and elevation of the Grand Chancellor Hotel (Kam et. al 2011)

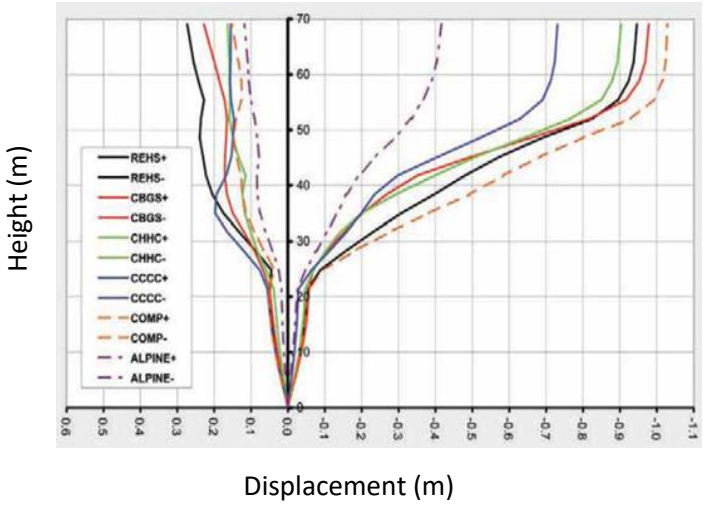

(b) Maximum displacement in east-west direction (Royal Commission, 2011)

Figure 2.5: Ratcheting in Grand Chancellor Hotel

The Canterbury Earthquake Royal Commission's investigation into the performance of the Hotel Grand Chancellor identified that the building was designed using a modal response spectrum method of analysis that assumed equal stiffness in the forward and reverse directions. Furthermore, if the building were designed to have the same lateral strengths in the forward and reverse directions when no eccentric loading was applied, the presence of the eccentric loading would decrease the building's effective capacity to resist lateral loads in one direction, and increase it in the other. The Royal Commission emphasises the inadequacy of elastic structural analyses adopted in practice to capture the effect of ratcheting, and stated that "the fact that this fundamental problem was not identified in the (investigation) reports received by the Royal Commission (2011) highlights the need for structural engineers to have a clear understanding of the basic assumptions involved in seismic design".

2.2 Causes of Seismic Ratcheting

2.2.1 Overview

Based on a review of existing literature, it was determined that ratcheting can occur due to the following effects:

- **Ground motion effect**: e.g., some ground motions, such as pulse-type motions, may cause structures to deform more in one direction than another.
- **Dynamic stability effect**: e.g., structures with a negative post-elastic stiffness due to structural or P-delta effects may tend to deform more in the direction of first yield.
- **Eccentric loading effect**: e.g., structures subjected to eccentric gravity loading may tend to deform more in the direction of the eccentricity.
- **Structural form effect**: e.g., structures with different lateral strengths in the forward and reverse directions may predominantly deform in the weak direction.

2.2.2 Ground Motion Effect

The ground motion effect is complicated due to it being heavily dependent on fault type, rupture mechanism, local soil site conditions, epicentral distance, and other factors. However, the tendency for seismic ratcheting due to the ground motion effect can be minimized with appropriate structural form (e.g., MacRae and Kawashima, 1993). As such, the following sections will focus more on the mechanics of seismic ratcheting due to the other three effects mentioned. Nevertheless, information on the effect of near-fault and pulse-type motion on seismic ratcheting of buildings can be found in the work done by Alavi and Krawinkler (2001), Jamnani et al. (2013), and Chen et al. (2014).

2.2.3 Dynamic Stability Effect

The effect of dynamic stability on seismic ratcheting of structures was first described by MacRae and Kawashima (1993). They considered two different cases of bilinear response that had no initial forces acting on them: one with a positive post-elastic stiffness (**Figure 2.6a**), and another with a negative post-elastic stiffness (**Figure 2.6b**), where F is the lateral force and Δ is the lateral displacement. If the building has a positive post-elastic stiffness and has a residual displacement at point A, the structure would have lower yield strength in the negative direction. This results in a greater tendency for the building to yield towards the zero-displacement position. In contrast, the building with the negative post-elastic stiffness would be more likely to yield away from the zero-displacement position, which results in ratcheting. Due to these observations, the first case is considered to be dynamically stable, while the second case dynamically unstable.

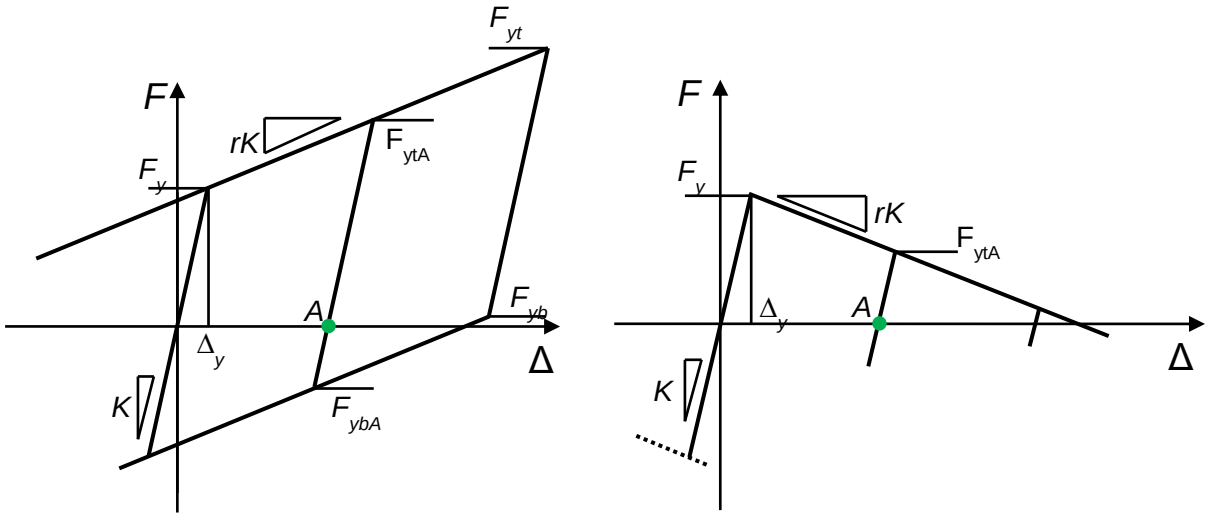

(a) Positive Bilinear Hysteresis **(b) Negative Bilinear Hysteresis**

Figure 2.6: Examples of dynamic stability (MacRae and Kawashima, 1993)

2.2.4 Eccentric Loading Effect

Structures subjected to eccentric gravity loads may also be susceptible to ratcheting effects during seismic events (MacRae and Kawashima, 1993). Consider a column with the lateral force–displacement backbone hysteresis shown in **Figure 2.7**. The effect of an eccentric moment applied to the column, M_E, on the lateral force capacity of the column can be approximated by applying an equivalent static lateral force, $F = M_E/L$, to the top of the column, where L is the column's height. This causes the baseline of the hysteresis curve to be shifted by M_E/L. Therefore, the provided strength in the forward direction will be increased by M_E/L and that in the opposite direction will be decreased by the same amount. These final strengths, which are the strengths provided after considering the effect of the eccentric moment, are referred to in this thesis as "effective strengths". As the column has different lateral strengths in each direction, it requires a smaller force to yield in the negative direction compared with the positive direction, resulting in the column ratcheting in the reverse direction.

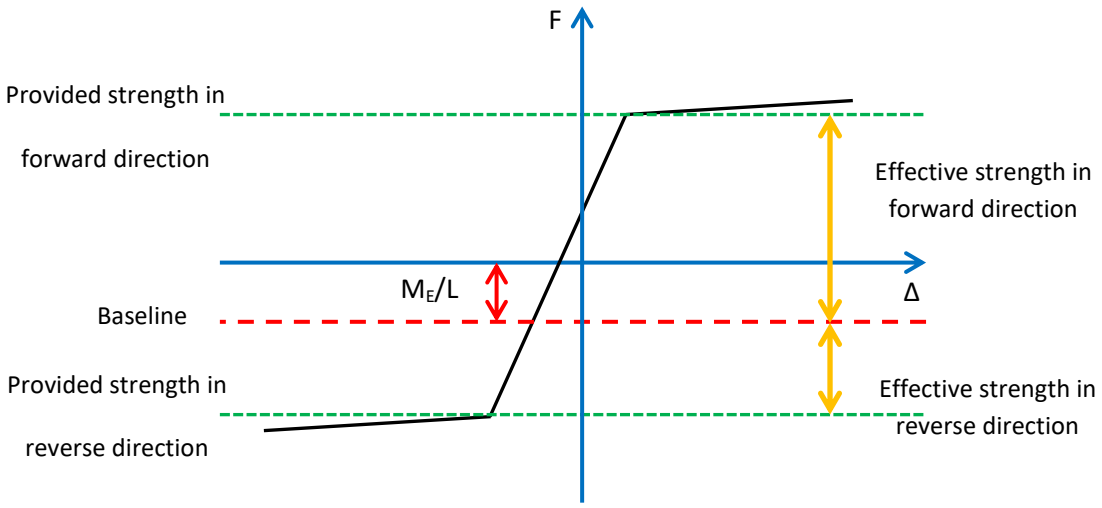

Figure 2.7: Eccentric loading effect on dynamic stability

2.2.5 Structural Form Effect

Structures with unequal strengths and/or stiffness in the back-and-forth directions may also exhibit ratcheting behaviour. Consider a column with the lateral force–displacement hysteresis curve shown in **Figure 2.8**, where the strength and stiffness in the positive direction is larger than that in the negative direction. If the stiffness is the same in both directions, then ratcheting would predominantly occur in the negative direction, as discussed previously. If the strength is the same in both directions, then increasing stiffness would also increase lateral force demands, which may instead cause yielding to first occur in the stiffer direction. However, structures tend to have larger displacements if the stiffness is lower. As such, it is not obvious how these factors would interact with each other. More in-depth discussion on these effects is detailed by Abdolahirad et al. (2017).

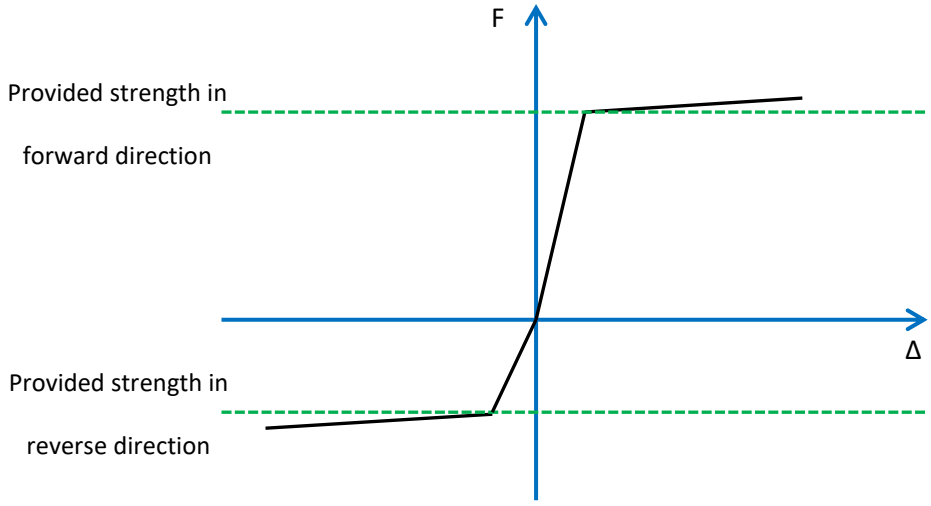

Figure 2.8: Structural form effect on dynamic stability

2.3 Studies Quantifying the Effect of Seismic Ratcheting

Dupuis et al. (2014) investigated the effect of gravity-induced lateral demand (GILD) on the seismic performance of shear-wall buildings. In their research, the strength in the weak direction was increased by the moment caused by the GILD, M_{GILD}, as shown in **Figure 2.9**. Based on their findings, they proposed actions to address the amplification in building displacements and drifts as shown in **Table 2-1**, where α is the ratio between the applied eccentric moment and the yield capacity of the member in the eccentric moment direction. They stated that if the applied eccentric moment is significantly smaller than the yield capacity, such that $\alpha < 0.1$ for systems with self-centring characteristics, and $\alpha < 0.03$ for other systems, the effects of ratcheting can be ignored. If the eccentric moment is sizable, such that $\alpha > 0.2$ for systems with self-centring characteristics and $\alpha > 0.06$ for other systems, nonlinear response history analysis is required. All other cases require displacements to be amplified by a factor of 1.2.

The range of α corresponding to these cases depends on the hysteresis loop shapes. Systems were divided into two types. These are (i) systems with self-centring characteristics such as shear walls with high axial load, where the hysteresis will take a flag shape, which results in self-centring response, and (ii) other systems which do not exhibit self-centring, such as elastic–perfectly plastic hysteretic behaviour. However, it was not mentioned in the standards how to determine whether the structure has self-centring or not, which creates confusion between engineers in practice. Another drawback is that the analyses forming the basis of the provision are for reinforced concrete structures only, which raises questions on how applicable they are to steel structures.

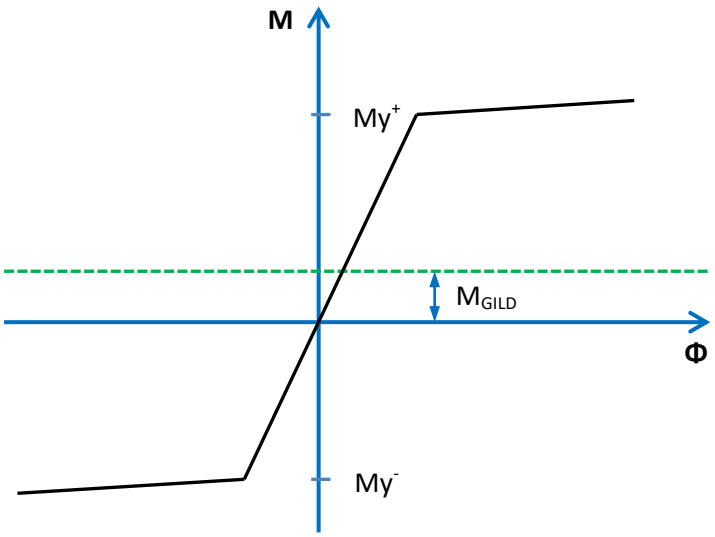

Figure 2.9 : Relationship between flexural demands and capacities for shear wall (Dupuis et al., 2014)

Table 2-1: Summary of proposed code requirements for new gravity-induced lateral demand irregularity (Dupuis et al., 2014)

Systems with self-centring characteristics	Other systems	Code requirement
$0.0 \le \alpha \le 0.1$	$0.0 \le \alpha \le 0.03$	No requirements
$0.1 < \alpha \le 0.2$	$0.03 < \alpha \le 0.06$	Multiply displacements by 1.2
$0.2 < \alpha$	$0.06 < \alpha$	Nonlinear response history analysis

Recently, Abdolahirad et al. (2017) conducted a study on the effect of unbalanced storey strength on the residual inter-storey drift ratio and how to reset the structure to its original position after an earthquake. They studied the feasibility of straightening low steel buildings after earthquakes using the dynamic properties of the buildings by adding tension braces to a 2D steel-frame building structure. They found that by increasing the storey strength in the same direction as the residual displacement after a first shake, the

residual inter-storey drift of the structure would decrease. Furthermore, they found that if the strength and stiffness of the storey is increased by 35% and 10% respectively, then the second shake will straighten the structure rather than doubling the residual displacement.

They used the energy method to explain the dynamic behaviour of structures. The concept is illustrated in **Figure 2.10** by considering an oscillator that has a potential energy at point **A1** which is equal to the area marked with (1), as shown in the figure. When releasing the load it will get back to zero force position at **A2**. Here the velocity is large and the system has already gained a large momentum that prevents the oscillator from stopping at point **A2** as the potential energy converts to kinetic energy. It will most likely move on to yield in the negative direction until all of the kinetic energy is consumed and transformed again into potential energy, which occurs at a distance where the energy under the curve in the negative direction equals that in the positive direction. Therefore, if the energy needed to yield in the positive direction is different from that in the negative direction, it will have a tendency to yield towards the direction which needs less energy.

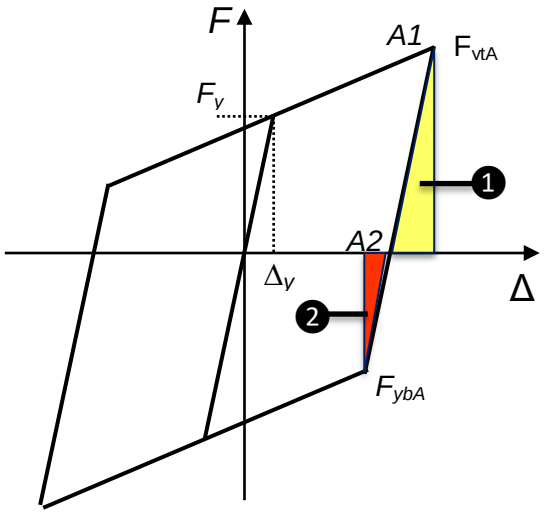

Figure 2.10: Energy method concept

2.4 Studies Examining Mitigation of Seismic Ratcheting

Past recommendations to mitigate ratcheting of bridge columns subjected to eccentric loading were to increase the strength in the direction of eccentricity as shown in **Figure 2.11**. If the direction of eccentricity acts in the "reverse direction", then the relationship between the design column's lateral strength in the forward and reverse directions (ϕS_{fn} and ϕS_{rn}, respectively), excluding the effect of eccentric moments, is shown in **Equation 2-2**.

$$\phi S_{rn} = \phi S_{fn} + \beta F_{ecc} \qquad (2\text{-}2)$$

Where F_{ecc} is the equivalent lateral load caused by eccentric loading, and β is the multiplier of F_{ecc} by which the strength is increased. It should be noted that if the eccentricity acts in the forward direction instead, then ϕS_{fn} and ϕS_{rn} should be swapped.

The Japanese Road Association (1991) proposed using β = 1.0 based on static loading considerations. In contrast, MacRae and Kawashima (1993) stated that columns exhibiting bilinear hysteretic response should have equal design lateral strengths in both directions, adjusted considering the eccentricity effect based on dynamic stability considerations. If S_f and S_r are denoted as the revised design lateral strengths in the forward and reverse directions considering the effect of F_{ecc}, respectively, then these can be calculated from **Equations 2-3** and **2-4**, respectively. For S_f and S_r to be equal, β must be equal to 2.0.

$$S_f = \phi S_{fn} + F_{ecc} \tag{2-3}$$

$$S_r = \phi S_{rn} - F_{ecc} \tag{2-4}$$

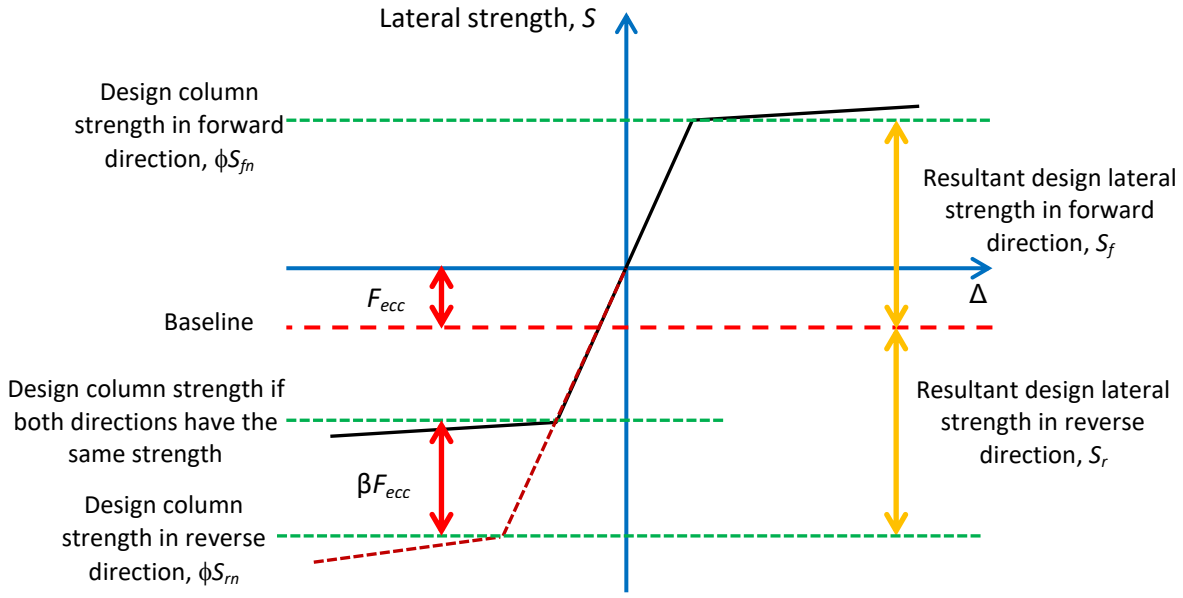

Figure 2.11: Ratcheting Mitigation

Yeow et al. (2013) showed that if column stiffness does not increase with strength, then β = 2.0 is still insufficient due to the P-delta effect. This is because there will be different yield displacements in both directions, resulting in a different levels of P-delta actions acting at the yield point in each direction. They proposed methods to estimate the actual β required for bilinear columns subjected to P-delta effects.

Yeow et al. (2013) also suggested that an even greater β is required for systems that have unequal elastic or reloading/unloading stiffness in the back-and-forth directions. They explained this by examining the elastic–perfectly plastic and Takeda hysteretic model with β = 2.0 excluding the effect of P-delta in **Figures 2.12a** and **2.12b**, respectively. In the elastic–perfectly plastic hysteresis case, the potential energy of the column at point *A* is equal to the amount required to yield in the opposite direction. In the Takeda hysteretic model case however, the potential energy at *A* is smaller than that required to yield in the opposite direction. While the same is true in the opposite direction, the difference in energies would be smaller. As such, the system is less likely to fully yield back towards the zero-displacement position for the Takeda hysteretic model case, and hence requires a higher β. They suggested that $\beta = 2.3M_e$ should be used for columns exhibiting the Takeda hysteretic model with the P-delta effect included. It should be noted that this study did not capture the interaction between an increase in strength and stiffness.

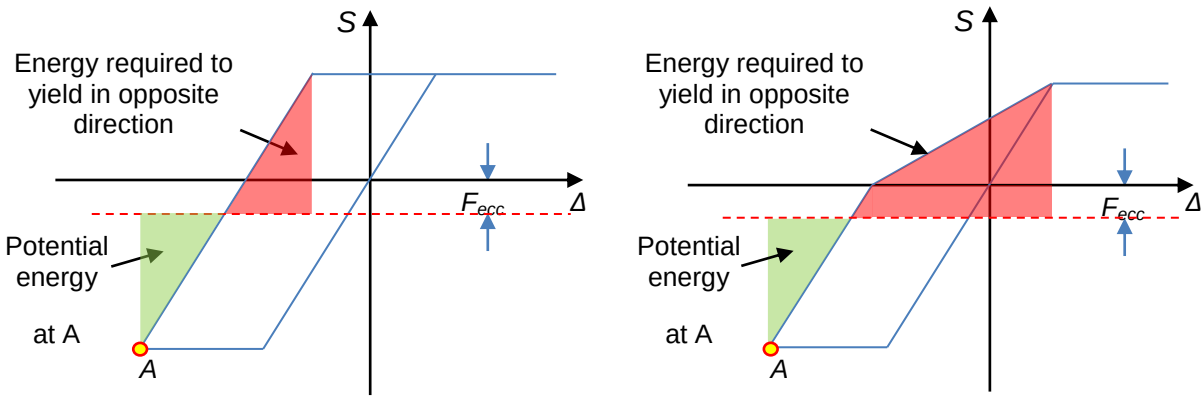

Figure 2.12: Comparison of potential energy versus energy required to yield in opposing direction for column subjected to eccentric loading; (a) elasto-plastic hysteretic curve, (b) Takeda hysteretic curve

2.5 NZS1170.5 New Provisions to Address Seismic Ratcheting

2.5.1 Provision Background and Applicability

The 2016 amendments to Part 5 of the New Zealand Structural Design Actions standards, NZS1170.5 (2016), provide provisions to determine the tendency and effect of seismic ratcheting for structures that behave in a ductile manner during strong shaking. Based on the descriptions provided in C7.2.1.3 of the 2016 NZS1170.5 commentary, the new ratcheting provisions were based on 1500 time-history analyses performed on single-degree-of-freedom structures with plastic hinge zone behaviour being represented by a Takeda hysteretic model. The column's natural period was varied from 0.5 s to 2.5s, ductility values ranged from 1 to 5, and ten different ground motion records were used. In discussion with the provision writer (Fenwick, 2017), P-delta effects, and stiffness and strength interactions of reinforced concrete members (e.g., Priestley, 2003), were not considered in the analyses. The results of these analyses have not yet been published.

It should be noted that C4.5.3 of the NZS1170.5's commentary (2016) stated that "in many cases, particularly in moment-resisting frames, moment redistribution associated with seismic actions and inelastic deformation reduces the difference in lateral strengths". This would apply to bays "b" and "c" in **Figure 2.13** where the lateral force capacity is controlled by the beam's plastic hinge capacity, and because such ratcheting is not likely to be significant for these cases, although plastic hinging may occur earlier on one side of the beam. However, the ratcheting effect is more severe for loading applied to cantilevered spans (e.g., bay "a") as the redistribution of moments in this case results in horizontal forces *T* and *C*, which induce shear in the storey.

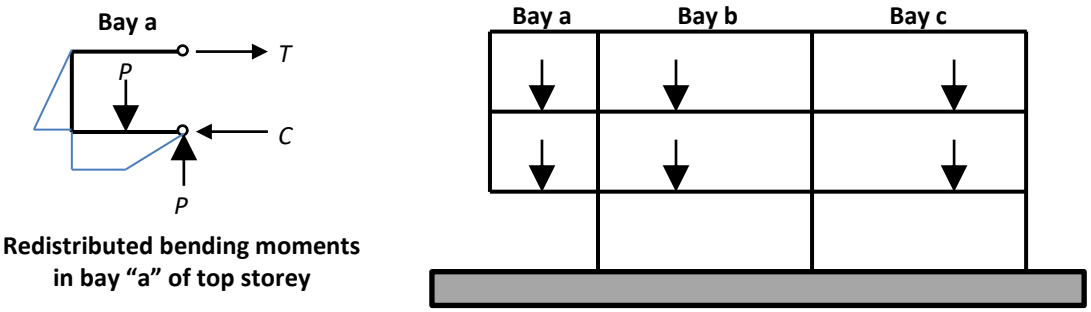

Figure 2.13: Illustration of additional lateral forces imposed on frame due to eccentric bay loading

2.5.2 Clause 4.5.3: The Ratcheting Index

Clause 4.5.3 describes the tendency of a building to exhibit seismic ratcheting by determining the ratcheting index, r_i, in **Equation 2-5**.

$$r_i = r_{i,1} + r_{i,2} \qquad \text{NZS } 1170.5\text{: } 4.5.3(\text{a}) \qquad (2\text{-}5)$$

The parameter $r_{i,1}$ is the ratio of the lateral design strength in the forward direction, S_f, to the corresponding strength in the reverse direction, S_r, according to **Equation 2-6**. The forward direction is taken as the direction of the higher lateral strength.

$$r_{i,1} = \frac{S_f}{S_r} \qquad \text{NZS } 1170.5\text{: } 4.5.3(\text{a: i}) \qquad (2\text{-}6)$$

The parameter $r_{i,2}$ accounts for the possibility of ratcheting occurring even if S_f and S_r are equal (NZS1170.5:4.5.3, 2016). This is consistent with observations by Yeow et al. (2013) for buildings exhibiting Takeda hysteretic behaviour. The parameter $r_{i,2}$ is calculated from **Equation 2-7**, where S_g is the "change in the lateral strength due to the portion of eccentric gravity load in the forward direction being balanced by a corresponding change in the lateral strengths of the structural elements" (Clause 4.5.3).

$$r_{i,2} = \frac{S_g}{S_r} \qquad \text{NZS } 1170.5\text{: } 4.5.3(\text{a: ii}) \qquad (2\text{-}7)$$

Ratcheting effect consideration depends on the design ductility level, as specified in Clause 6.1.1 (NZ1170.5, 2016). For example, it should be considered for limited ductile and ductile structures. The value of the ratcheting index can also be used to indicate whether to account for ratcheting or not. If r_i is less than 1.15, ratcheting effects can be neglected, as stated in Clause 6.1.1 (NZS1170.5, 2016). If r_i is greater than 1.5, time history analysis must be used to determine the structure's displacements. If r_i is between these two boundaries, amplification factors from Clause 7.2.1.3 may be used to modify displacements obtained via elastic analysis approaches, and the base shear strength in the weak direction should be equal to or larger than the horizontal seismic force (NZS1170.5:6.2.1.2, 2016).

2.5.3 Clause 7.2.1.3: Increased Displacements Due to Ratcheting

Clause 7.2.1.3(b) states that the displacements should be increased by an amount equal to $0.75(r_i - 1)$ times the lateral deflections obtained using the equivalent static or modal response spectrum methods if $1.15 < r_i < 1.5$. It is stated in the C7.2.1.3 of NZS1170.5 (2016) commentary that this value was based on the average obtained from the unpublished analyses that form the basis of the provisions, and is further increased by 20% to consider the potential for increased ratcheting due to interaction with P-delta actions. That is, the total increase in displacement accounting for both P-delta and ratcheting simultaneously may be greater than the sum of its individual effects; and the 20% approximates the difference between the simultaneous case versus the combined individual effects. Discussions with Fenwick (2017) indicated that the consideration of P-delta effects from other clauses within NZS1170.5 (2016) is still required.

2.5.4 Ratcheting Index Calculation Examples

The following describes the supplementary examples to calculate r_i provided in NZS1170.5's Commentary (2016) to Clause 4.5.3, the summary of which is shown in **Table 2-2**. In case A, the reinforcement layout on the "a" and "b" sides of the column are identical, resulting in the lateral strengths in both directions being 100, as shown in **Figure 2.14a,** when there are no eccentric gravity loads applied. If there is an eccentric gravity load causing an equivalent lateral demand of 15, the lateral strength in the forward direction (S_f) will increase to 115, while the strength in the reverse direction (S_r) will decrease to 85, as shown in **Figure 2.14b**. The value of S_g is 0 since none of the eccentric load is balanced by any change in the lateral strength, and hence $r_{i,2} = 0$. The ratcheting index is therefore $r_i = r_{i,1} = 1.35$. This implies that seismic ratcheting is not negligible, but time history analysis is not required. Clause 7.2.1.3 can then be examined to determine the displacement modification factor required if displacements were estimated using elastic analysis, although examples for this were not provided. An illustration of this example is shown in **Figure 2.15a**.

Table 2-2: Calculation of ratcheting indices

Case ID in commentary	S_f	S_r	S_g	$r_{i,1}$	$r_{i,2}$	r_i
A	115	85	0	1.35	0	1.35
B	115	100	15	1.15	0.15	1.30
C	115	115	15	1.00	0.13	1.13
D	115	130	15	0.88	0.12	1.00

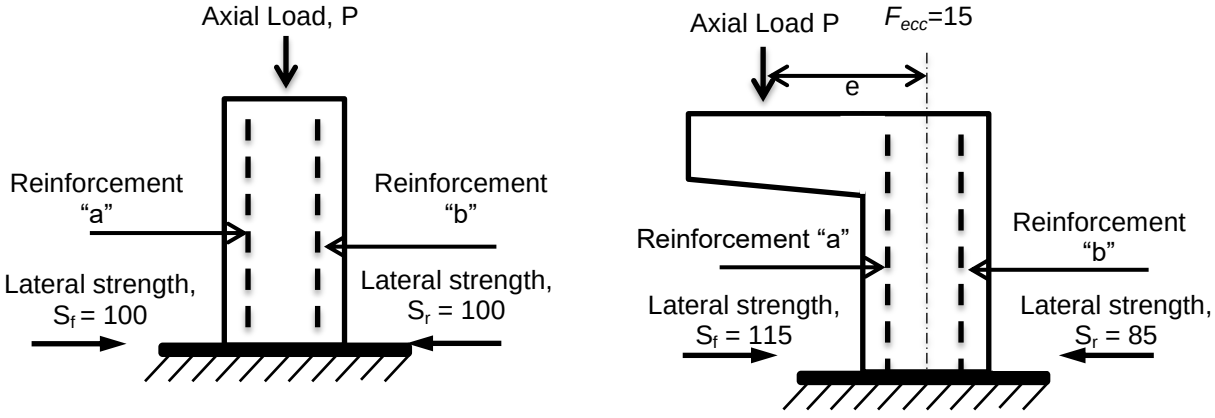

(a) Column without eccentric loading **(b) C-bent column with eccentric loading**

Figure 2.14: Ratcheting index example for Case A

In Case B, the quantity of reinforcement on side "b" is increased so that S_r increases to 100 from 85. The strength in the forward direction remains 115. Therefore, $r_{i,1}$ = 115/100 = 1.15. As the reinforcement is increased enough to balance the eccentric loading, S_g = 15. Therefore, $r_{i,2}$ = 15/100 = 0.15, and r_i for this case is 1.3. This still requires the use of Clause 7.2.1.3 to determine the displacement modification factor. An illustration of this example is shown in **Figure 2.15b**.

In Case C, the quantity of reinforcement on side "b" is increased even further so that S_r is now 115, while S_f remains at 115. Here, $r_{i,1}$ = 115/115 = 1.0. Because the strength increase in the reverse direction (which is 30 larger than Case A) is greater than the full portion of eccentric gravity load (15), S_g is again taken as 15. Therefore, $r_{i,2}$ = 15/115 = 0.13, and r_i for this case is 1.13. Ratcheting effects do not need to be considered further in this case. An illustration of this example is shown in **Figure 2.15c**.

In Case D, the quantity of reinforcement on side "b" is increased so that the S_r increases to 130, while the S_f remains at 115. The example in the commentary calculates $r_{i,1}$ = 115/130 = 0.88. This is, however, inconsistent with Clause 4.5.3 as $r_{i,1}$ should be greater than 1.0. The value of S_g is kept at 15, and hence $r_{i,2}$ = 15/130 = 0.12 and the ratcheting index r_i for this case is 1.0. No ratcheting would be anticipated, as mentioned in the NZS1170.5 commentary (2016). An illustration of this example is shown in **Figure 2.15d**.

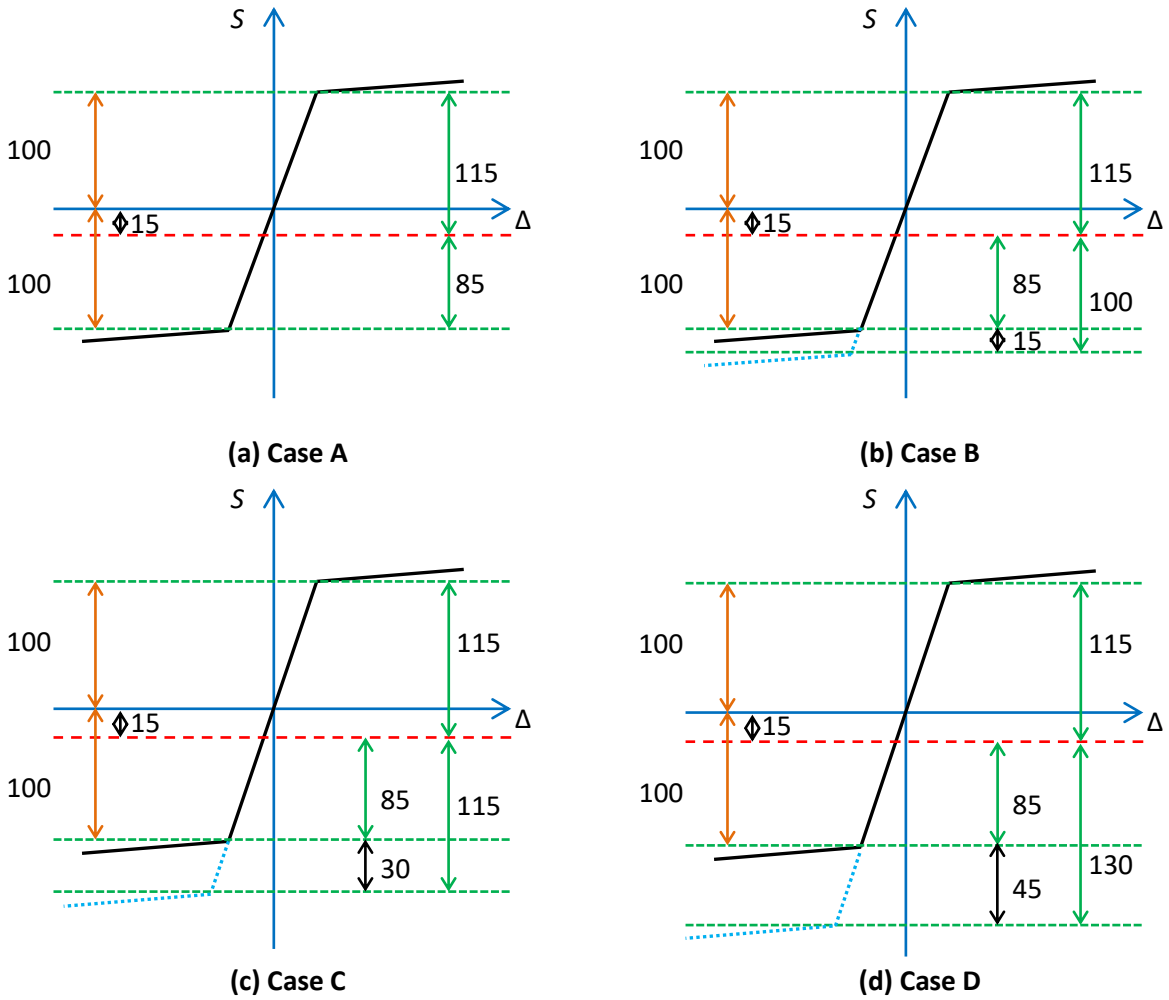

Figure 2.15: Visual Representation of 2016 NZS1170.5 Clause 4.5.3 Commentary Examples

2.6 National Building Code of Canada (NBCC) Recommendations on Ratcheting

A new vertical irregularity clause was added to the National Building Code of Canada (NBCC) in 2015, under type 9 irregularity in 4.1.8.6, which is based on the effect of gravity-induced lateral demand on the seismic performance of shear-wall buildings. Unlike the NZS1170.5, the Canadian clause divided the structural systems into two categories: (i) systems with self-centring characteristics, where the hysteresis loops are flag shaped, (ii) other systems, where the hysteresis loops are wider and dissipate more energy. Their recommendations are according to **Table 2-3**, where α is the ratio between the applied eccentric moment and the yield capacity of the members.

Table 2-3: Summary of proposed code requirements for new gravity induced lateral demand irregularity, Dupuis et al. (2014)

Systems with self-centering characteristics	Other systems	Code requirement
$0.0 \le \alpha \le 0.1$	$0.0 \le \alpha \le 0.03$	No requirements
$0.1 < \alpha \le 0.2$	$0.03 < \alpha \le 0.06$	Multiply displacements by 1.2
$0.2 < \alpha$	$0.06 < \alpha$	Nonlinear response history analysis

3. METHODOLOGY

In this research, a cantilever bridge pier was used to perform nonlinear time history analyses considering the reinforcement arrangement and stiffness effect on ratcheting, to overcome the limitations in the previous studies, which were conducted on the C-bent piers. OpenSees (McKenna et al., 2016) was used to model the pier and to run the analyses. Peak and residual displacements were used as indicators to measure the tendency of ratcheting. This chapter describes the material and model details, the analytical framework, and ground motion records that were used in the research. The scripts that were used in this research can be found in Section 9.3 and 9.4 in the appendices.

3.1 Material and Modelling Details

The column adopted for this case study was based on a reinforced concrete bridge pier with a scale of 2/5 used by Chang et al. (2004). As the column has a rectangular cross section, it was easy to quantify the amount of reinforcement added to the tension side to mitigate ratcheting. This column has a height of 3.25 m with a cross section of 750 mm x 600 mm, as shown in **Figure 3.1**. An axial force, *P*, and an eccentric moment, M_E, were applied at the top of the column. This scaled model was chosen as it was hard to find a full-scale bridge pier with square or rectangular cross section designed according to the international standards in the literature, as most of the bridges have circular piers, to provide equal strength in all directions, or long squat walls.

The column was modelled as a fibre section such that each fibre size is 23 mm x 23 mm. The unconfined concrete strength was taken as 30 MPa and the strain at maximum strength was taken as 0.002. The confined concrete strength was found to be 37 MPa and the strain at maximum strength was 0.0043. The modulus of elasticity for the concrete was calculated using $5000\sqrt{fc'}$. Concrete04 material, which is based on a uniaxial Popovics (1973) concrete material object, was used to model the concrete. The confined concrete area, which had a stress–strain curve as shown in **Figure 3.2a**, was assumed to be the rectangular area enclosed by the centroids of the longitudinal reinforcing bars, while the concrete in the cover area was assumed to be unconfined. Steel02 material, which is based on a uniaxial Giuffre-Menegotto-Pinto (1973) steel material object, was used to model longitudinal reinforcement and has a stress–strain curve as shown in **Figure 3.2b**. The yield strength was taken as 300 MPa with modulus of elasticity of 200 GPa and post elastic stiffness ratio of 0.01. The parameters that control the transition from elastic to plastic branches, as well as to consider the Bauschinger effect (1881), were taken as R0=20, cR1=0.925, and cR2=0.15.

Dynamic inelastic time history analyses were performed using 5% initial stiffness proportional Rayleigh damping. Nonlinear beam-column force-based elements, which consider the spread of plasticity along the element, were used to model the nonlinear behaviour of the structural elements with four integration points

that are based on the Gauss-Lobatto quadrature rule. The P-delta effect was considered using the co-rotational method. The natural period, *T*, was calculated based on the secant stiffness from the origin (0,0) to the first yield point, considering cracked properties.

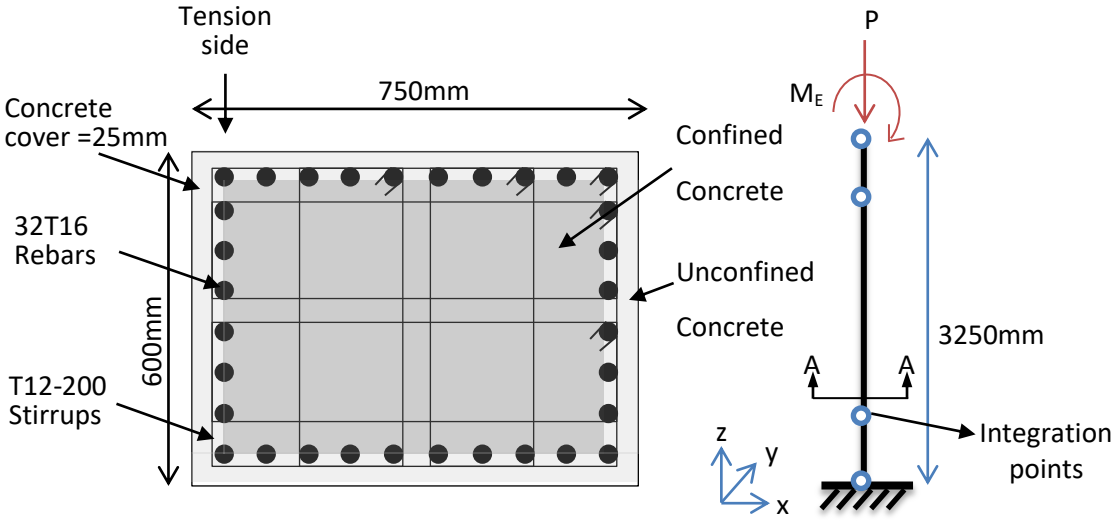

(a) Section A-A **(b) Column**

Figure 3.1: C-bent column model (Chang et al., 2004)

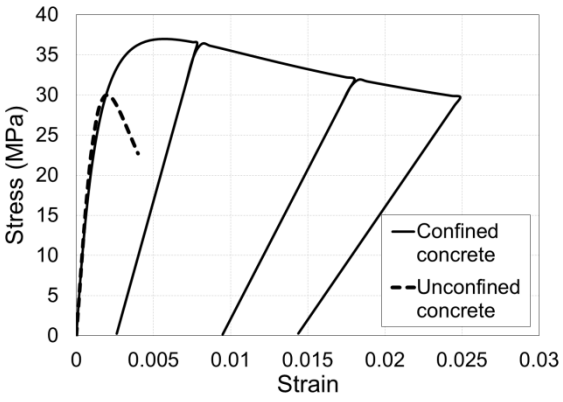

(b) Stress-strain curve for Concrete04 material, where the maximum confined compression stress = 37MPa and the maximum unconfined compression stress = 30MPa

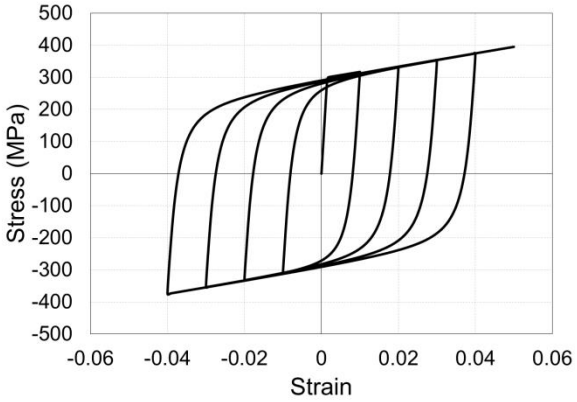

(a) Stress-strain curve for Steel02 material, where the yield stress = 300MPa

Figure 3.2: Stress-strain behaviour for the material used in the model

3.2 Analytical Framework

The analysis framework adopted is shown in **Figure 3.4**. The values of axial load ratio, which is the axial load, *P,* normalized by the axial load capacity, $A_g f_c'$, were varied from 0.0 to 0.2 with a step size of 0.05; here A_g is the column's gross cross-sectional area and f_c' is the unconfined concrete strength. The value of the design force reduction factor, *R* (which is equivalent to k_μ/S_p from Clause 5.2.1.1 in NZS1170.5), was varied from 1 to 6 with a step of 1.0. The eccentric moment ratio, α, is defined as the eccentric moment, M_E, normalized by the column's first yield moment when there is no eccentric moment applied and with balanced reinforcement, M_y, as shown in **Equation 3-1**, was varied from 0.0 to 0.4 with a step of 0.1. The eccentric moment was applied at the top of the pier, as shown in **Figure 3.1b**, so the cantilever part of the C-bent pier did not need to be explicitly modelled.

$$\alpha = \frac{M_E}{M_y} \tag{3-1}$$

The strength increment ratio, β, was increased by increasing M^- and was calculated using **Equation 3-2**, where M^+ is the column's moment capacity in the same direction of the eccentric moment, and M^- is the moment capacity in the opposite direction, as shown in **Figure 3.3**. The value of β was varied from 0.0 to 4.0 with step of 1.0 in order to find the optimal strength increment ratio, β_o, at which no ratcheting in peak displacement will occur.

$$\beta = \frac{M^+ - M^-}{M_E} \tag{3-2}$$

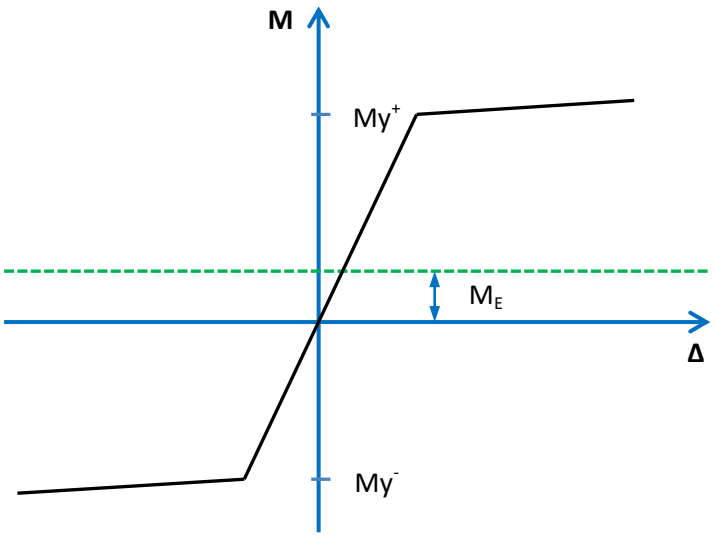

Figure 3.3: Moment–displacement relationship including the eccentric moment effect

Two parameters were used to define the degree of ratcheting: the maximum displacement ratio (*MDR*) and the residual displacement ratio (*RDR*). *MDR* and *RDR* are defined by **Equations 3-3** and **3-4**, respectively.

$$MDR = \frac{Maximum\ displacement\ (\beta, \alpha, \frac{P}{P_o}, R, T)}{Maximum\ displacement\ (\beta = 0, \alpha = 0,\ \frac{P}{P_o},\ R,\ T)} \quad (3\text{-}3)$$

$$RDR = \frac{Residual\ displacement\ (\beta, \alpha, \frac{P}{P_o}, R, T)}{Maximum\ displacement\ (\beta = 0, \alpha = 0,\ \frac{P}{P_o},\ R,\ T)} \quad (3\text{-}4)$$

In these equations, the displacement demands at a specific values of β, α, P/P_o, R, and T are normalized by the maximum displacement when the strength is the same in both directions and no eccentric moment is applied (i.e., β = 0 and α = 0). This is because in practice the latter value is usually obtained by engineers using static analysis, and hence they can simply multiply their analysis output by the *MDR* and the *RDR* ratios to estimate the maximum and the residual displacements due to ratcheting, respectively.

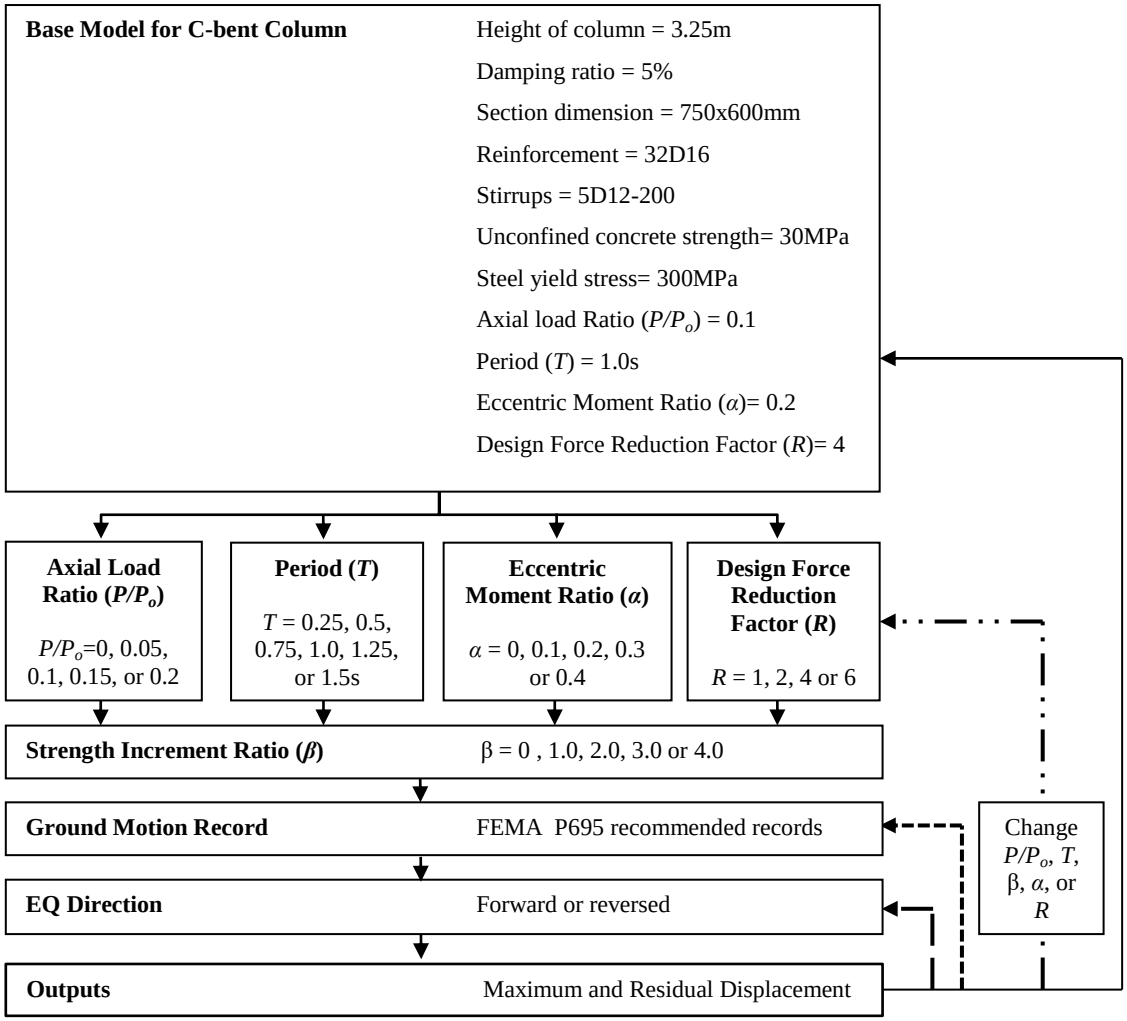

Figure 3.4: Time-history analysis procedure for C-bent column

3.3 Earthquake Ground Motions and Scaling

The far-field records in the sets of ground motion records in Appendix A of FEMA P695 (FEMA, 2009) were used and the horizontal components only were considered. The far-field records were chosen for reasons of practicality, and in recognition of the fact that there are many unresolved issues concerning characterization of near-fault hazard and ground motion effects (FEMA, 2009). There are 22 ground motion records in total, as shown in **Table 3-1**, where the PGA_{max} and PGV_{max} are the maximum values of as-recorded peak ground acceleration and peak ground velocity, respectively. Structural analyses were performed twice for each individual record to eliminate directionality effects; once with the record applied in the forward direction, and then again in the reverse direction. As such, 44 analyses were performed for each column reinforcing and loading case considered.

The record scaling for R = 1 was first found by trial and error for the column with no strength increment and no eccentric moment (i.e., α = 0 and β = 0) and when the axial force is considered, such that yield first occurred in the rebar. To account for higher values of R, the record magnitude scale factor calculated for R = 1.0 was multiplied by the target value of R, as illustrated in **Figure 3.5**. This approach of scaling the ground motion records, rather than changing the member's strength, was chosen for simplicity of the analysis.

Table 3-1: Summary of the Normalized Ground Motions for the Far-Field Record Set (FEMA, 2009)

ID No.	Earthquake			Station	Site class	Normalization factor	Normalized motions	
	M	Year	Name				PGA_{max} (g)	PGV_{max} (cm/s)
1	6.7	1994	Northridge Beverly	Beverly Hills - Mulhol	D	0.65	0.34	41
2	6.7	1994	Northridge Canyon	Canyon Country-WLC	D	0.83	0.40	38
3	7.1	1999	Duzce, Turkey	Bolu	D	0.63	0.52	39
4	7.1	1999	Hector Mine	Hector	C	1.09	0.37	46
5	6.5	1979	Imperial Valley	Delta	D	1.31	0.46	43
6	6.5	1979	Imperial Valley	El Centro Array #11	D	1.01	0.39	43
7	6.9	1995	Kobe, Japan	Nishi-Akashi	C	1.03	0.53	39
8	6.9	1995	Kobe, Japan	Shin-Osaka	D	1.10	0.26	42
9	7.5	1999	Kocaeli, Turkey	Duzce	D	0.69	0.25	41
10	7.5	1999	Kocaeli, Turkey	Arcelik	C	1.36	0.30	54
11	7.3	1992	Landers Yermo	Yermo Fire Station	D	0.99	0.24	51
12	7.3	1992	Landers Coolwater	Coolwater	D	1.15	0.48	49
13	6.9	1989	Loma Prieta	Capitola	D	1.09	0.58	38
14	6.9	1989	Loma Prieta	Gilroy Array #3	D	0.88	0.49	39
15	7.4	1990	Manjil, Iran	Abbar	C	0.79	0.40	43
16	6.5	1987	Superstition Hills	El Centro Imp. Co.	D	0.87	0.31	40
17	6.5	1987	Superstition Hills	Poe Road (temp)	D	1.17	0.53	42
18	7	1992	Cape Mendocino	Rio Dell Overpass	D	0.82	0.45	36
19	7.6	1999	Chi-Chi, Taiwan	CHY101	D	0.41	0.18	47
20	7.6	1999	Chi-Chi, Taiwan	TCU045	C	0.96	0.49	38
21	6.6	1971	San Fernando	LA - Hollywood Stor	D	2.10	0.44	40
22	6.5	1976	Friuli, Italy	Tolmezzo	C	1.44	0.50	44

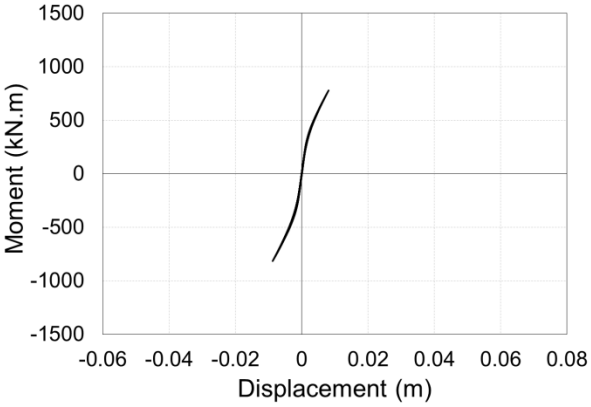

(a) Hysteresis loop for R = 1
(α = 0, P/P_o = 0.1, T = 1s, and β = 0)

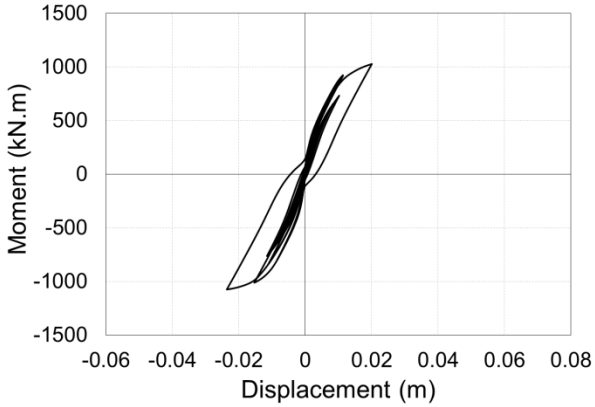

(b) Hysteresis loop for R = 2
(α = 0, P/P_o = 0.1, T = 1s, and β = 0)

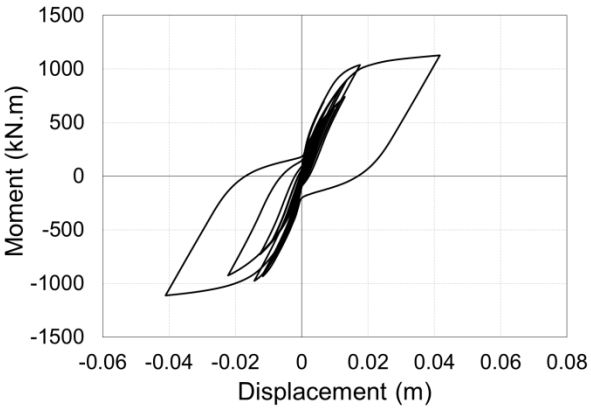

(c) Hysteresis loop for R = 4
(α = 0, P/P_o = 0.1, T = 1s, and β = 0)

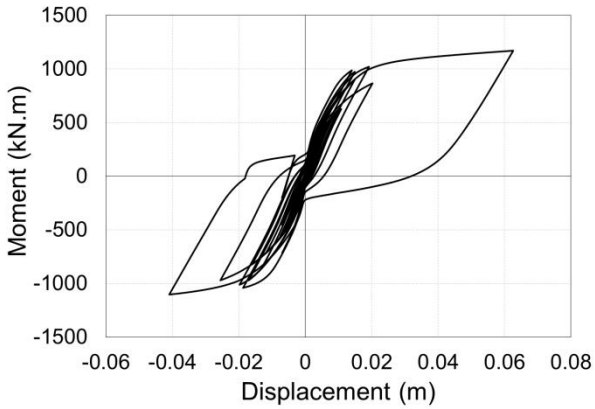

(d) Hysteresis loop for R = 6
(α = 0, P/P_o = 0.1, T = 1s, and β = 0)

Figure 3.5: Hysteresis loops showing the hysteretic behaviour when the ground motion is scaled to achieve specific R values.

4. INTERPRETATION AND EVALUATION OF NZS1170.5 2016 PROVISIONS FOR SEISMIC RATCHETING

4.1 General View of NZS1170.5 Issues

New Zealand Industry has stated that the wording of Clause 4.5.3 may be confusing. This possibly results in different interpretations of the provisions. These issues are elaborated upon in the following sections.

4.1.1 The Definition of "Design Lateral Strength"

Based on the examples provided in the Commentary of NZS1170.5 (2016), the "design lateral strength" used in S_f and S_r are the lateral strengths of the system considering the presence of eccentric loads. However, NZS1170.5 (2016) Appendix A defines design strength as "the nominal strength multiplied by the strength reduction factor as given in the appropriate material standard". As such, the design lateral strength resulting from the design strength of the members excluding eccentric loading effects may be used instead in the calculation of r_i, which would be incorrect.

4.1.2 The Definition of Forward and Reverse Directions

According to Clause 4.5.3, the forward direction corresponds to the direction of the higher lateral strength; that is, S_f must be greater than S_r. However, example Case D (NZS1170.5:C4.5.3, 2016) violates this as S_f is smaller than S_r. If code definitions were followed, then S_f and S_r should have been taken as 130 and 115 in Case D, respectively. In this case, perhaps S_g should be taken as a negative value (-15) since it acts in the "forward" direction, in that the forward and reverse directions have swapped. This would result in $r_{i=}$ 1.13-0.13 = 1.0. While r_i happens to be identical to that calculated in the commentary despite the different calculation approach, there will be differences for other cases. Further clarity for the examples and definition are required.

4.1.3 The Definition of S_g

As described earlier, S_g is defined as "the change in the lateral strength due to a portion of the eccentric gravity load in the forward direction being balanced by a corresponding change in the lateral strength of the structural elements". One potential misinterpretation is regarding the words "change in lateral strength", as it is not made clear what strength this increase is relative to. For example, an engineer's initial design is identical to that in Case D, as shown in **Figure 4.1a**, where S_g = 15. If the strength acting in the opposite direction of the eccentricity was increased from 115 to 130 as shown in **Figure 4.1b**, the change in lateral strength is 15 in the direction opposing the eccentric gravity load. One interpretation would be that S_g is now 0 (as the lateral strength was not changed to balance the eccentric gravity load). As S_f and S_r are the same in this case, $r_{i,1}$ = 1.0 and hence r_i = 1.0. However, this is essentially identical to example Case B in the

NZS1170.5's commentary (2016) where $S_f = S_r$ and r_i is greater than 1.0. It is therefore obvious that r_i should be greater than 1.0.

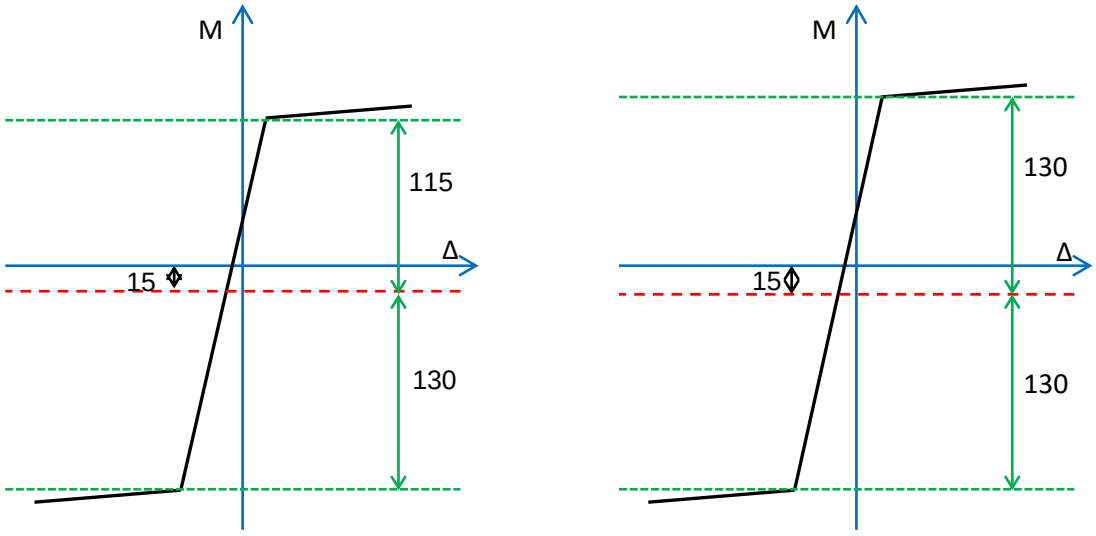

Figure 4.1: Illustration of example demonstrating complication of S_g; (a) case "D", and (b) increase in lateral strength in direction opposing eccentricity

It should be noted that in the examples provided, the "change in lateral strength" was for the reverse direction, S_r, relative to the case where the same amount of reinforcing was applied on both sides of the column. This needs to be clarified.

4.1.4 Consideration of P-Delta Effects

As mentioned previously, discussions with Fenwick (2017) indicated that the 20% increase in displacement amplification factor only addresses possible P-delta and ratcheting interactions. It does not replace the need to assess P-delta effects from Clause 7.2.1.2 of NZS1170.5 (2016). This is not clear from the wording in C7.2.1.3 of the Commentary of NZS1170.5 (2016).

Furthermore, the P-delta effect would cause the resultant lateral design strengths to decrease, which may cause the ratcheting index, r_i, to increase. As such, there needs to be some clarity regarding whether the effect of P-delta should be included in the calculation of r_i.

4.2 Proposed Revised Definitions

This section provides recommendations on clarification of the various complications related to Clause 4.5.3, based on the interpretation of the provisions and its application in the examples provided in the Commentary. These do not seek to provide derivation or validate assumptions of the ratcheting clauses in NZS1170.5 (2016); they aim to provide one means of ensuring that the NZS1170.5 (2016) provisions can be modified in a way that is easy to interpret, and that provides one way to assess the likelihood and effect of ratcheting for a particular structure.

Firstly, for the purpose of clarity it should be re-emphasized in the ratcheting clauses that "design lateral strength" considers the effect of eccentric loading. This will minimize the possibility of engineers using the strength of the structure without adjusting for eccentric loads.

Secondly, two separate alternative approaches are proposed here to address complications regarding the forward/reverse direction. Both alternatives give similar results if they are applied consistently. These are:

Alternative 1: Retain the definition that the forward direction corresponds to the direction of larger strength, and change example Case D to be consistent with this.

Alternative 2: Redefine S_f as the direction opposing the eccentricity, which ensures consistency with example Case D. In the event that $S_f + S_g$ is smaller than S_r (i.e., the column is more likely to ratchet in the direction opposite to eccentricity), then the inverse of r_i should be taken to indicate the tendency for ratcheting in the forward direction. The latter condition means that, if no eccentric moments were applied, the selection of S_f and S_r becomes arbitrary.

The absolute value of S_g can be defined by **Equation 4-1**, where, F_{ecc} is the lateral force caused by the eccentric gravity load. If Alternative 1 is used for determining the "forward" and "reverse" directions, then S_g is negative if the eccentric moment acts in the forward direction and positive otherwise. If Alternative 2 is used, then S_g is always positive as the eccentric moment is assumed to always act in the reverse direction in this case.

$$S_g = \begin{cases} \min\left\{ \begin{matrix} F_{ecc} \\ \max\left(S_r - S_f + 2F_{ecc}, 0\right) \end{matrix} \right. & \text{if eccentricity acts in reverse direction} \\ -\min\left\{ \begin{matrix} F_{ecc} \\ \max\left(S_f - S_r + 2F_{ecc}, 0\right) \end{matrix} \right. & \text{if eccentricity acts in forward direction} \end{cases} \quad (4\text{-}1)$$

Finally, it should be made clear in the Commentary that the increase of 20% in the displacement amplification factor does not discount the need to perform separate P-delta checks. Furthermore, imposed lateral loads due to P-delta effects should be included in the calculation of S_r and S_f. For a single-degree-of-freedom system, the P-delta effects shown in **Figure 4.2a** can be approximated by an equivalent lateral force of $P\Delta/L$, shown in **Figure 4.2b**; where P is the axial force, Δ is the displacement, and L is the length of the column. The resulting design lateral strength considering P-delta can be reduced by $P\Delta_y/L$ as shown in shown in **Figure 4.2c**; where Δ_y is the displacement at yield. In the case of multi-degree-of-freedom systems, Clause 6.5.4.2 in NZS1170.5 can be used to estimate the P-delta contribution to storey-shear.

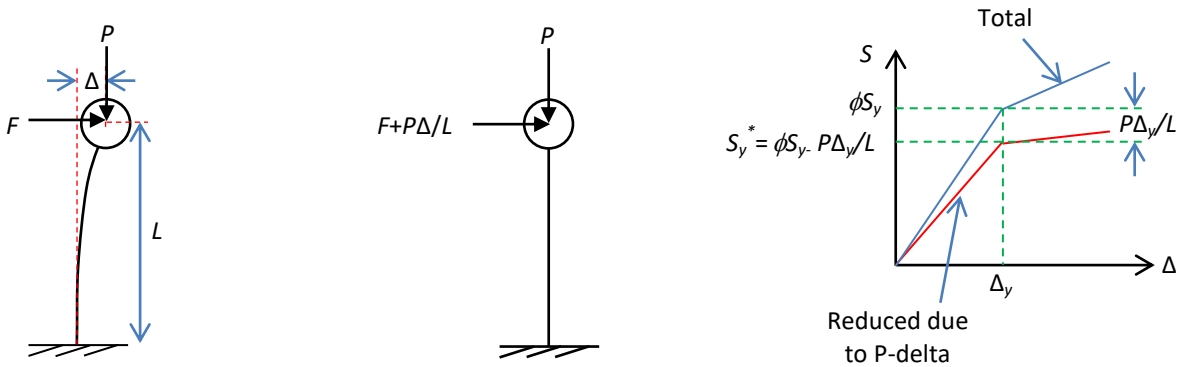

Figure 4.2: Consideration of P-delta effect; (a) effect acting on single column, (b) equivalent representation using lateral forces, and (c) reduction in capacity due to P-delta

4.3 Additional Examples to Demonstrate Application of Proposed Revised Definitions

Three examples are examined here to demonstrate the proposed recommendations discussed, and the results are detailed in **Table 4-1**. The first example demonstrates the calculation of S_g using **Equation 4-1**.

Example 1: Consider case "II", where design lateral strength in the reverse direction including eccentric load effects, S_r, is increased from 85 in Case A to 95. The design lateral strength in the forward direction including eccentric load effects, S_f, remains the same at 115. Therefore, $r_{i,1} = S_f/S_r = 115/95 = 1.21$. Using $F_{ecc} = 15$, $S_g = S_r-S_f+2F_{ecc} = 10$. Therefore, $r_{i,2} = S_g/S_r = 10/95 = 0.11$. The ratcheting index, r_i, for this case is $r_{i,1}+r_{i,2} = 1.32$. In this case, displacement modifiers from Clause 7.2.1.3 are required if elastic methods of analysis were used.

The next two examples consider the same column configuration, but are based on the different interpretations of the forward and reverse direction. The wording, consistent with Clause 4.5.3, which is alternative 1, is examined first.

*Example 2: Consider case "VI(a)", where the design lateral strength including eccentric load effects is 145 in the direction of eccentricity and 115 in the opposite direction, and $F_{ecc} = 15$. Based on this, and using alternative 1 where the forward direction is in the larger strength direction, $S_f = 145$ and $S_r = 115$. As the eccentricity acts in the forward direction, $S_g = -15$ using **Equation 4-1**. Therefore, $r_{i,1} = 145/115 = 1.26$ and $r_{i,2} = -15/115 = -0.13$. The ratcheting index, r_i, for this case is 1.13, and seismic ratcheting need not be considered further.*

*Example 3: "VI(b)" considers the same scenario as example 2, but using alternative 2 where the forward direction is in the direction opposing the eccentricity. Based on this, $S_f = 115$ and $S_r = 145$. This is because the eccentricity acts in the direction corresponding with the design lateral strength of 145. Using **Equation 4-1**, $S_g = 15$. Therefore, $r_{i,1} = 115/145 = 0.79$ and $r_{i,2} = 15/145 = 0.10$. As the sum of $r_{i,1}$ and $r_{i,2}$ is smaller than 1.0,*

the inverse is taken instead. This results in r_i = 1.12, which is near identical to the other interpretation, which indicates that either approach is reasonably consistent.

Table 4-1: Calculation of ratcheting indices with new examples

Case ID in thesis	Case ID in commentary	P-delta effect included?	S_f	S_r	S_g	$r_{i,1}$	$r_{i,2}$	r_i
I	A	No	115	85	0	1.35	0	1.35
II	-	No	115	95	10	1.21	0.11	1.32
III	B	No	115	100	15	1.15	0.15	1.30
IV	C	No	115	115	15	1.00	0.13	1.13
V	D	No	115	130	15	0.88	0.12	1.00
VI(a)	-	No	145	115	-15	1.26	-0.13	1.13
VI(b)	-	No	115	145	15	0.79	0.10	1.12

4.4 Evaluation Displacement Increase Estimates from Clause 7.2.1.3

4.4.1 Approach

An independent numerical study was performed to examine the performance of bridge columns with eccentric loadings and to evaluate if the displacement increase estimates provided in Clause 7.2.1.3 are reasonable. Furthermore, comparisons were also made with recommendations from Dupuis et al. (2014) and the National Building Code of Canada (NBCC, 2015) discussed previously in Sections 2.3 and 2.6. To enable this, the α (=$F_{ecc}/\phi S_{fn}$) parameter needs to be converted back to r_i. Dupuis et al. (2014) and NBCC (2015) consider $\phi S_{fn} = \phi S_{rn}$, and hence S_g and $r_{i,2}$ is zero. The parameters α and r_i can therefore be related as shown in **Equation 4-2**. If the system has self-centring characteristics, then the r_i equivalent of the Canadian code (NBCC, 2015) form is as shown in **Table 4-2**.

$$r_i = r_{i,1} = \frac{S_f}{S_r} = \frac{\phi S_f + F_{ecc}}{\phi S_f - F_{ecc}} = \frac{\phi S_f + \alpha \phi S_f}{\phi S_f - \alpha \phi S_f} = \frac{1+\alpha}{1-\alpha} \tag{4-2}$$

Table 4-2: Ratcheting provisions in NBCC (2015) in terms of ratcheting index

Systems with self-centring characteristics	Other systems	Code requirement
$1.00 \le r_i \le 1.22$	$1.00 \le r_i \le 1.06$	No requirements
$1.22 < r_i \le 1.5$	$1.06 < r_i \le 1.13$	Multiply displacements by 1.2
$1.5 < r_i$	$1.13 < r_i$	Nonlinear response history analysis

4.4.2 Methodology

The reinforced concrete cantilever column fibre model considered is shown in **Figure 4.3**. This is based on a scaled reinforced concrete bridge column used by Chang et al. (2004). The analyses were performed using OpenSees (McKenna et al., 2016) with 5% Rayleigh damping and co-rotational analyses to consider the P-delta effect. The natural period, T, was 1.0 s and R (the k_μ/S_p factor from Clause 5.2.1.1 in NZS1170.5) was selected to be 4.0. An axial load ratio of P/P_o=0.1 was applied at the top of the column.

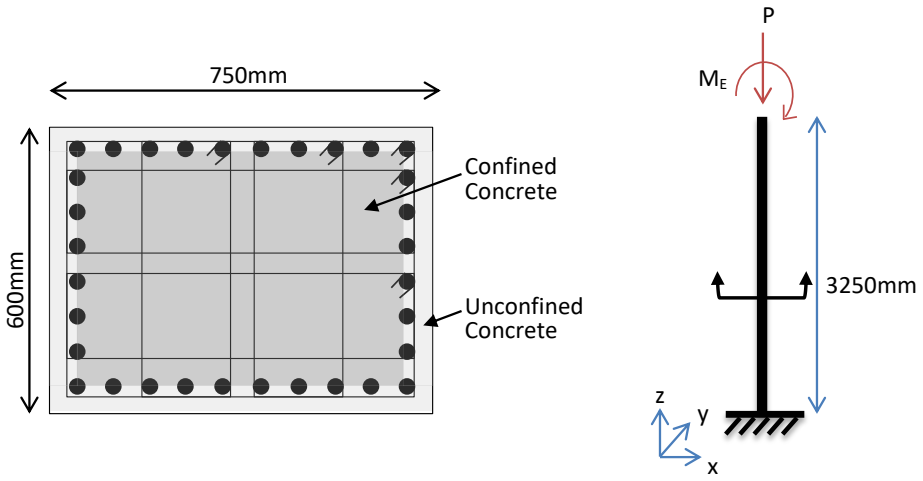

Figure 4.3: Cantilevered column model

Three cases were considered: (i) symmetrically reinforced columns subjected to eccentric loads, (ii) unsymmetrically reinforced columns without eccentric loads, and (iii) unsymmetrically reinforced columns with eccentric loads. In the first two cases, there was no reinforcement change to balance the eccentric moment, therefore S_g = 0 and $r_{i,2}$ = 0. The lateral force caused by the eccentric load, F_{ecc}, considered in cases (i) and (iii) were varied from 0 to 0.3 times ϕS_{fn} in steps of 0.1. The ratcheting index r_i was then calculated for each reinforcement layout.

The far-field record suite provided in Appendix A of FEMA P695 (FEMA, 2009) was used in the analyses. This record suite contains 22 sets of ground motion records, each with two horizontal and one vertical component. Each horizontal component was treated as an individual event, and vertical components were not considered. For each record and each of the three cases considered, the displacement at a given r_i was normalized by the displacement at r_i = 1.0. The average of the normalized displacements for each individual case was calculated and termed the "displacement amplification".

4.4.3 Increase in Displacements Due To Eccentric Moments Alone

The displacement amplification factors for columns (i) with varying F_{ecc} without modifying the strength of the column, and (ii) with unbalanced strength without any eccentric loading applied are both shown in **Figure 4.4a** and **4.4b**, where the axial load ratio applied was P/P_o=0.1 and 0, respectively. The two different axial loads applied resulted in the column exhibiting different degrees of self-centring, as shown in

Figure 4.4c and **4.4d**. It can be seen that for both of these cases, the NZS1170.5 (2016) estimates are slightly larger than that observed from the numerical study. This indicates that NZS1170.5 (2016) provides a reasonable but conservative estimate of the displacement amplification. In contrast, the Canadian code (NBCC, 2015), which already increased the strength in the weak direction by the eccentric moment, underestimates the displacement amplification in the case where the column's hysteresis curve exhibits self-centring behaviour when r_i is greater than 1.35 (**Figure 4.4a**); and overestimates the displacement amplification in cases where the column does not exhibit self-centring behaviour over the range where it may be applied.

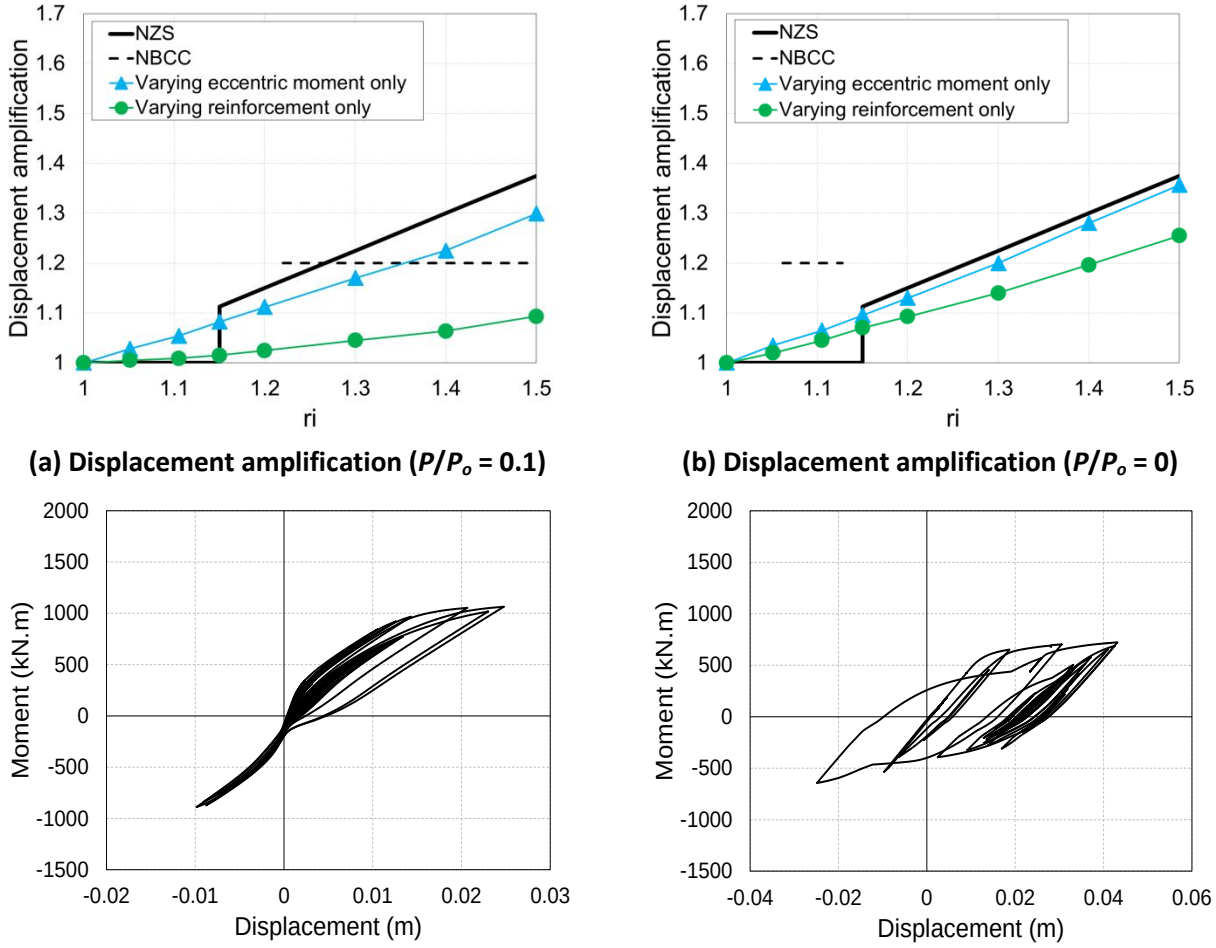

(a) Displacement amplification (P/P_o = 0.1)

(b) Displacement amplification (P/P_o = 0)

(c) Hysteresis shape for P/P_o = 0.1

(d) Hysteresis shape for P/P_o = 0

Figure 4.4: Evaluation of displacement amplification factors for case of varying eccentric moment or reinforcing separately (S_g = 0, T = 1.0s, R = 4, damping 5%, and using fibre section)

In the third case where both the eccentric moment and reinforcing content was varied at the same time, the effect of additional parameters was also investigated to check their effect on the displacement amplification factor. In **Figure 4.5a**, the eccentric moment ratio, α, was changed from 0.1 to 0.4 with a step of 0.1. It can be seen that at a fixed value of r_i, the displacement amplification generally decreases with increasing eccentricity. This seems counter-intuitive as one would expect the displacement amplification factor to

increase with α. However, a column with a lower α would be designed with a lower value of β (less reinforcement) at a given value of r_i compared with a column with a larger α, and would therefore be more sensitive to ratcheting effects. If no strength increase were provided, then the displacement amplification factor increases with α as expected. This, however, raises the issue that consideration of the relative ratio of effective strengths may not be sufficient on its own to estimate the increase in displacements.

In **Figure 4.5b**, the axial load ratio was varied to represent the degree of self-centring. It can be seen that NZS1170.5 (2016) provided a reasonable estimate of displacement amplification factors when the applied axial load is high, for cases with axial loads applied. It is however non-conservative in the case where no axial loads were applied when the column did not exhibit self-centring behaviour. Conversely, the National Building Code of Canada (2015) provided reasonable estimates when no axial loads were applied, but was otherwise non-conservative for the case of P/P_o=0.1. The same trends were observed for varying the lateral force reduction factor, R, and period, T, in **Figures 4.5c** and **4.5d**, respectively. It can be seen, however, that the displacement amplification factor tends to increase noticeably with R and slightly with T.

Based on these observations, although NZ1170.5 (2016) is mostly conservative for r_i < 1.4, it is proposed that it should be modified where the displacement amplification factors are adjusted to take into account the degree of self-centring, and R. Based on the limited influence of T, it is perceived that this factor does not need to be explicitly considered.

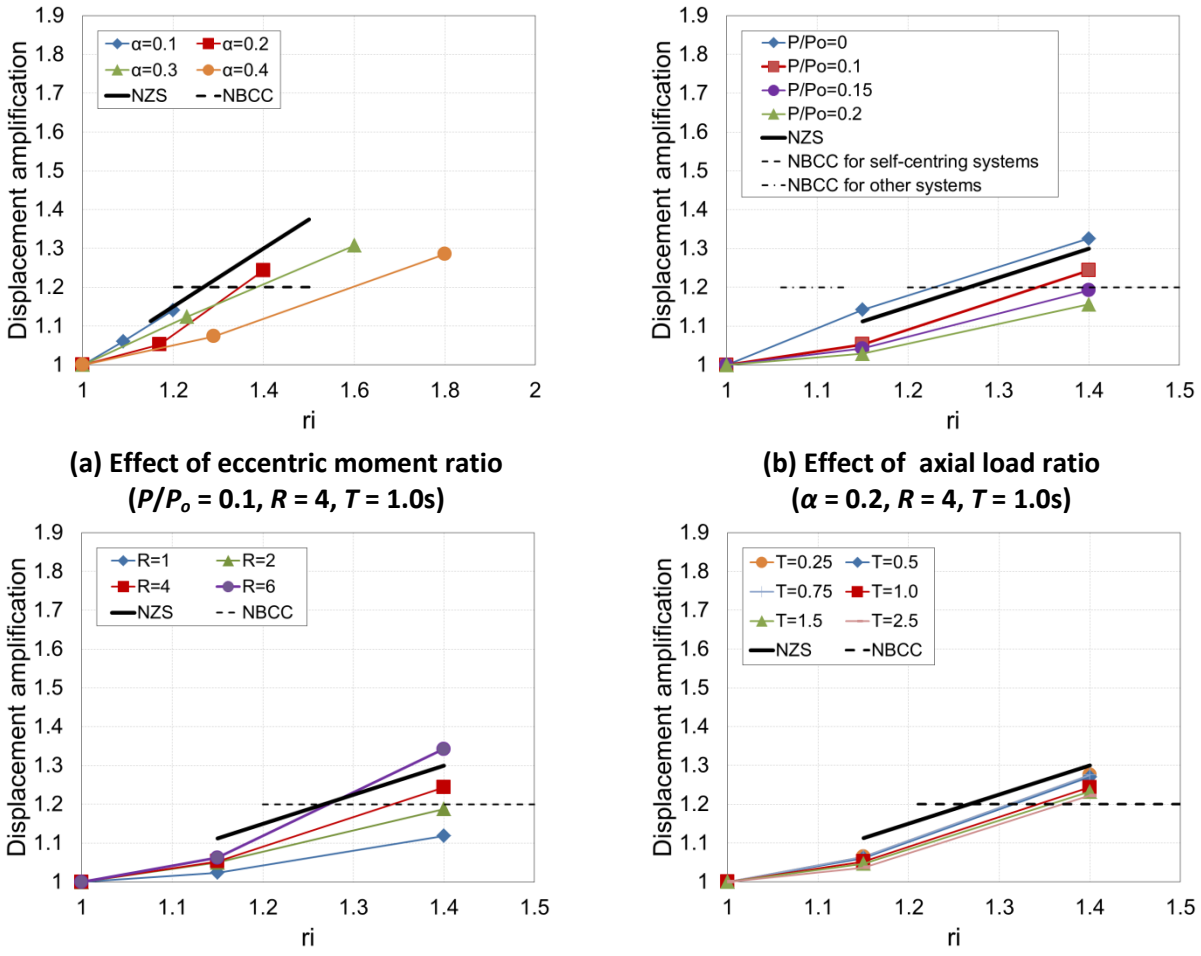

(a) Effect of eccentric moment ratio (P/P_o = 0.1, R = 4, T = 1.0s)

(b) Effect of axial load ratio (α = 0.2, R = 4, T = 1.0s)

(c) Effect of R (P/P_o = 0.1, α = 0.2, T = 1.0s)

(d) Effect of natural period (P/P_o = 0.1, α = 0.2, R = 4)

Figure 4.5: Effect of various parameters on displacement amplification (including P-delta)

4.4.4 Use of NZS1170.5 Provisions to Mitigate Ratcheting

One method to prevent the need for modifying the displacements to address the effect of ratcheting is to design for $1.0 \leq r_i \leq 1.15$. Assuming that the eccentric moment acts in the reverse direction, the design lateral capacity in the forward direction excluding the effect of eccentricity is ϕS_f, and that the equivalent lateral force to represent the eccentric moment as $F_{ecc} = \alpha.\phi S_f$, the design lateral strength in the reverse direction excluding the effect of eccentric moment, ϕS_r, can be calculated from **Equations (4-3)** and **(4-4)**. This assumes that the increase in strength required in the reverse direction is greater than F_{ecc}, so $S_g = F_{ecc}$.

$$1.15 = r_{i,1} + r_{i,2} = \frac{S_f + F_{ecc}}{S_r} = \frac{\left(\phi S_{fn} + \alpha.\phi S_{fn}\right) + \alpha.\phi S_{fn}}{\phi S_{rn} - \alpha.\phi S_{fn}} \qquad (4\text{-}3)$$

$$\phi S_{rn} = (0.87 + 2.74\alpha).\phi S_{fn} \qquad (4\text{-}4)$$

The approaches proposed by MacRae and Kawashima (1993) for bilinear hysteretic behaviour, and Yeow et al. (2013) for Takeda hysteretic behaviour including the P-delta effect discussed previously in section 2.4, are shown in **Equations 4-5** and **4-6**, respectively.

$$\phi S_{rn} = (1.00 + 2.00\alpha).\phi S_{fn} \quad (4\text{-}5)$$

$$\phi S_{rn} = (1.00 + 2.30\alpha).\phi S_{fn} \quad (4\text{-}6)$$

Comparisons of the three approaches are shown in **Figure 4.6**. Here, the y-axis starts at 0.5 so that differences in the lines could be observed more clearly. It can be seen that simply satisfying $r_i < 1.15$ may not be adequate to mitigate seismic ratcheting when compared with Yeow et al. (2013). However, it should be emphasised that the purpose of Clause 4.5.3 is to assess whether the tendency for seismic ratcheting is significant enough to warrant further considerations, and not mitigating ratcheting completely. Nonetheless, this shows that by simply following the approach by Yeow et al. (2013), r_i should be less than or similar to 1.15 for the range of α considered, and hence no further modifications to displacements would be required.

In contrast, the approach of MacRae and Kawashima (1993) would still require further modifications to displacements if α were greater than 0.2. This is due to the differences between bilinear and Takeda hysteretic behaviours, as discussed previously in section 2.3, where bilinear responding columns do not require as large a strength increase due to it not being affected by the potential versus yielding energy effect. This again raises the question of how suitable the code clauses are for steel or timber buildings.

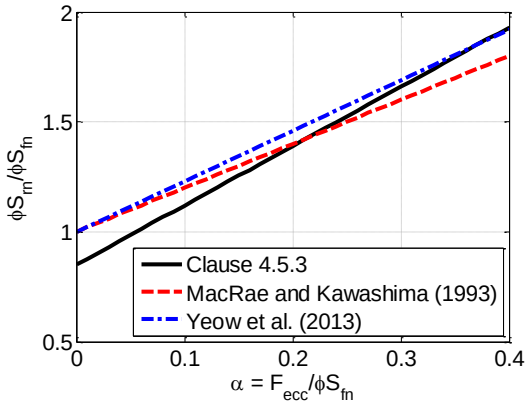

Figure 4.6. Comparison of mitigation strategies

4.4.5 Avenues for Future Work

Based on the assessment of NZS1170.5 (2016) described above, it is noted that the displacement amplification factors proposed are mostly conservative where $r_i < 1.4$ for structures exhibiting self-centring behaviour. However, its inability to address the influence of self-centring behaviour and R results in (i) some "extreme" cases that still have $r_i < 1.5$ being underestimated, and (ii) over-conservatism in buildings that appear to be less prone to ratcheting, such as stronger buildings (i.e., lower R). Furthermore, the code clauses were derived from analyses of single-degree-of-freedom systems with Takeda hysteretic behaviour. It is not certain if these are therefore applicable to multi-storey buildings or to buildings exhibiting other hysteretic behaviours.

It is proposed that more robust analyses should be conducted to provide an approach to consider these factors, among others, in future estimation of displacement amplification factors. Furthermore, comprehensive provisions for different types of systems should be provided to account for ratcheting, and should be written in a clear way without any deficiency, such that practicing engineers can easily follow them. Finally, more detailed methods of mitigating ratcheting effects should be explored and provided as an alternative to amplifying displacements.

5. SEISMIC RATCHETING AND DESIGN OF RC C-BENT COLUMNS CONSIDERING STRENGTH AND STIFFNESS DEPENDENCY AND AXIAL-MOMENT INTERACTION

In practice, modal or equivalent static analyses, which are unable to capture the effect of eccentric moments, are often used. Therefore, this chapter provides methods to estimate the maximum and the residual displacements when ratcheting is considered for both reinforced concrete and steel columns with eccentric gravity loads. It also presents the optimal strength increment ratio at which ratcheting in maximum displacement will not occur due to eccentric moment for cases where displacements were obtained by elastic methods. Design examples are also presented, explaining how to use the suggested approaches.

5.1 Influence of Adding Strength in Direction of Eccentricity on Back-and-Forth Stiffness

This section assesses if the approximation that strength and stiffness are proportional (Priestley, 2003) is captured by the fibre modelling. Pushover analysis was performed using the cantilever model described in the methodology with different reinforcing bar diameters, d_b. The results are shown in **Figure 5.1**. It can be seen that the points of first yield all occur at approximately the same displacement. Therefore, the stiffness–strength relationship is approximately linear. Cyclic pushover was also performed on the model, where the strength on one side was increased by adding more reinforcing bars compared with the other side. The results are shown in **Figure 5.2**, where it can be seen that when the strength is increased, by adding more reinforcing bars on one side, the stiffness also increases, as shown by the values for the unloading stiffness.

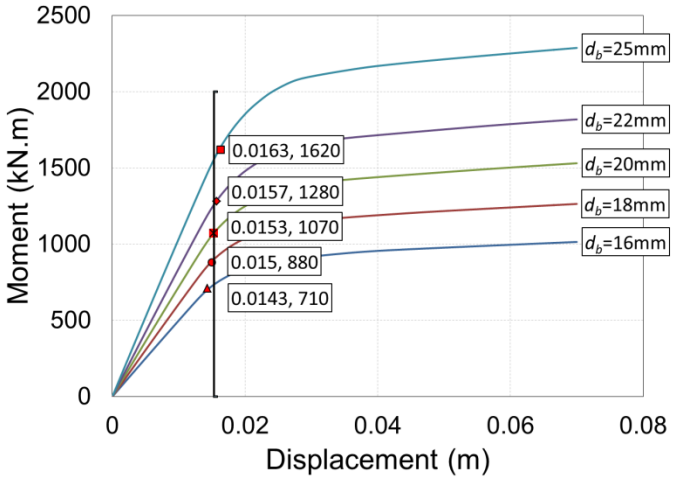

Figure 5.1: Pushover analysis results using different bar diameters (the yield displacements are based on the first yield point)

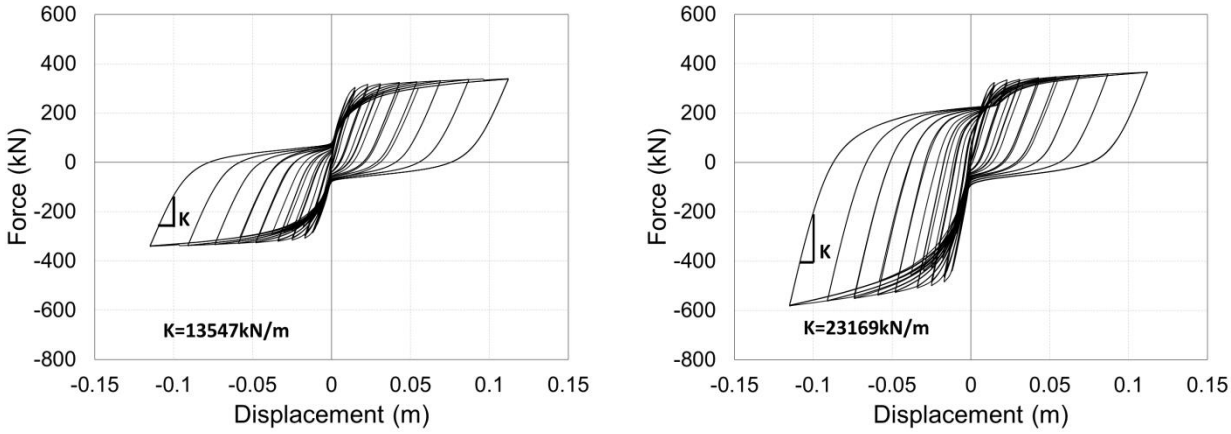

(a) Hysteresis loop with same reinforcement on both sides

(b) Hysteresis loop with more reinforcement on one side

Figure 5.2: Stiffness–strength relationship with different reinforcement layout

5.2 Effect of Eccentric Moment on Seismic Ratcheting

In this section, the influence of the eccentric moments on the column's response was defined by two parameters: maximum displacement ratio (*MDR*) and residual displacement ratio (*RDR*), as defined by **Equations 5-1** and **5-2**, respectively. Both *MDR* and *RDR* were calculated for each individual record, and the average from all records is shown in the figures.

$$\text{MDR} = \frac{\text{Maximum displacement at } \alpha}{\text{Maximum displacement at } \alpha = 0} \tag{5-1}$$

$$\text{RDR} = \frac{\text{Residual displacement at } \alpha}{\text{Maximum displacement at } \alpha = 0} \tag{5-2}$$

5.2.1 Reinforced Concrete Cantilever Column

First, the effect of the eccentric moment on the displacement demands for a reinforced concrete column was studied. **Figure 5.3** shows that displacements increase with increasing eccentric moment ratio, α. *MDR* is higher for a higher force reduction factor, *R*, as shown in **Figure 5.3a**. This is because a weaker column would yield earlier with a greater value of *R*, and therefore is more susceptible to eccentric loading effects. In contrast, the *RDR* shown in **Figure 5.3b** is smaller for a higher value of *R*. This can be explained by referring to the *RDR* definition in **Equation 5-2**, where both the residual and the maximum displacements increase with *R*; however, since the RC column has re-centring characteristics the increment in the residual displacement will be lower than that in the maximum displacement, which results in a low *RDR* for high values of *R*. As can be seen from **Figure 5.3** when α = 0.3, the maximum displacement could increase up to 60% for *R* = 6 and up to 35% for *R* = 1.

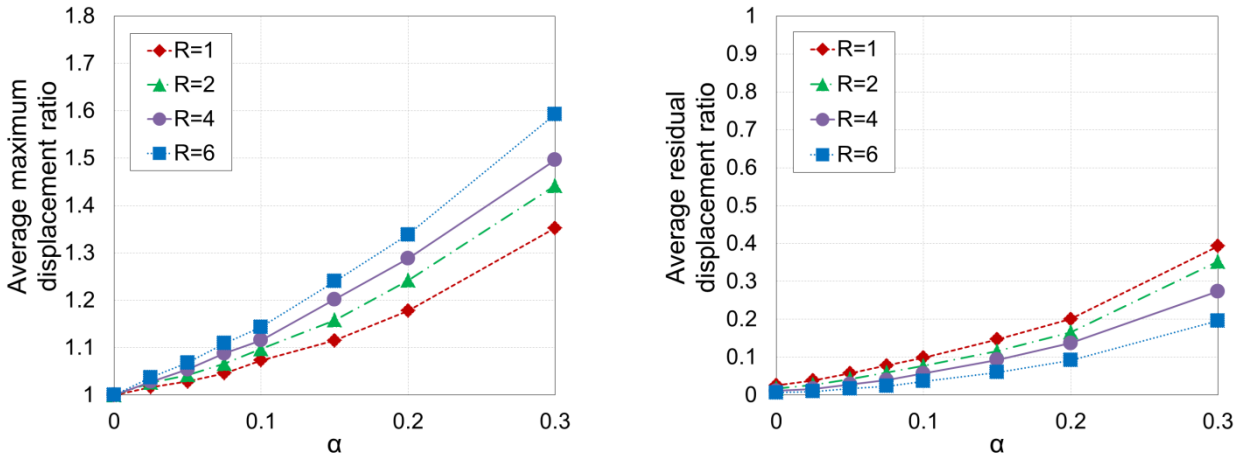

(a) Average maximum displacement ratio **(b) Average residual displacement ratio**

Figure 5.3: Effect of eccentric moments on displacement response with change in *R* (*T* = 1.0s and P/P_o = 0.1) for RC column

Figure 5.4 shows the effect of the eccentric moment on displacements for different axial load ratios, where the displacement demands increase with the increasing eccentric moment. This effect decreases with an increase in axial force. This is because the axial force enhances the re-centring capability of the column, resulting in reduced maximum and residual displacements. An example of this is shown in **Figure 5.5**, where the column subjected to P/P_o= 0.2, where $P_o=A_g f_c'$, exhibited re-centring characteristics, while the P/P_o= 0 case predominantly deformed in the positive direction. **Figure 5.4** also shows that the maximum and residual displacement ratios can increase from 1.45 to 1.68 and 0.2 to 0.9, respectively, as a result of P/P_o changing from 0.2 to 0.0 when α = 0.3.

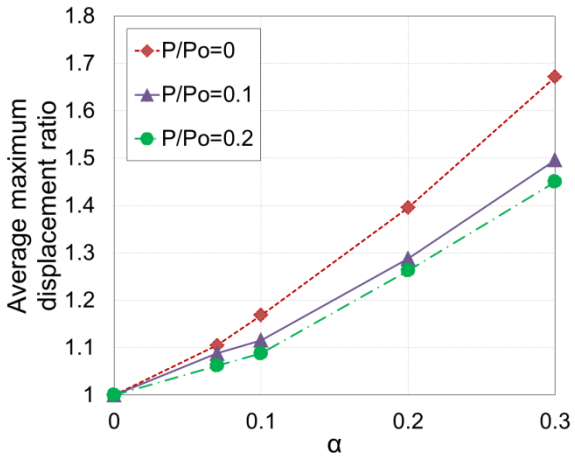

(a) Average maximum displacement ratio

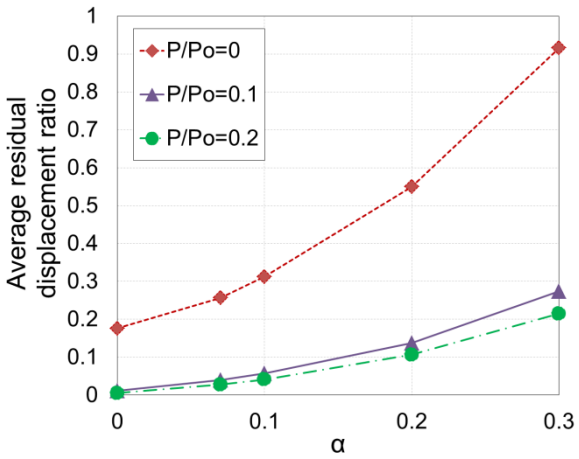

(b) Average residual displacement ratio

Figure 5.4: Effect of eccentric moments on displacement response with change in P/P_o (T = 1.0s and R = 4) for RC column

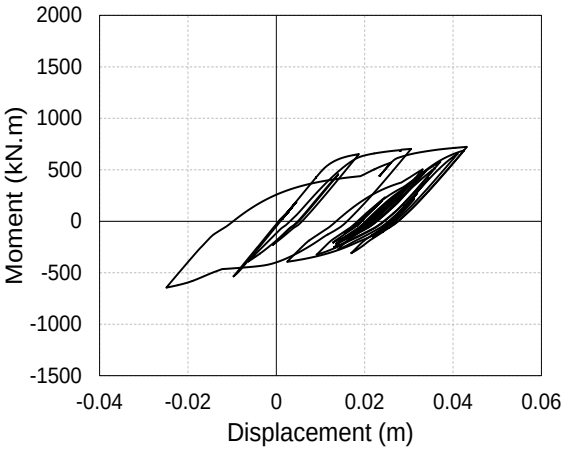

(a) Hysteresis loop for P/P_o = 0

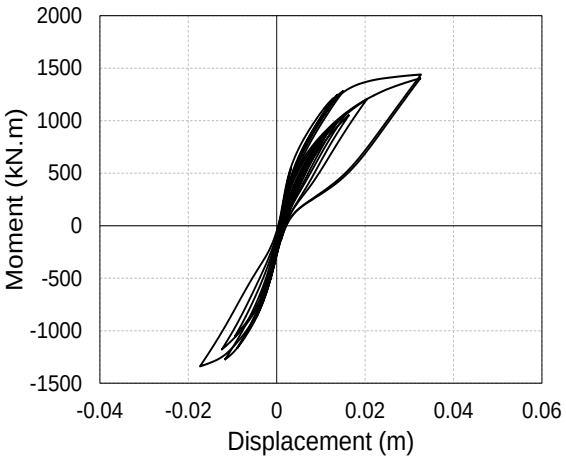

(b) Hysteresis loop for P/P_o = 0.2

Figure 5.5: Effect of axial loading on hysteretic re-centring characteristics (T = 1.0s, α = 0.2 & R = 4) for RC column

Figure 5.3 and **Figure 5.4** can be useful to estimate the maximum and residual displacements, for columns with eccentric moments that cause ratcheting, not considered by engineers when the displacement demands were calculated. For example, consider a column designed for P/P_o = 0.1 and R = 4 that has an estimated maximum displacement of 100 mm without considering the moment eccentricity. If α = 0.2, the corresponding maximum and residual displacement ratios are 1.3 and 0.15, respectively, according to **Figure 5.3**. Therefore, the expected maximum and residual displacement considering eccentricity will be approximately 130 mm and 15 mm, respectively.

5.2.2 Steel Cantilever Column

The same assessment performed for the RC column was also applied to a steel column, where 350WC with F_y = 300 MPa was used. **Figure 5.6** shows the displacement ratios for different values of *R*. The trend is the same as in the RC column, where the displacement demands increase with the eccentric moment, and the maximum displacements ratio is higher for higher *R* as the column becomes weaker and yields earlier. However, it can be noticed that the *RDR* increases with *R*. This can be explained by referring to the *RDR* definition in **Equation 5-2**, where both the residual and the maximum displacements increase with *R*, but since there are no re-centring characteristics in steel columns, the residual displacement is higher than the maximum displacement with no ratcheting (α = 0) which results in higher *RDR* with *R*. It can also be seen from the figure that both the *MDR* and the *RDR* of the steel column are much higher than that of the RC section. This is because of the re-centring characteristics of the RC column, which decrease the displacement demands and makes the column return to its initial position, which is not a property of steel columns.

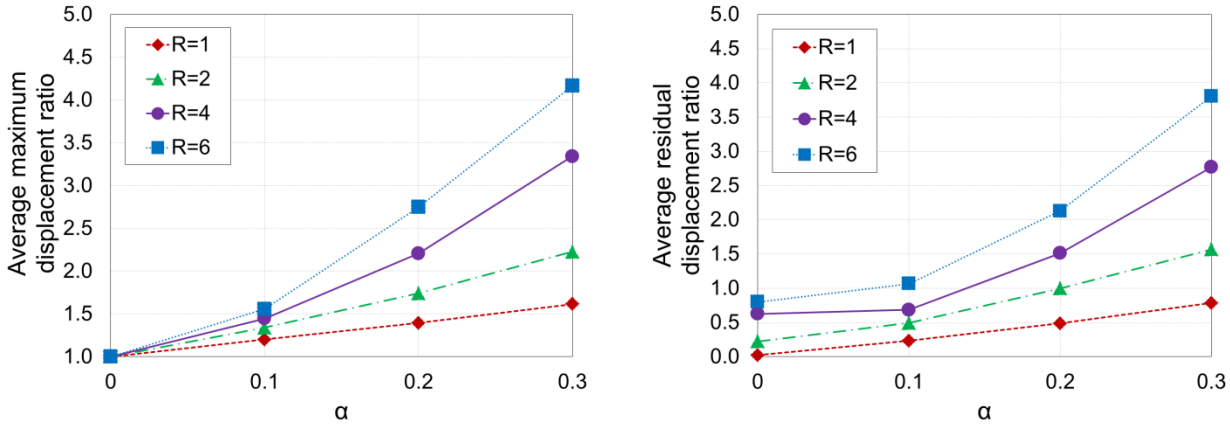

(a) Average maximum displacement ratio **(a) Average residual displacement ratio**

Figure 5.6: Effect of eccentric moments on displacement response with change in *R* (*T* = 1.0s and P/P_o = 0.1) for steel columns

The effect of the axial load ratio is shown in **Figure 5.7**. It can be seen that the displacement ratios increase with increasing α. Here, the displacement ratios for steel columns are higher than those in RC columns, as there is reduced re-centring in steel columns. Furthermore, unlike the concrete columns, the *MDR* and *RDR* increased with increasing axial load, which can be explained by the dynamic stability concept mentioned in the literature. This is shown in **Figure 5.8**, where the post-yield stiffness is negative when P/P_o = 0.2, for example. Therefore, an increased axial load on steel columns has a significant detrimental effect, unlike reinforced concrete columns where increasing the axial force may result in increased self-centring behaviour.

Figure 5.6 and **Figure 5.7** can be useful to estimate the maximum and residual displacements for steel columns with eccentric moments if the engineers did not consider ratcheting effects in calculating the displacement demands. The same procedure for the RC column can be followed.

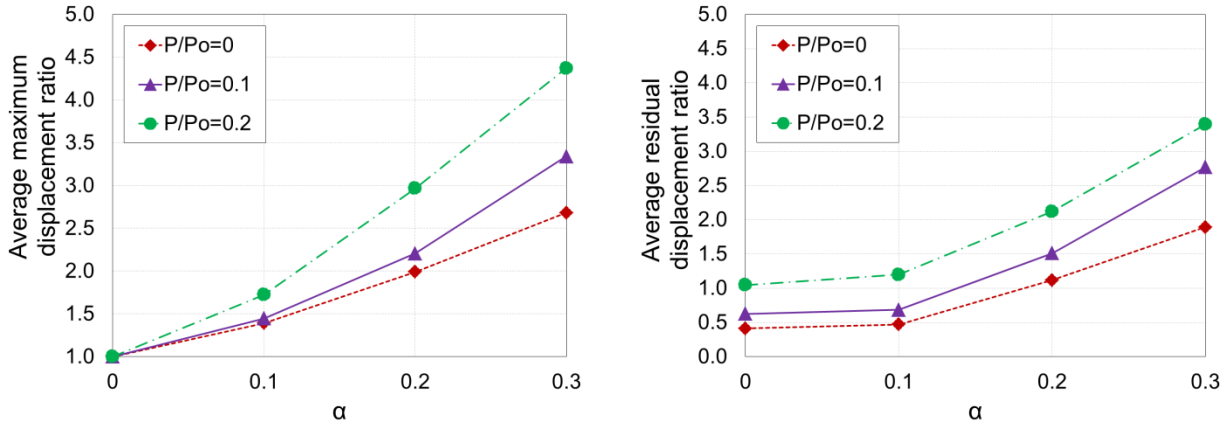

(a) Average maximum displacement ratio **(b) Average residual displacement ratio**

Figure 5.7: Effect of eccentric moments on displacement response with change in P/P_o (T = 1.0s and R = 4) for steel columns

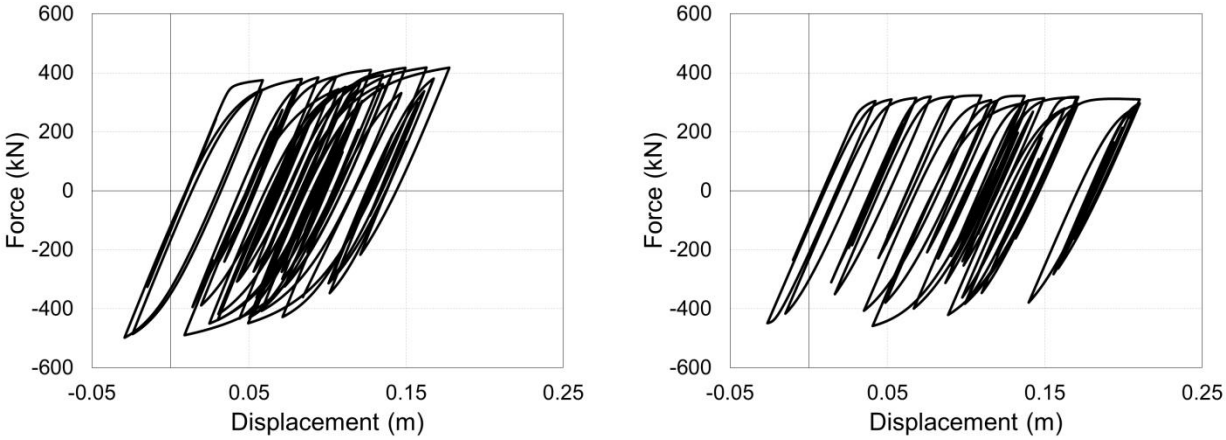

(a) Hysteresis loop for P/P_o = 0 **(b) Hysteresis loop for P/P_o = 0.2**

Figure 5.8: Effect of axial loading on hysteretic characteristics (T = 1.0s, α = 0.2 and R = 4) for steel column

5.3 Displacement Estimation and Optimal Design of C-Bent Columns

5.3.1 Estimation of Displacements and Optimal Strength Increment for C-Bent Piers

In this section, the analysis results will be presented in the form of graphs that can be used to estimate maximum and residual displacements of C-bent bridge piers with eccentric moment and different values of β. The graphs can also be used to indicate the optimal strength increment ratio, β_o. Only RC columns will be considered as it is hard to change the lateral strength for steel columns. Hysteresis loops for each case considered are shown in Section 9.1 in the appendices.

5.3.1.1 Effect of Axial Loading (P/P_o)

The effect of increasing the strength on one side of the column with different axial loads and with R = 4, α = 0.2 is shown in **Figure 5.9**. It can be seen that higher axial load ratios generally result in lower displacement ratios, as explained previously.

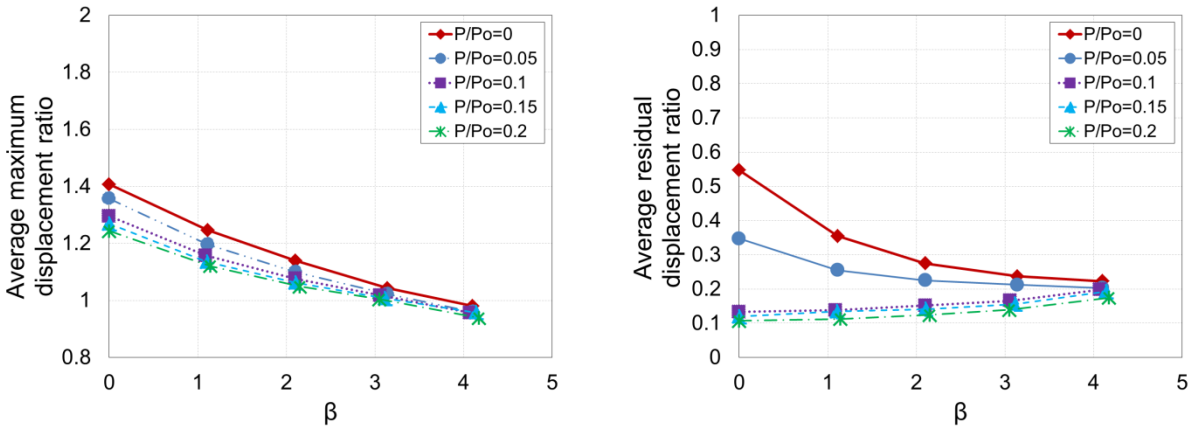

(a) Average maximum displacement ratio **(b) Average residual displacement ratio**

Figure 5.9: Displacements ratio for different values of axial load ratio P/P_o using fibre model and including P-delta effect (α = 0.2, R = 4, and T = 1.0s)

It can also be seen from **Figure 5.9a** that the *MDR* decreases with increasing β in the weak direction. However, that is not the case for the *RDR* as it increases with β for P/P_o > 0.05 but the trend is reversed when $P/P_o \leq 0.05$, as shown in **Figure 5.9b**. In the case where the column has a relatively high axial load, like the case where P/P_o > 0.05, the hysteresis loop will be flag-shaped with re-centring characteristics. When the reinforcement is balanced, that is, β=0, the residual displacement will be closer to the zero displacement, as shown in **Figure 5.10a**. However, when β is increased the re-centring effect is reduced as the added reinforcement increases the energy dissipation, and the hysteresis becomes larger, as shown in **Figure 5.10b**.

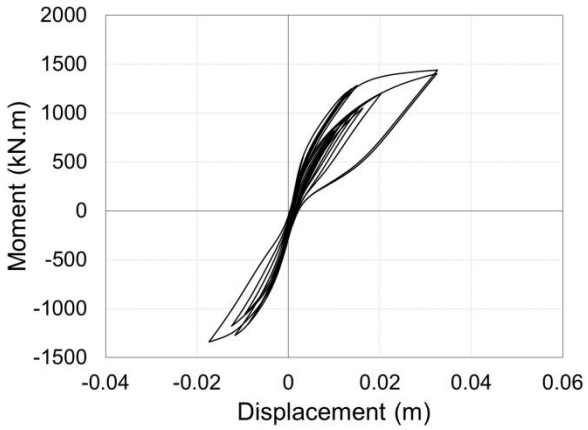

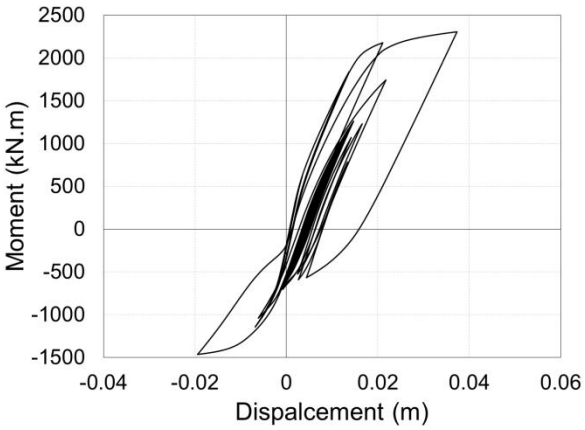

(a) Hysteresis loop for P/P_o = 0.2 and β = 0 **(b) Hysteresis loop for P/P_o = 0.2 and β = 3**

Figure 5.10: Increasing β effect on systems with re-centring characteristics (T = 1.0s, α = 0.2 & R = 4) for RC column

In the case where the column has relatively low axial load, like the case where $P/P_o \leq 0.05$, the residual displacement decreases with increasing β. This can be explained using the energy method. Consider a balanced column that has experienced an earthquake event and reached point "A" as shown in **Figure 5.11a**. The potential energy at point A is lower than the energy required to yield in the negative direction. Therefore, the column will most likely yield in the positive direction, increasing the residual displacement. However, when increasing β, the energy required to yield in the negative direction becomes less than that in the positive direction, as shown in **Figure 5.11b**. Therefore, the column will most likely yield in the negative direction towards zero displacement position, which reduces the residual displacement.

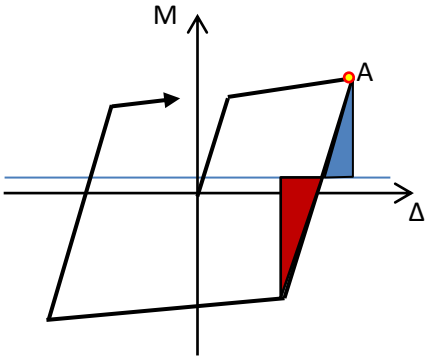

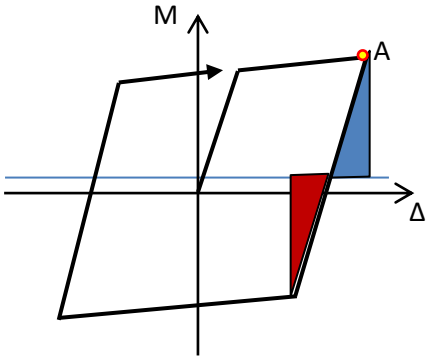

(a) Balance reinforcement **(b) Increasing the reinforcement in the positive direction**

Figure 5.11: Increasing β in systems with no re-centring characteristics

Optimal strength increment ratio, β_o, can be defined as the strength increment ratio at which no ratcheting in maximum displacement will occur. In **Figure 5.9**, β_o is that value where the lines cross the MDR = 1.0 value, which means the maximum displacement obtained is equal to that when β = 0 and α = 0 (i.e., no ratcheting in maximum displacement). However, if more reinforcement is added, that is, $\beta > \beta_o$, ratcheting

will occur in the opposite direction. In this case, β_o = 3.5 for axial load ratio $P/P_o > 0$, and β_o = 3.8 for $P/P_o = 0$. However, since the axial load is usually there and not equal to zero, then β_o = 3.5 will be considered.

Effect of Eccentric Moment (α)Figure **5.12** shows displacements ratios, *MDR* and *RDR*, with different eccentric moment ratio, α, with P/P_o = 0.1 and R = 4. It can be seen from **Figure 5.12a** that *MDR* decreases with β as more reinforcement is added to the weak side. In contrast, the *RDR* increases with β, as shown in **Figure 5.12b,** because the hysteresis loop of the column becomes larger by increasing the number of reinforcing bars, which is consistent with **Figure 5.9b** for P/P_o = 0.1. The figure also shows that the displacement ratio is higher for larger α due to ratcheting. This can be explained by **Figure 5.13** where it can be seen that if the eccentric moment increases, the difference between the lateral strength in each direction increases, making the column more prone to yield predominantly in one direction than the other, causing more ratcheting. The optimal strength increment ratio, β_o, can be obtained from **Figure 5.12** and it was found to be β_o = 3.3.

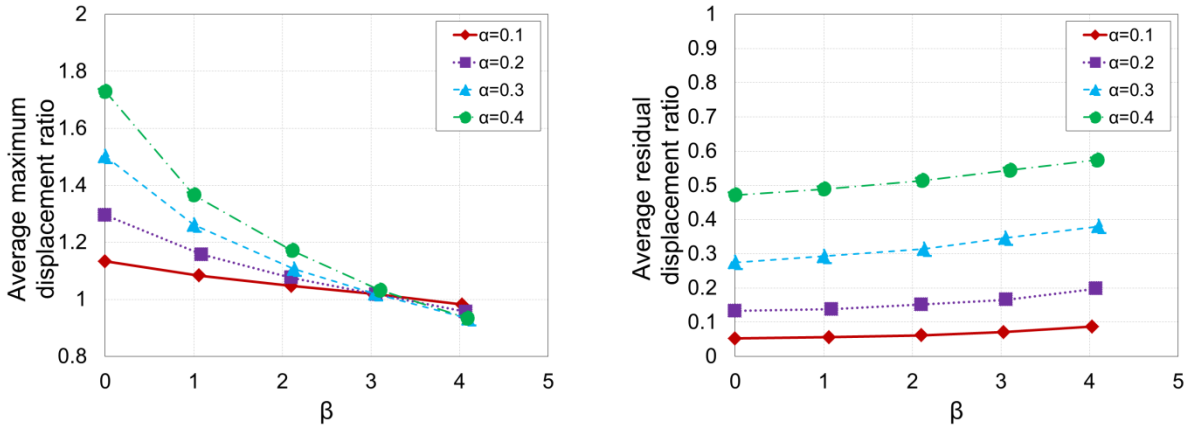

(a) Average maximum displacement ratio **(b) Average residual displacement ratio**

Figure 5.12: Displacements ratio for different values of eccentric moment, α using fibre model and including P-delta effect (P/P_o = 0.1, R = 4, and T = 1.0s)

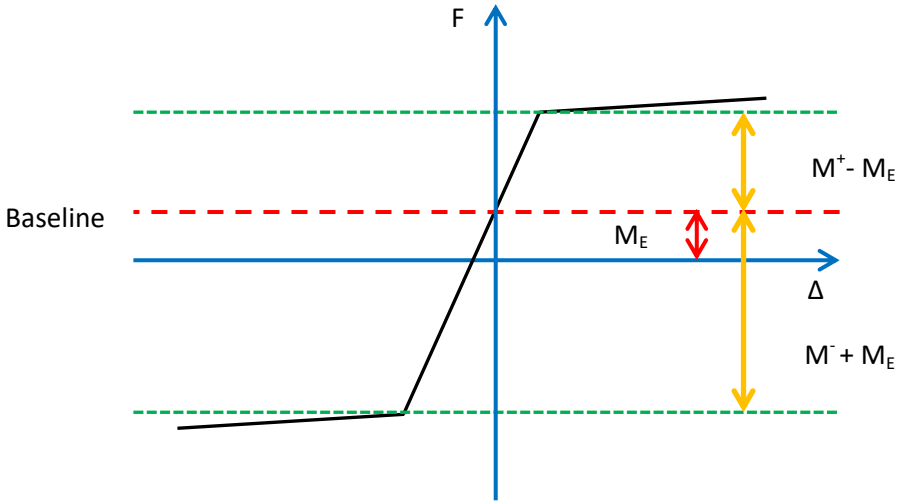

Figure 5.13: Eccentric loading effect on moment capacities

Effect of Force Reduction Factor (*R)*Figure **5.14** shows the effect of the force reduction factor, *R*, on the ratios *MDR* and *RDR* , where the general trend of the graph is similar to that obtained by varying the eccentric load ratio, where the *MDR* decreases with β, while the *RDR* increases except for the case where *R* = 1. That is because, although the column just reaches the yielding point when *R* = 1, there is an eccentric moment acting on the column at β = 0 which makes it yield and has a residual displacement. This eccentric moment, however, is balanced by increasing β, and therefore *MDR* tends towards 1.0 and *RDR* drops to zero. It also shows that a higher *R* will result in higher displacement demands; that is because the columns get weaker and yield at an earlier stage, which increases the displacements demands. The optimal strength increment ratio was found from the graph to be around β_o = 3.5.

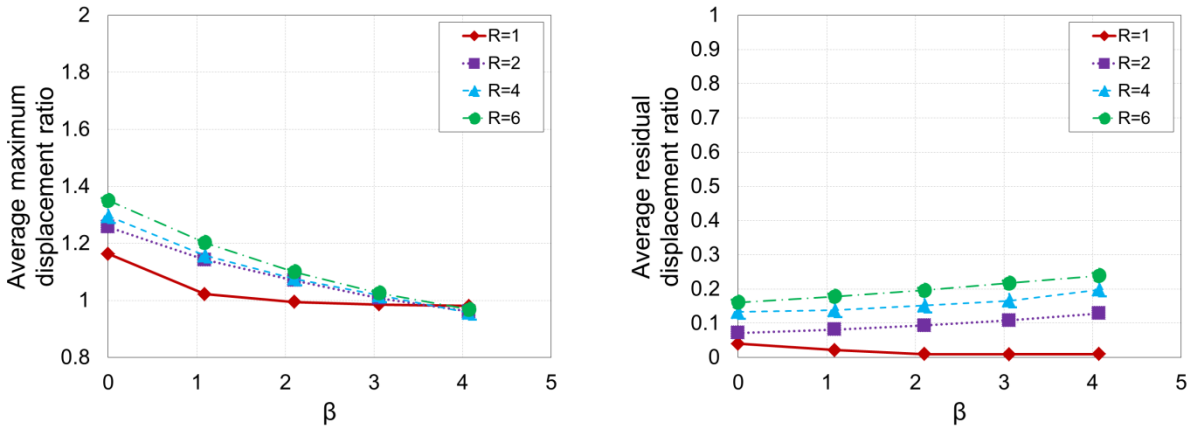

(a) Average maximum displacement ratio **(b) Average residual displacement ratio**

Figure 5.14: Displacements ratio for different force reduction factor, *R* using fibre model and including P-delta effect (*P/P*$_o$ = 0.1, *α* = 0.2, and *T* = 1.0s)

5.3.1.2 Effect of Period (*T*)

Columns with different structural period, *T*, were considered and the results are shown in **Figure 5.15**. The results also showed a similar trend to before, where the *MDR* decreases with β, while the *RDR* increases. However, it was noticed that the results were almost the same and varied by less than 5% for different values of *T*, and therefore, it can be concluded that the structural period does not have a great effect on the RC bridge pier considered. It can be seen that all lines pass the value of 1.0 at β_o = 3.4 which is considered to be the optimal strength increment ratio.

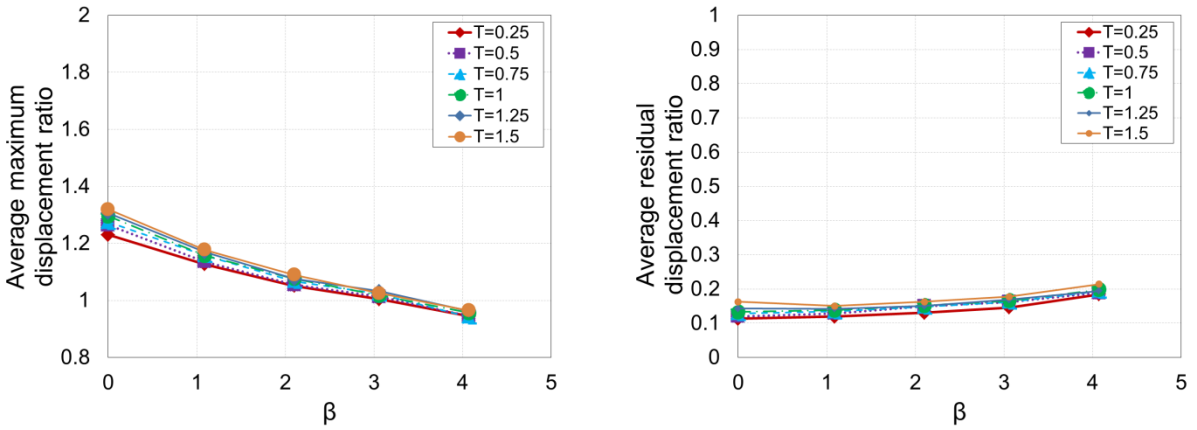

(a) Average maximum displacement ratio **(b) Average residual displacement ratio**

Figure 5.15: Displacements ratio for different values or period, *T* using fibre model and including P-delta effect (α = 0.2, P/P_o = 0.1, and R = 4)

5.3.2 Seismic Response of Full Scale RC Bridge Pier

In order to validate the results obtained using the scaled column, another full-scale column was used. The column is shown in **Figure 5.16** and was a design used by Kawashima et al. (2010). The Japanese Road Association design code (JRA, 2002) was used to design the pier. The properties and parameters used in this column were the same as those used in the main model, and the column was modelled as a cantilever column with a moment applied at the top. Fibre section was used, P-delta effect was considered, and the force reduction factor effect was investigated.

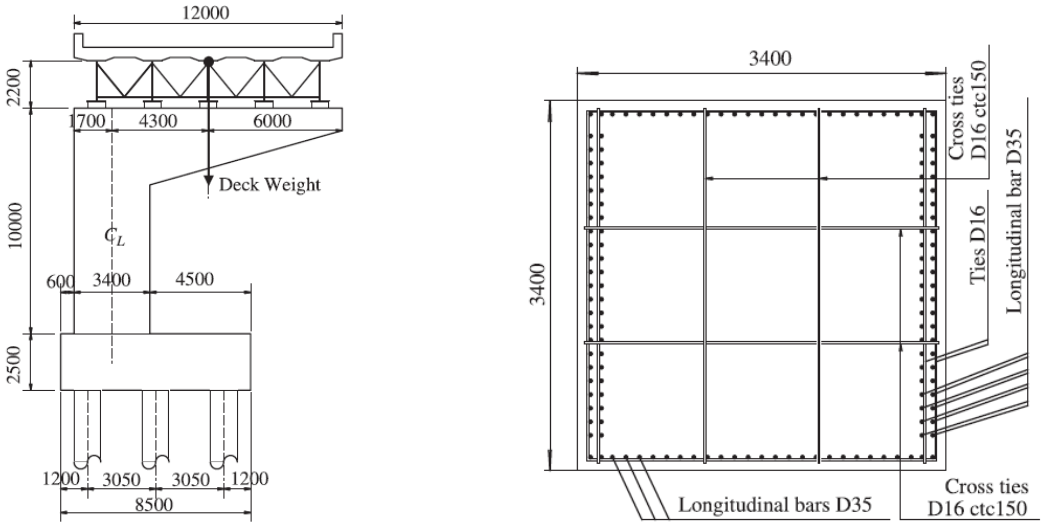

(a) The column's elevation **(b) The column's cross section**

Figure 5.16: Full scale C-bent bridge pier model (Kawashima at al., 2010)

The analysis results are shown in **Figure 5.17**. It can be seen that the results are almost identical to those obtained using the scaled model in **Figure 5.14** although the results of the full-scale model are slightly lower.

This increases the confidence in the results obtained using the scaled model, and indicates that the results in this research may be representative of different sizes of C-bent piers.

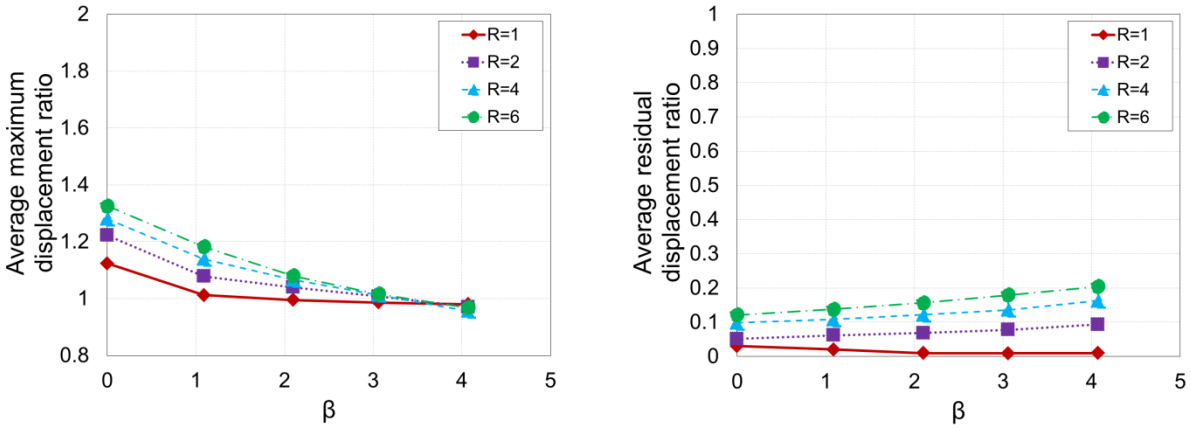

(a) Average maximum displacement ratio **(b) Average residual displacement ratio**

Figure 5.17: Displacements ratio for different force reduction factors, *R*, using a full-scale pier (α = 0.2, P/P_o = 0.1, and *T* = 1.0s)

5.3.3 Examples

The previous graphs can be used to estimate the maximum and residual displacements of C-bent piers to account for seismic ratcheting. For example, consider a C-bent pier with R = 4, α = 0.4, P/P_o= 0.1, and T = 1.0s, which has a maximum displacement of 200 mm, calculated using static analysis and balanced reinforcing on both sides of the column. From **Figure 5.12**, *MDR* = 1.73 and the *RDR* = 0.47. Therefore, the expected maximum displacement when ratcheting is considered is 346 mm (= 1.73 x 200 mm) and the expected residual displacement is 94 mm (= 0.47 x 200 mm). Thus, since this column was not designed using the optimal strength increment ratio, it has a maximum displacement 73% larger than expected and the residual displacement can be almost half of the expected maximum displacement calculated using static analysis and balance reinforcing.

To illustrate how the graphs can be used for a different combination of parameters not previously reported in this chapter, consider a similar column to that examined previously, except that it has been designed for R = 6 instead of R = 4. From **Figure 5.14**, it can be seen that for α = 0.2, P/P_o = 0.1, and T = 1.0, *MDR* is 1.25 and 1.28 for R = 4 and 6, respectively, and that *RDR* is 0.15 and 0.18, respectively. This means that the maximum and residual displacements for R = 6 would be 1.02 (1.28/1.25) and 1.2 (0.18/0.15) times greater than that for R = 4, respectively. Therefore, the resulting maximum and residual displacements in this case are 353 mm and 113 mm, respectively.

Practicality to Balance Ratcheting **Figure 5.18** shows the amount of reinforcement needed to achieve the optimal strength increment ratio, β_o, for different eccentric moment ratios, α. To indicate whether it is practical to reach β_o, the following guidelines were used:

- The reinforcement ratio, ρ, where the maximum reinforcement ratio should not exceed 8% (NZS3101:10.3.8.1, 2006).
- Minimum spacing of reinforcement, where the clear spacing between bars, S, should be $S >$ max (4mm, 1.5 d_b) where d_b is the bar diameter (NZS3101:8.3.7, 2006).

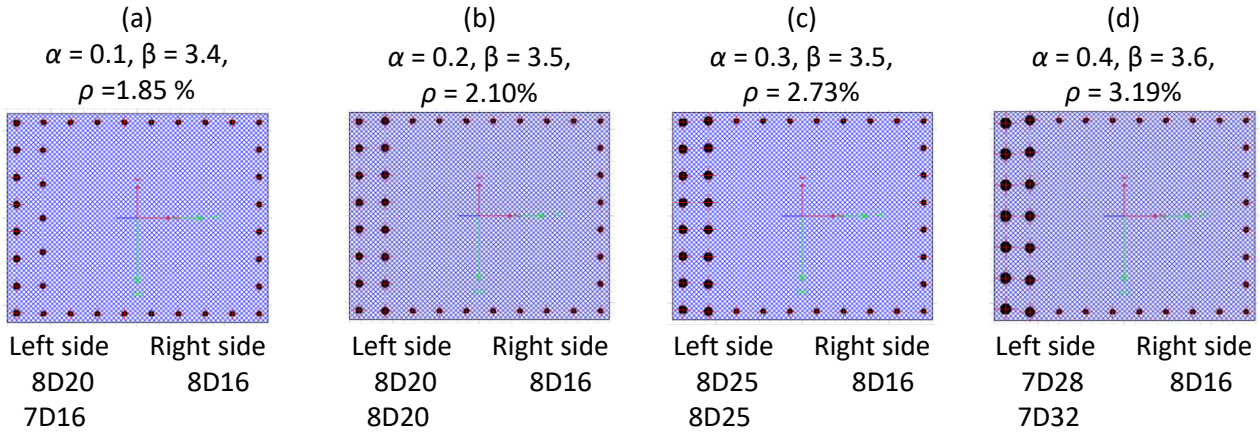

Figure 5.18: Graphical representation for the number of reinforcing bars that are needed to achieve different values of the optimal strength increment ratio, β_o

All the reinforcement arrangements in **Figure 5.18** satisfied the criteria mentioned earlier. Therefore, it was found that it is practical to obtain the optimal strength increment ratio, β_o, which was found to be less than 4.0 as mentioned in the previous section. It should be noted that this assessment is from the viewpoint of practicality, and that financial feasibility is not considered at this stage. However, it is the view of the author that while the material cost of the reinforcing will increase, other construction costs should be relatively similar due to the consistent layout adopted. Furthermore, the maximum displacement demands may decrease by up to 43% by designing for a more optimal column, and hence would have greater longevity. The cost-benefit assessment regarding the value proposition of designing and constructing these columns should be examined in future studies.

5.4 Simple Approach to Account for Ratcheting

A more simple approach to estimate the displacement demands is proposed in this section, which is based on empirical equations. All curves were assumed to be linear for simplicity, and linear best-fit lines were plotted on each graph. The equation for each linear line was determined and is noted beside each case. Using these equations, a general formula is presented to estimate *MDR* and *RDR* for each parameter considered. These formulas can be used for columns with no reinforcement change, that is, β = 0, and they can also be used when more reinforcement is added to the tension side of the column, when β > 0. **Figure 5.19** shows the equations for different values of α. Using the equations mentioned on the figure, the following formulas are derived:

$$\begin{aligned} MDR &= A\beta + C \\ A &= -0.67\alpha + 0.027 \\ C &= 2\alpha + 0.94 \end{aligned} \tag{5-3}$$

$$\begin{aligned} RDR &= D\beta + E \\ D &= 0.06\alpha \\ E &= 1.4\alpha - 0.09 \end{aligned} \tag{5-4}$$

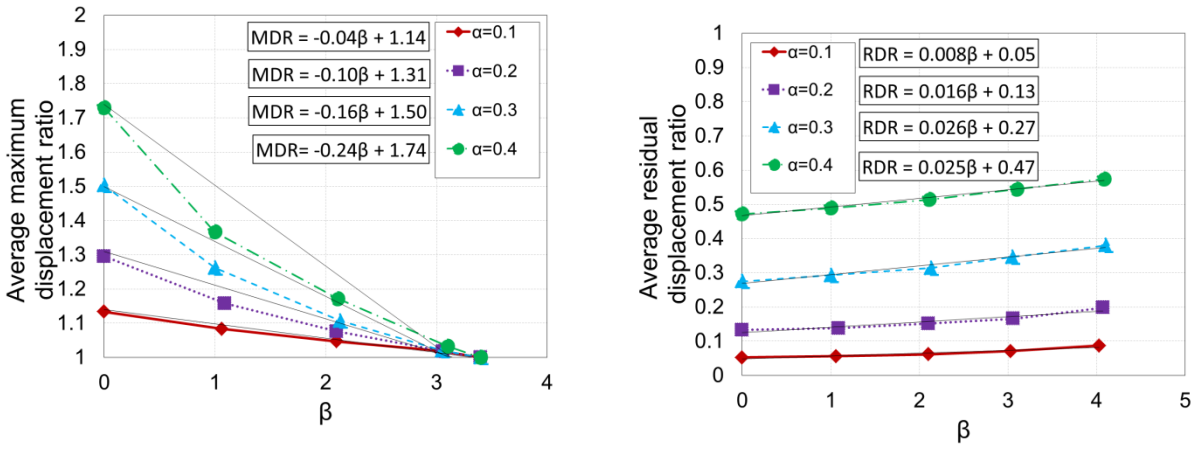

(a) Average maximum displacement ratio **(b) Average residual displacement ratio**

Figure 5.19: Equations for estimating *MDR* and *RDR* for different values of α using fibre model and including P-delta effect (P/P_o = 0.1, *R* = 4, and *T* = 1.0s)

Figure 5.20 shows the equations for different values of P/P_o. It can be seen from **Figure 5.20b** that the trend for $P/P_o \leq 0.05$ is different from that of $P/P_o > 0.05$. Therefore, two cases were considered for the calculation of *RDR*. Using the equations mentioned on the figure, the following formulas are derived:

$$\begin{aligned} MDR &= A\beta + C \\ A &= 0.25\frac{P}{P_o} - 0.13 \\ C &= 0.9\frac{P}{P_o} + 1.24 \end{aligned} \tag{5-5}$$

$$RDR = D\beta + E$$
$$\text{For}\frac{P}{P_o} \leq 0.05:\ D = 1.06\frac{P}{P_o} - 0.1$$
$$\text{and}\ E = -4.0\frac{P}{P_o} + 0.56$$
$$\text{For}\frac{P}{P_o} > 0.05:\ D = 0.04\frac{P}{P_o} + 0.004 \quad (5\text{-}6)$$
$$\text{and}\ E = -0.3\frac{P}{P_o} + 0.17$$

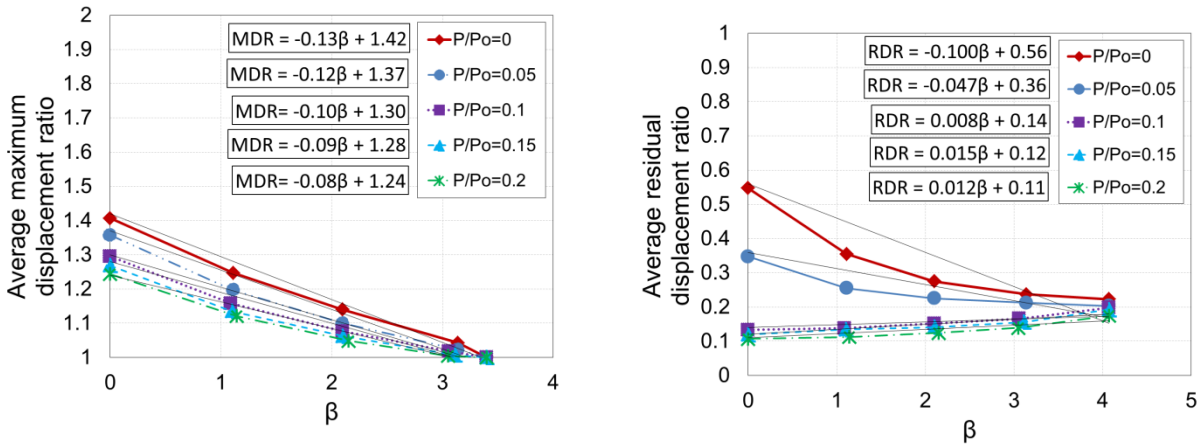

(a) Average maximum displacement ratio **(b) Average residual displacement ratio**

Figure 5.20: Equations for estimating *MDR* and *RDR* for different values of P/P_o using fibre model and including P-delta effect (α = 0.2, *R* = 4, and *T* = 1.0s)

Figure 5.21 shows the equations for different values of *R*. Constant values were given to the case when *R* = 1 as the eccentric moment is balanced at β = 1, and for β > 1 there will be no ratcheting in the maximum displacement and the column will be elastic, that is, with no residual displacement. Using the equations mentioned on the figure, the following formulas are derived:

$$MDR = 1.16 \text{ for } R = 1 \text{ and } \beta = 0$$
$$MDR = 1 \text{ for } R = 1 \text{ and } \beta > 0$$
$$MDR = A\beta + C \quad R > 1 \quad (5\text{-}7)$$
$$A = -0.01R - 0.06$$
$$C = 0.03R + 1.21$$

$$RDR = 0.04 \text{ for } R = 1 \text{ and } \beta = 0$$
$$RDR = 0 \text{ for } R = 1 \text{ and } \beta > 0$$
$$RDR = D\beta + E \quad R > 1 \quad (5\text{-}8)$$
$$D = 0.001R + 0.012$$
$$E = 0.023R + 0.025$$

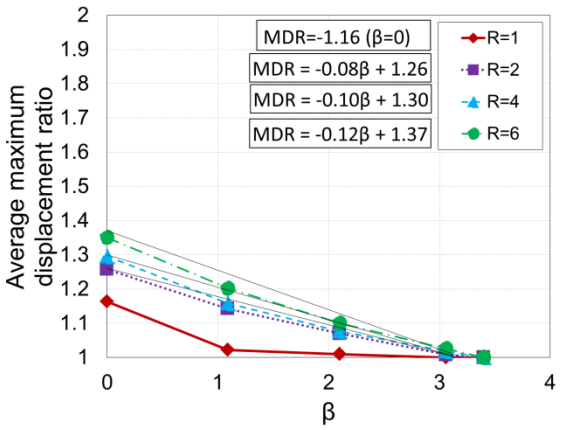

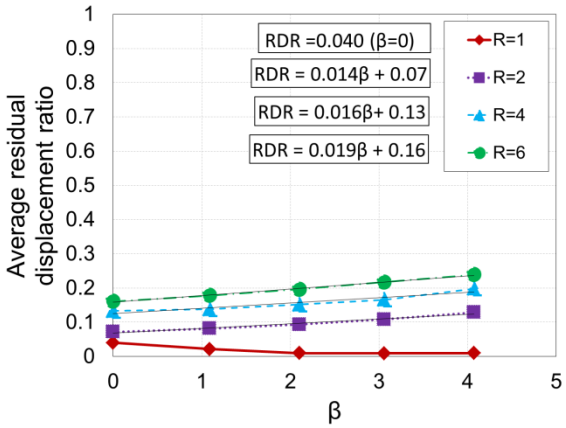

(a) Average maximum displacement ratio **(b) Average residual displacement ratio**

Figure 5.21: Equations for estimating *MDR* and *RDR* for different values of *R* using fibre model and including P-delta effect (α = 0.2, P/P_o = 0.1, and *T* = 1.0s)

Figure 5.22 shows the equations for different values of *T*. As the curves are close to each other, one equation was presented which represent the conservative case. Using the equations mentioned on the figure, the following formulas are derived:

$$MDR = -0.1\beta + 1.32 \quad (5\text{-}9)$$

$$RDR = 0.009\beta + 0.16 \quad (5\text{-}10)$$

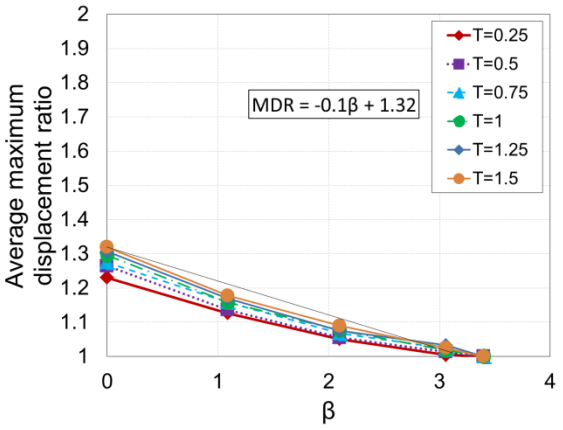

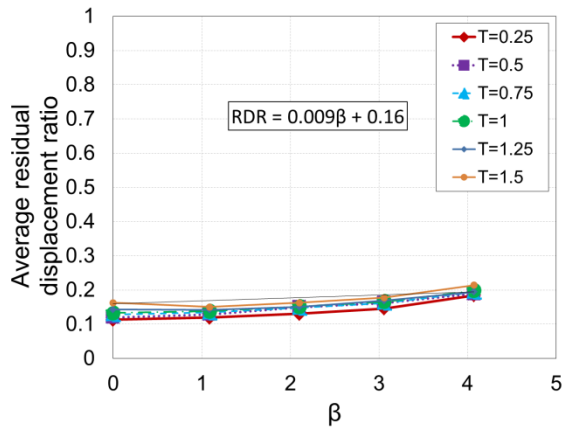

(a) Average maximum displacement ratio **(b) Average residual displacement**

Figure 5.22: Equations for estimating *MDR* and *RDR* for different values of *T* using fibre model and including P-delta effect (α = 0.2, P/P_o = 0.1, and *R* = 4)

5.5 Conclusions

Dynamic inelastic time history analyses for reinforced concrete C-bent bridge pier were conducted. The key conclusions are:

1. Strength and the stiffness are related and the fibre model was able to capture this relationship.
2. Graphs to estimate maximum and residual displacements to account for ratcheting when β = 0 for both reinforced concrete and steel columns were provided along with examples to demonstrate their use.
3. Steel structures are more sensitive to ratcheting than reinforced concrete structures, as they have less re-centring characteristics.
4. The strength increment, β, to mitigate ratcheting in maximum displacement was found to be approximately 3.4 M_E and was not sensitive to α, P/P_o, R, or T.
5. Using the column's maximum reinforcement ratio and specifications for spacing of reinforcing bar in the New Zealand Standards (NZS3101, 2006), it was found that it may be practical to balance ratcheting in C-bent bridge piers.

6. DEVELOPMENT OF DESIGN AND ASSESSMENT TOOLS

6.1 Chapter Summary

This chapter evaluates alternative methods to quantify the strength increase required to mitigate ratcheting in maximum displacement. Of the approaches examined, it was found that the method of equalizing the secant period to first yield in each direction relative to the static position, and the method which was based on equalizing the potential energy to peak displacements, gave the best results. A design approach that is simple and easy to follow is proposed, and an example demonstrating its use is provided.

6.2 Evaluations of Hypothetical Approaches

The energy concept was used by Yeow et al. (2013) and Abdolahirad et al. (2017) to explain the dynamic behaviour of structures which yield in one direction over another. They found that the structure tends to yield in the direction which needs less energy. Using the same concept, five methods will be evaluated:

1) Equalizing potential energy under secant stiffness to point of first yield
2) Equalizing potential energy under hysteretic curve to point of first yield
3) Equalizing potential energy to peak displacements
4) Equalizing the ratio of potential energy at peak displacement to energy required to yield in reverse direction
5) Equalizing the ratio of periods using secant stiffness to first yield relative to initial static conditions.

For the first four methods, It was assumed that when the energy ratio, which is the energy needed to yield in one direction divided by the one needed to yield in the opposite direction, is equal to 1.0, then no ratcheting in peak displacement would occur. The energy and period ratios were changed by increasing the reinforcement in the weak direction, until these ratios were equal to 1.0. After that, the results which were obtained using the nonlinear time history analysis were used to evaluate if the assumption was correct or not. The detailed results can be found in Section 9.2 in the appendices.

6.2.1 Method 1: Equalizing Potential Energy under Secant Stiffness to Point of First Yield

In this method, the energy was approximated as the area under the line measured from the origin, considering eccentric moment, until the first yielding point, as shown in **Figure 6.1**. The area in the positive direction marked as “A1” and the area in the negative direction, marked as “A2”, was obtained by calculating the area of the two triangles, as shown by **Equation 6-1**. It was hypothesized that when the energy ratio is equal to 1.0 then no ratcheting in peak displacement will occur.

$$\text{Method 1 energy ratio} = \frac{A_1}{A_2} \quad \text{(6-1)}$$

The *MDR* values that were obtained by the nonlinear time history analysis described in the previous chapter were used here. Since the maximum displacements were normalized to the maximum displacements when the column has equal strength in both directions and with no eccentric moment effect, no ratcheting in maximum displacement will occur when the *MDR* equals 1.0. The results are plotted in **Figure 6.2**. Generally, it can be seen from the figure that the *MDR* decreases when the area ratio decreases. This is because more reinforcement is added to the weak side of the pier, which reduces the maximum displacement. The figure also shows that when the *MDR* is equal to 1.0, the area ratio will be around 0.5 for the different parameters that were considered except for α = 0.1 where the *MDR* is about 0.8. This means that no ratcheting will occur when the energy ratio is equal to 0.5. Therefore, this method can be used to mitigate ratcheting.

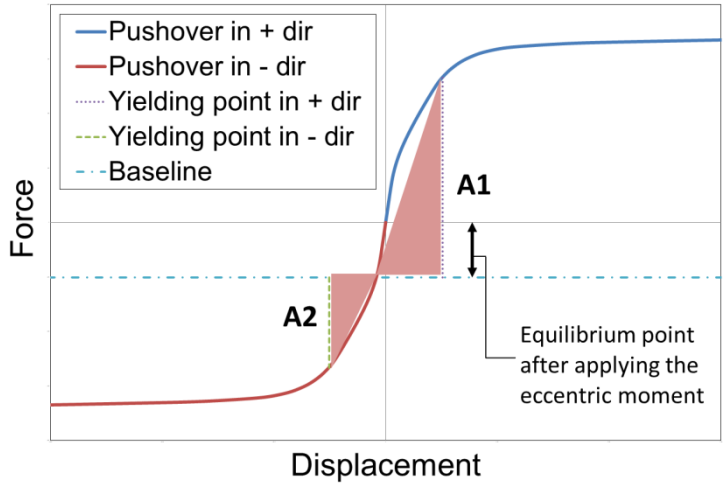

Figure 6.1: Method 1: Equalizing potential energy under secant stiffness to point of first yield

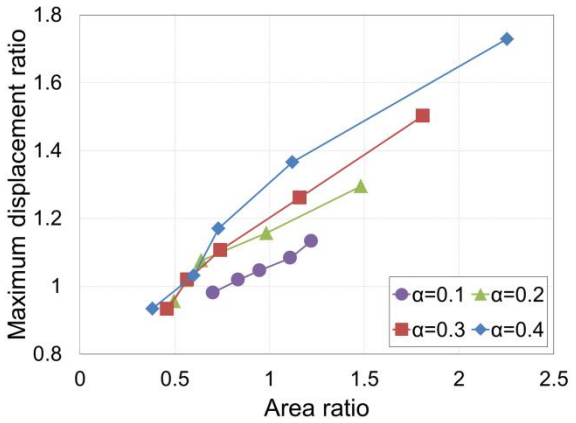

(a) Average maximum displacement ratio for different values of eccentric moment ratio, α (P/P_o = 0.1, R = 4, and T = 1.0s)

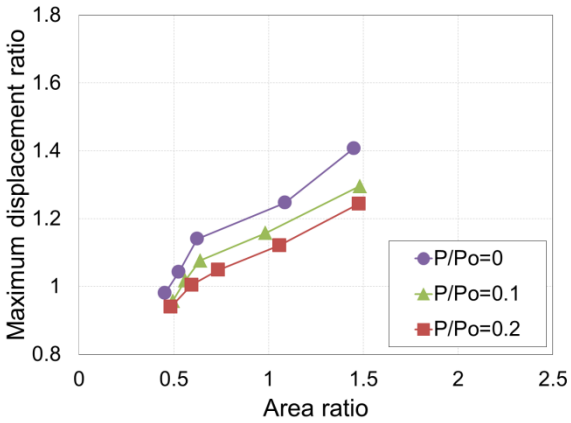

(b) Average maximum displacement ratio for different values of axial load ratio, P/P_o (α = 0.2, R = 4, and T = 1.0s)

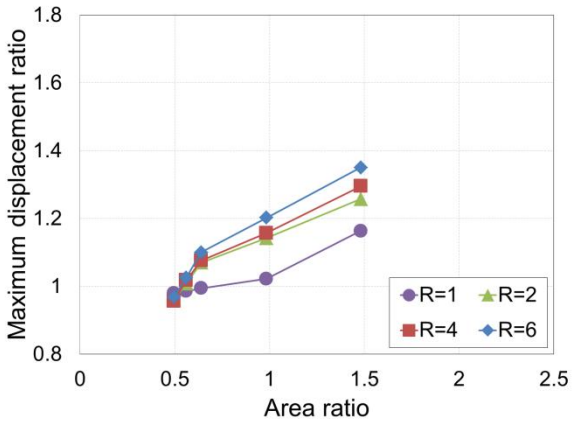

(c) Average maximum displacement ratio for different values of force reduction factor, R (P/P_o = 0.1, α = 0.2, and T = 1.0s)

Figure 6.2: Dynamic response for C-bent bridge pier with different parameters using method 1

6.2.2 Method 2: Equalizing Potential Energy under Hysteretic Curve to Point of First Yield

In this method no linearization of the energy considered, where the total area under the curve, measured from point of origin to the first yielding point, was calculated taking the curvature into consideration, as shown in **Figure 6.3**. The energy needed to yield in the positive direction was marked as "B1" while the energy needed to yield in the negative direction was marked as "B2" and then the ratio was calculated using **Equation 6-2**. It was assumed that when B1/B2 is equal to 1.0 then no ratcheting in the maximum displacement will occur. The results are shown in **Figure 6.4**. It can be seen from **Figure 6.4a** that *MDR* is equal to 1.0 when the area ratio ranges between 0.6 and 0.9. However, for different P/P_o and R the area ratio is about 0.75, as can be seen from **Figure 6.4b** and **c**. As the optimal ratio which mitigates ratcheting is not unique but is scattered among several values, this method was not considered as an accurate method to mitigate ratcheting.

$$\text{Method 2 energy ratio} = \frac{B_1}{B_2} \qquad (6\text{-}2)$$

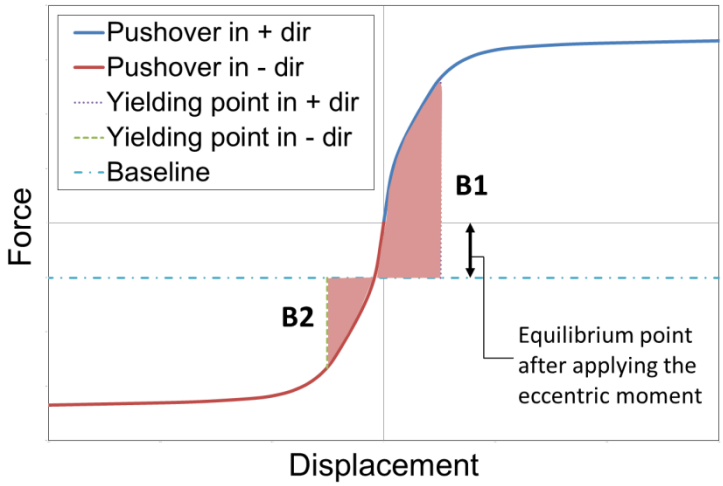

Figure 6.3: Equalizing potential energy under hysteretic curve to point of first yield

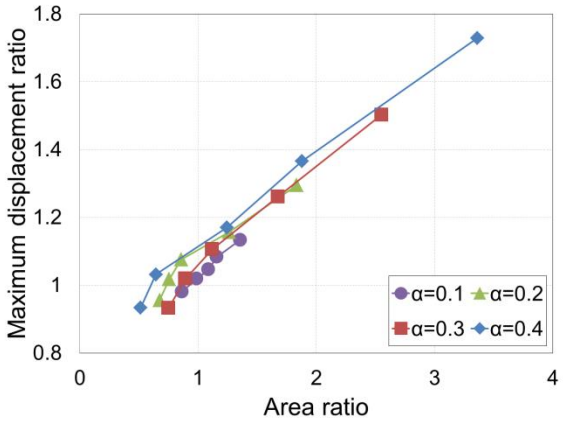

(a) Average maximum displacement ratio for different values of eccentric moment ratio, α (P/P_o = 0.1, R = 4, and T = 1.0s)

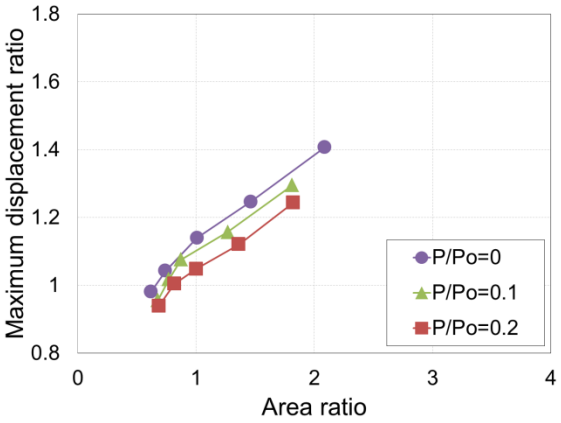

(b) Average maximum displacement ratio for different values of axial load ratio, P/P_o (α = 0.2, R = 4, and T = 1.0s)

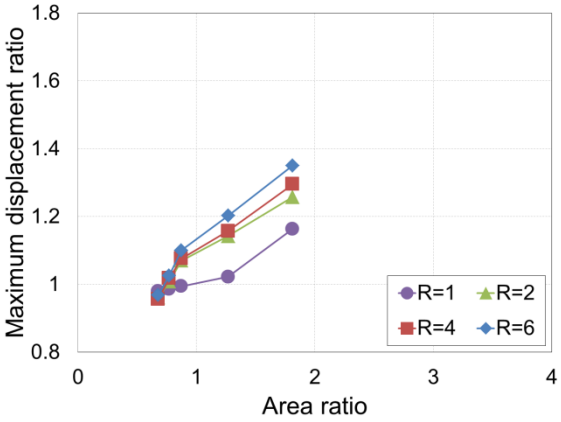

(c) Average maximum displacement ratio for different values of force reduction factor, R (P/P_o = 0.1, α = 0.2, and T = 1.0s)

Figure 6.4: Dynamic response for C-bent bridge pier with different parameters using method 2

6.2.3 Method 3: Equalizing Potential Energy to Peak Displacements

The total positive and negative area under the curve was calculated in this method, as shown in **Figure 6.5**. The energy under the curve in the positive direction was marked as "C1" while the energy under the curve in the negative direction was marked as "C2", then the ratio was calculated using **Equation 6-3**. The results are shown in **Figure 6.6**. The figure shows that the *MDR* is equal to 1.0 when the area ratio is equal to 1.0 when changing α and R, as shown in **Figure 6.6a** and **b**, respectively, while it is around 1.1 for P/P_o = 0.1 and 0.2, and around 0.9 when P/P_o = 0.0 as shown in **Figure 6.6b**. So far, this method provides the most accurate results, because when the energy ratio equal to 1.0, the *MDR* is equal to 1.0, as assumed before. Therefore, this method can be used as an alternative method to mitigate ratcheting.

$$\text{Method 3 energy ratio} = \frac{C_1}{C_2} \tag{6-3}$$

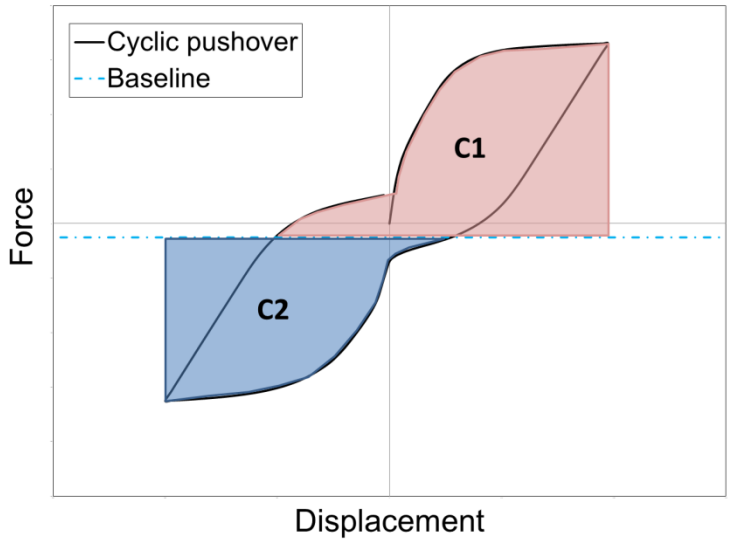

Figure 6.5: Equalizing potential energy to peak displacements

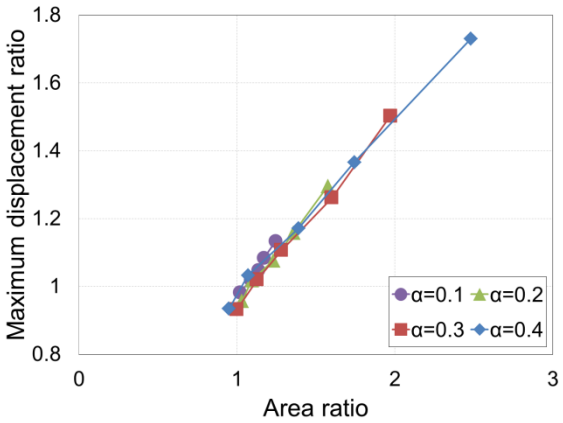

(a) Average maximum displacement ratio for different values of eccentric moment ratio, α (P/P_o = 0.1, R = 4, and T = 1.0s)

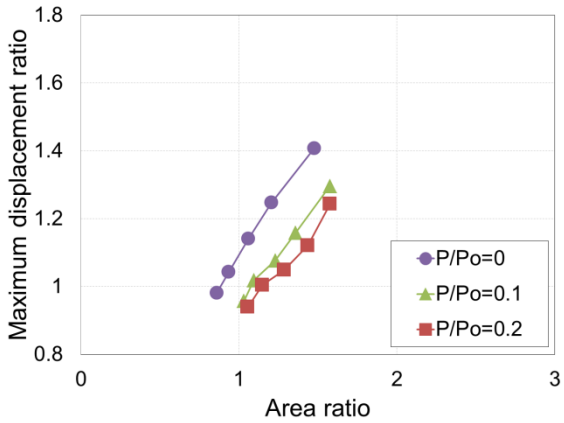

(b) Average maximum displacement ratio for different values of axial load ratio, P/P_o (α = 0.2, R = 4, and T = 1.0s)

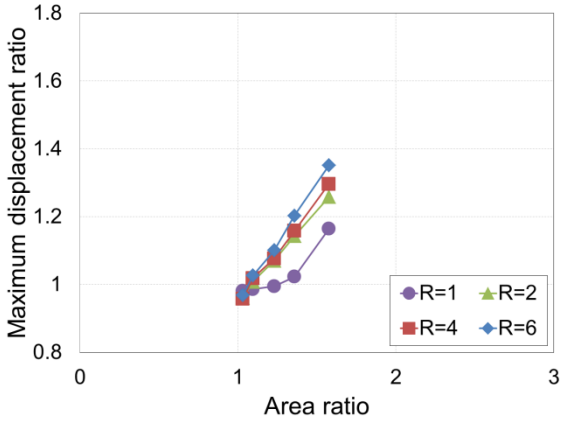

(c) Average maximum displacement ratio for different values of force reduction factor, R (P/P_o = 0.1, α = 0.2, and T = 1.0s)

Figure 6.6: Dynamic response for C-bent bridge pier with different parameters using method 3

6.2.4 Method 4: Equalizing Ratio of Potential Energy at Peak Displacement to Energy Required to Yield in Reverse Direction

In this method, the energy needed to unload the column in the positive direction, U1, was determined and then the distance in the opposite direction that the column will move to dissipate U1 was determined and marked as X1. The same was calculated for the opposite direction, where the unloading energy in the negative direction was marked as U2 and the distance required to dissipate it was marked as X2, as shown in **Figure 6.7**, and then the distance ratio was calculated using **Equation 6-4**. **Figure 6.8** shows the results where It can be seen from **Figure 6.8a** that when the *MDR* is equal to 1.0 the area ratio has different values, depending on α, where it is 1.25 when α = 0.1, 1.6 for α = 0.2 and 0.3, and 1.7 for α = 0.4. While **Figure 6.8b** shows that when the *MDR* is 1.0 the area ratio is 1.3 for P/P_o = 0.0 and 1.4 for both P/P_o = 0.1 and 0.2. The force reduction factor effect is shown in **Figure 6.8c**, and when the *MDR* is 1.0 the area ratio is around 1.4. This method showed scattered optimal values. Therefore, this method was not considered as an alternative option to mitigate ratcheting.

$$\text{Method 4 ratio} = \frac{X_1}{X_2} \tag{6-4}$$

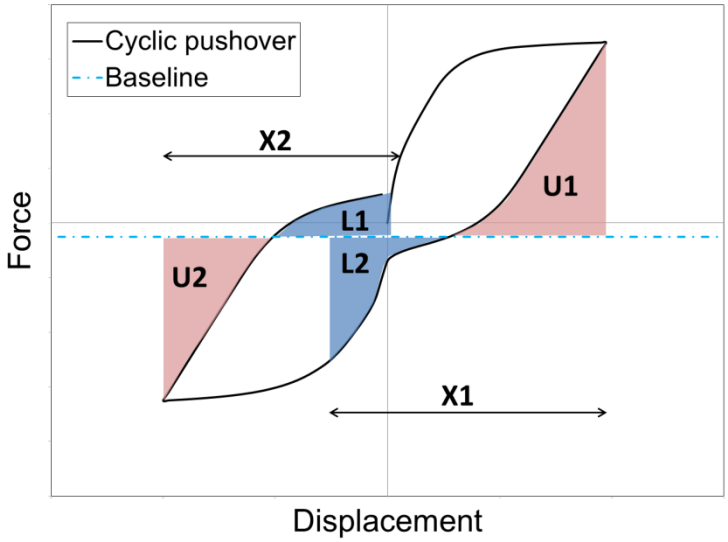

Figure 6.7: Method 4: Equalizing ratio of potential energy at peak displacement to energy required to yield in reverse direction

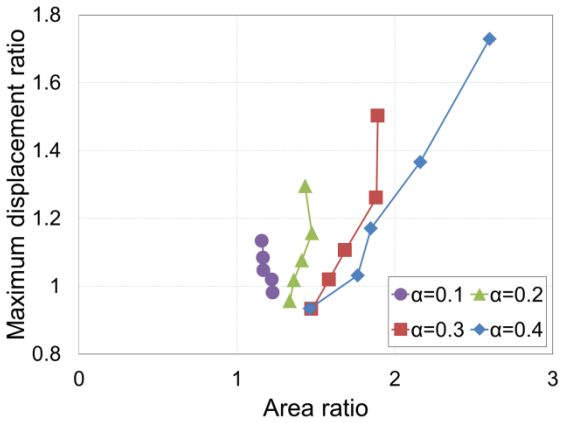

(a) Average maximum displacement ratio for different values of eccentric moment ratio, α (P/P_o = 0.1, R = 4, and T = 1.0s)

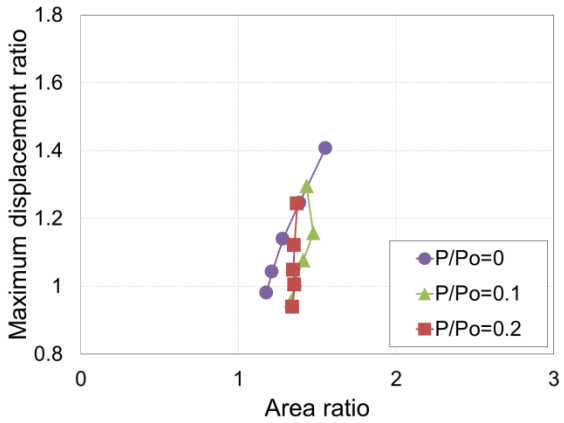

(b) Average maximum displacement ratio for different values of axial load ratio, P/P_o (α = 0.2, R = 4, and T = 1.0s)

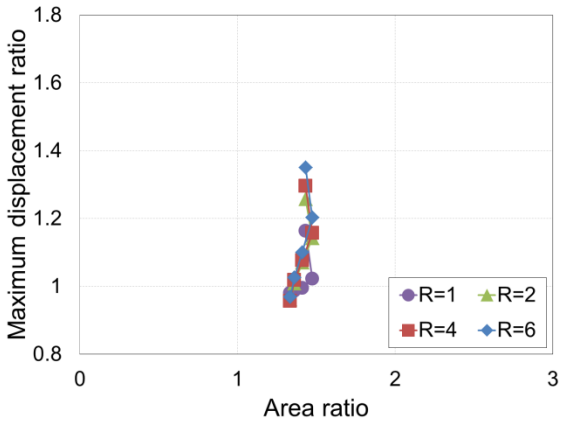

(c) Average maximum displacement ratio for different values of force reduction factor, R (P/P_o = 0.1, α = 0.2, and T = 1.0s)

Figure 6.8: Dynamic response for C-bent bridge pier with different parameters using method 4

6.2.5 Method 5: Equalizing Ratio of Periods Using Secant Stiffness to First Yield Relative to Initial Static Conditions

In this method, the effective period was calculated in each direction, the stiffness was calculated to the first yielding point, as shown in **Figure 6.9**. The strength of the weak direction was increased and the ratio of the periods was calculated using **Equation 6-5**. In this method, like the other methods, the maximum value of α was 0.4. The data results are plotted in **Figure 6.10**. It can be seen from **Figure 6.10a** and **c** that when the *MDR* is equal to 1.0 the period ratio is also almost 1.0, while in **Figure 6.10b**, the period ratio is almost 1.0 for P/P_o = 0.0 and 0.1, but it is 1.1 for P/P_o = 0.2. This means that no ratcheting will occur when the period ratio is equal to 1.0, as assumed before. Therefore, this method can be used to mitigate the ratcheting effect in maximum displacement. It should be noted that if the period ratio is 1.0, this implies that the stiffness in each direction is the same but does not imply that the strength is the same in both directions.

$$\text{Method 5 ratio} = \frac{T_2}{T_1} = \frac{2\pi\sqrt{\frac{m}{K_2}}}{2\pi\sqrt{\frac{m}{K_1}}} = \sqrt{\frac{K_1}{K_2}} \tag{6-5}$$

It is worth noting that the period method can be equivalent to method 1 assuming that the yielding displacement is constant, as suggested by Priestley (2003). **Equation 6-6** can be written as:

$$\frac{T_2}{T_1} = \sqrt{\frac{F_2.U_2}{F_1.U_1}.\frac{U_1^2}{U_2^2}} = \sqrt{\frac{A_2}{A_1}}x\ \frac{U_1}{U_2} = \sqrt{\frac{1}{method\ 1\ ratio}}x\ constant \tag{6-6}$$

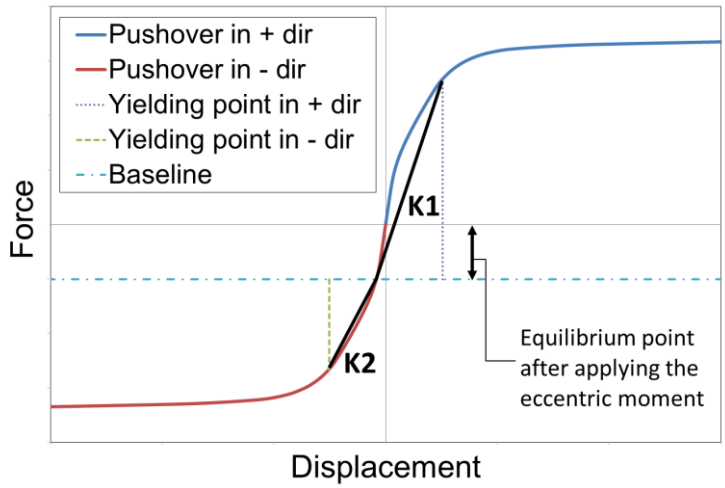

Figure 6.9: Method 5: Equalizing ratio of periods using secant stiffness to first yield relative to initial static conditions

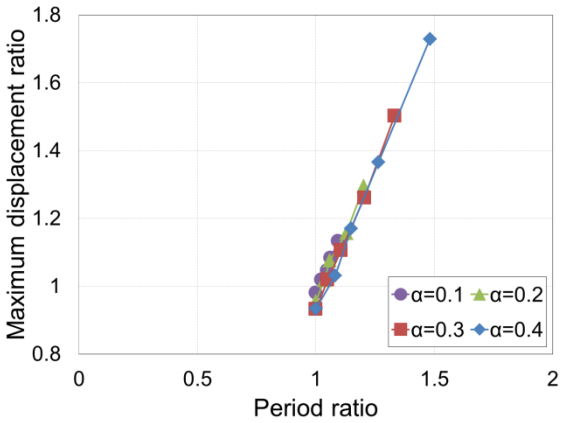

(a) Average maximum displacement ratio for different values of eccentric moment ratio, α (P/P_o = 0.1, R = 4, and T = 1.0s)

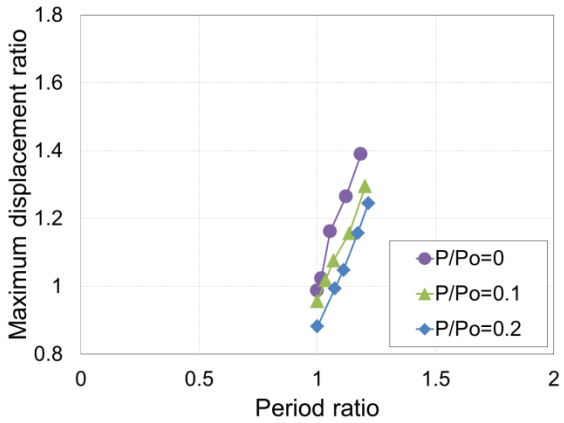

(b) Average maximum displacement ratio for different values of axial load ratio, P/P_o (α = 0.2, R = 4, and T = 1.0s)

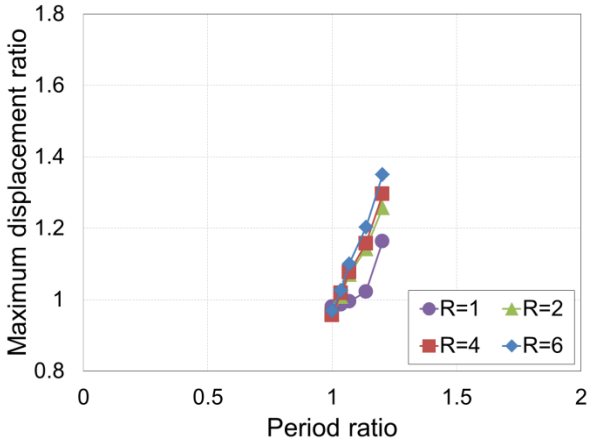

(c) Average maximum displacement ratio for different values of force reduction factor, R (P/P_o = 0.1, α = 0.2, and T = 1.0s)

Figure 6.10: Dynamic response for C-bent bridge pier with different parameters using method 5

6.2.6 Comparison between the Different Methods

The summary of each method of obtaining *MDR* is shown in **Table 6-1**. The methods were ranked based on the scatteredness of the optimal ratio that mitigates the ratcheting effect and how practical and easy it is for engineers to use the method. Among the five methods provided in the previous section, the period method was found to be the best option to mitigate ratcheting in maximum displacement. That is because it has the lowest value for scatteredness and, in practice, the engineers are familiar with the period calculation. Therefore, this can be an alternative method for engineers, where they can calculate the period in each direction and aim to get a period ratio of 1.0 to mitigate ratcheting in the maximum displacement.

Table 6-1: Summary for obtaining MDR using different methods

Ratio Method	MDR for different parameters			Method Rank
	α	R	P/P_o	
(A1/A2)=0.5	1.05, 1.15, 1.2, 1.3	1.02, 1.15, 1.17, 1.2	1.1, 1.15, 1.22	2
(B1/B2)=1	1.02, 1.05, 1.1, 1.12	1.0, 1.1, 1.12, 1.15	1.05, 1.15, 1.16	3
(C1/C2)=1	0.94, 0.95, 0.96, 1	0.97, 0.98, 0.99, 1.0	0.92, 0.93, 1.1	2
(X1/X2)=1	N/A	N/A	N/A	5
(T2/T1)=1	0.94, 0.95, 0.96, 0.98	0.98, 0.98, 0.99, 0.99	0.9, 0.95, 1.0	1

6.3 Period Ratio Detailed Analysis

As the period ratio was found to be the best method to mitigate ratcheting, further analyses were conducted using this method to produce graphs that can be used to estimate the maximum displacement.

6.3.1 Parametric Study

It can be seen from **Figure 6.10a** that *MDR* is independent of α; also **Figure 6.10c** shows that *MDR* is also independent of *R*. For the case of $R = 1$, the column has just reached the yielding point at period ratio of 1.2, then as the period ratio decreases (by adding more reinforcement) the eccentric moment effect is balanced, and therefore, the *MDR* decreases to 1.0.

Finally, the effect of axial load is shown in **Figure 6.10b**. It can be seen that the *MDR* is dependent on P/P_o and reached a value of 1.0 at different period ratios. However, for $P/P_o = 0.2$ *MDR* is equal to 1.0 when the period ratio is about 1.08. Higher P/P_o results in lower *MDR* as the re-centring behaviour reduces the displacement demands.

The detailed analyses results for different P/P_o were plotted in **Figure 6.11b**, **c**, and **d** and the mean, 84th percentile and the 16th percentiles were calculated and plotted on the graphs. The best-fit linear line and its equation were drawn for each case. These equations can be used to calculate the point at which the *MDR* equals 1.0 for different cases. It was found that the *MDR* reaches the value of 1.0 when the period ratio equals 1.0 when $P/P_o = 0$, 1.03 when $P/P_o = 0.1$, and 1.08 when $P/P_o = 0.2$. As the difference between these ratios is not significant, the period ratio method is still a reasonable approach to estimate the maximum displacement ratio.

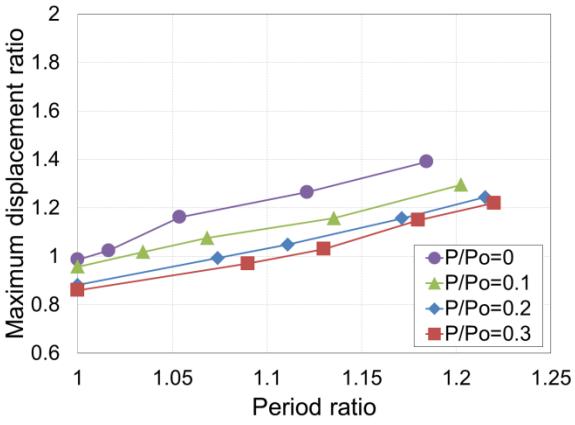

(a) Maximum displacement ratio with period ratio for different values of axial load, P/P_o

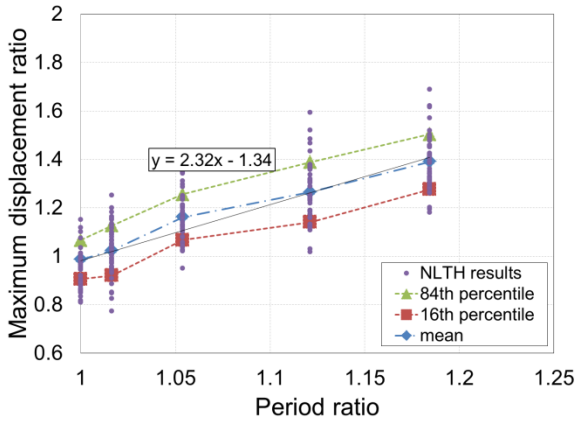

(b) Mean, 84th, and 16th percentiles for the maximum displacement ratio values for axial load $P/P_o = 0$

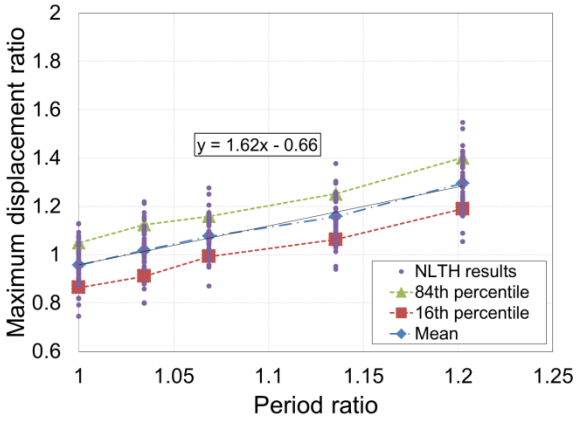

(c) Mean, 84th, and 16th percentiles for the maximum displacement ratio values for axial load $P/P_o = 0.1$

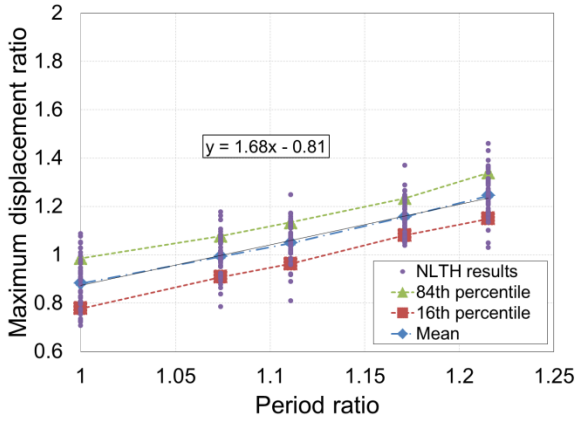

(d) Mean, 84th, and 16th percentiles for the maximum displacement ratio values for axial load $P/P_o = 0.2$

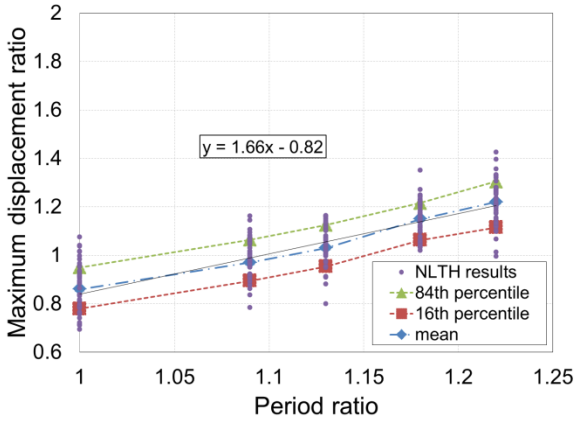

(e) Mean, 84th, and 16th percentiles for the maximum displacement ratio values for axial load $P/P_o = 0.3$

Figure 6.11: Maximum displacement ratio with period ratio for different values of axial load, P/P_o (α = 0.2, R = 4, and T = 1.0s)

6.3.2 Method Verification Using NLTH

The previous results were obtained by averaging the results of nonlinear time history analysis (NLTH) of 22 ground motions which were run in both directions. **Figure 6.12** shows the results of NLTH of one ground motion, which is the first ground motion in the far-field set suggest by FEMA (2009) that was mentioned in the methodology chapter, where the hysteresis loop and the displacement history were plotted for each case. The period was changed in each case by increasing the strength in the weak direction, which increases the stiffness, and then the period ratio was calculated. The strength was increased until the period ratio reached 1.0. It can be seen from **Figure 6.12** that when T2/T1 = 1.0 the peak displacement in both directions is the same, which means no ratcheting will occur in the maximum displacement. Therefore, based on this example, it can be said that the period ratio is a reasonable approach and there will be no ratcheting in peak displacement when the period in each direction is the same. It can be seen that the residual displacement is increasing with the period ratio (by adding more reinforcement), which was explained in the previous chapter.

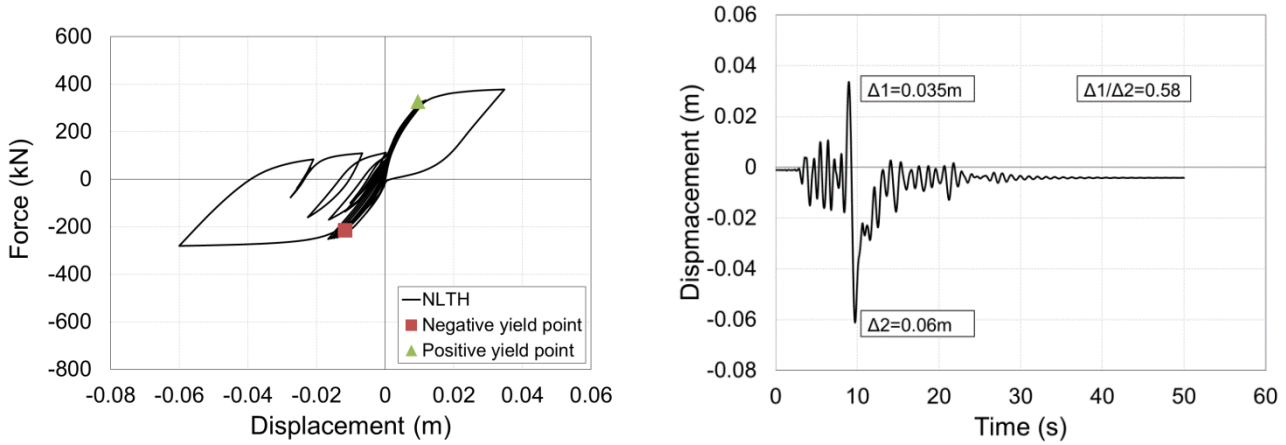

(a) Hysteresis loop and displacement history for a column with T1 = 0.91s, T2 = 1.23s and period ratio 1.34

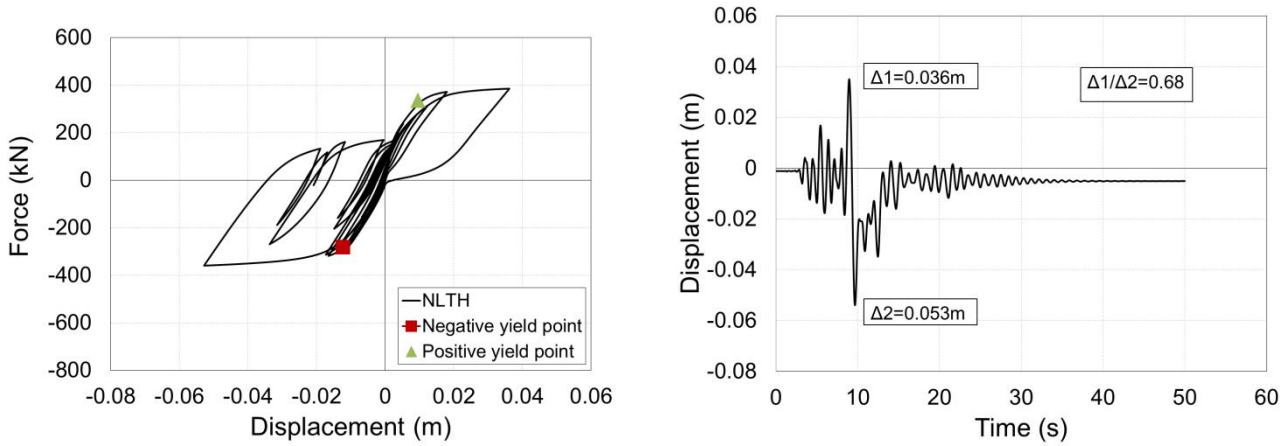

(b) Hysteresis loop and displacement history for a column with T1 = 0.90s, T2 = 1.10s and period ratio 1.22

Figure 6.12: Dynamic response of RC cantilever bridge pier (α = 0.2, R = 4, P/P_o = 0.1, and T = 1.0s)

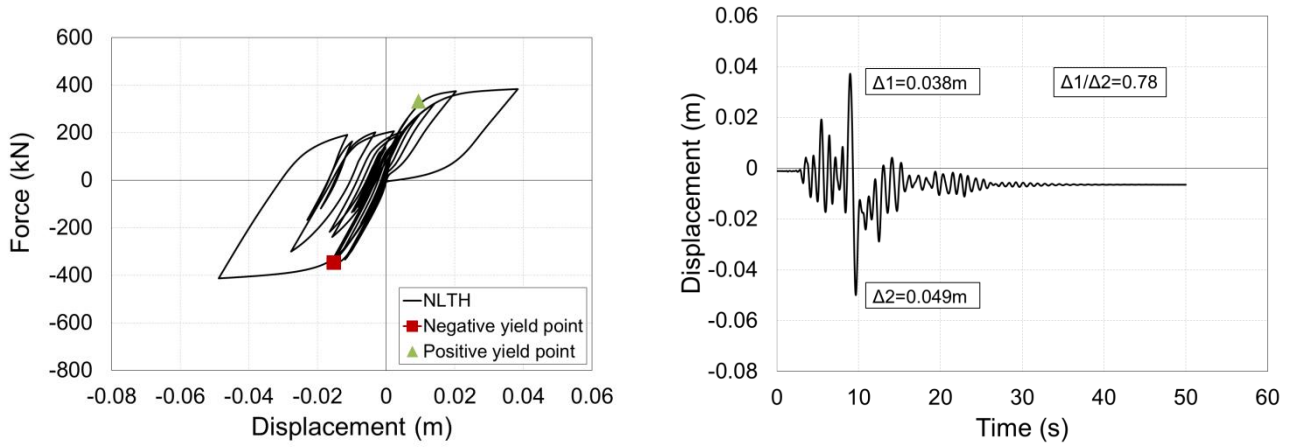

(c) Hysteresis loop and displacement history for a column with T1 = 0.89s, T2 = 1.05s and period ratio 1.16

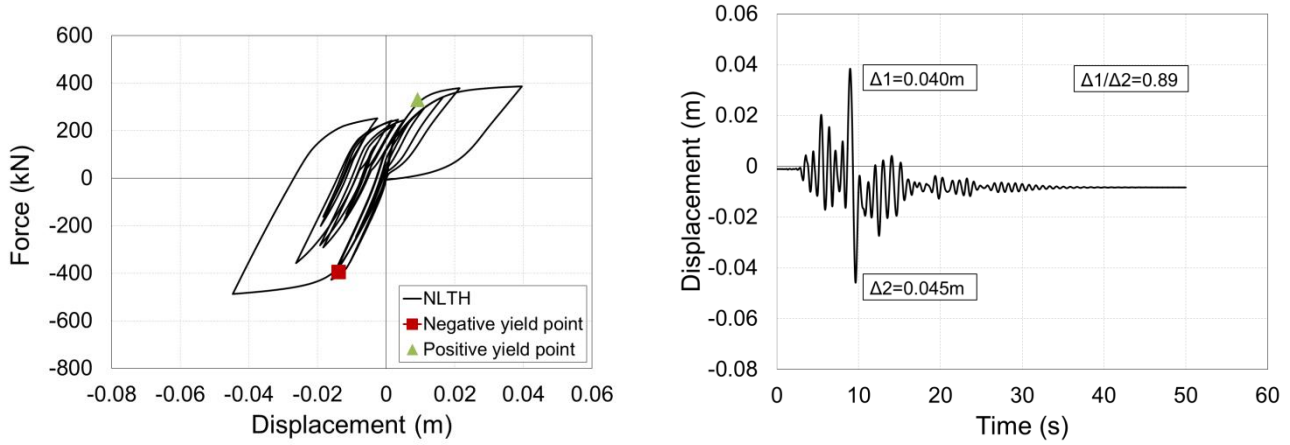

(d) Hysteresis loop and displacement history for a column with T1 = 0.88s, T2 = 0.98s and period ratio 1.11

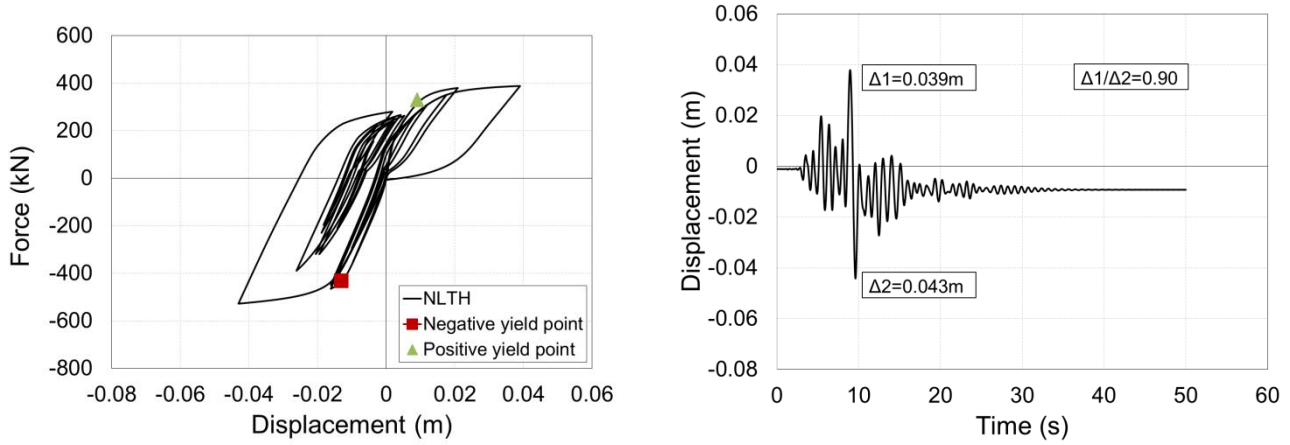

(e) Hysteresis loop and displacement history for a column with T1 = 0.88s, T2 = 0.95s and period ratio 1.08

Figure 6.12 (continued): Dynamic response of RC cantilever bridge pier (α = 0.2, R = 4, P/P_o = 0.1, and T = 1.0s)

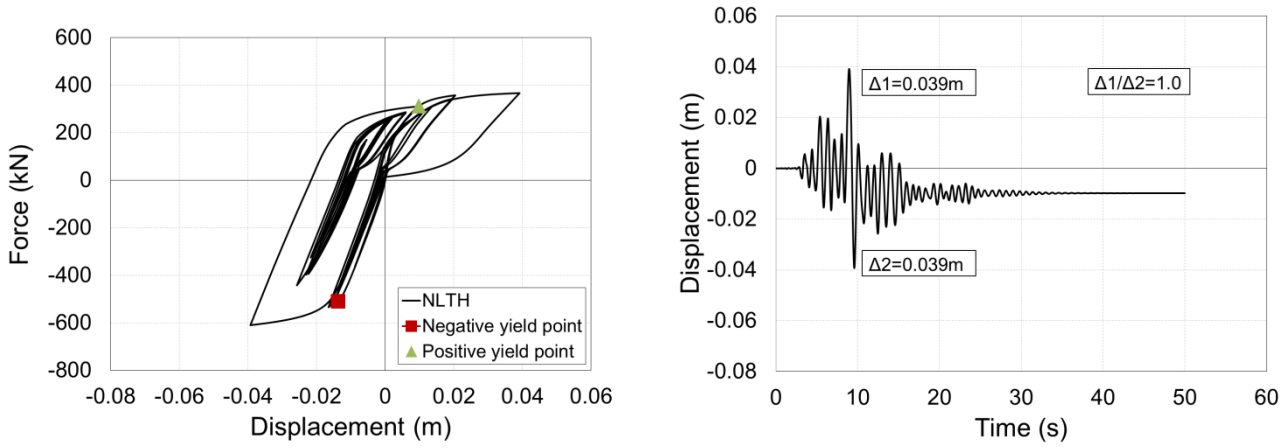

(f) Hysteresis loop and displacement history for a column with T1 = 0.88s, T2 = 0.89s and period ratio 1.01

Figure 6.12 (continued): Dynamic response of RC cantilever bridge pier (α = 0.2, R = 4, P/P_o = 0.1, and T = 1.0s)

6.3.3 Maximum Displacement Estimation Example

To explain how to use the period ratio to estimate the maximum displacement when ratcheting is accounted for, consider a cantilever column designed for R = 4, α = 0.4, and P/P_o = 0.1. The designer did not consider ratcheting and estimated a maximum displacement of 200 mm. When the period ratio was calculated, it was found to be 1.30 and it is required to estimate the maximum displacement of the column when ratcheting is considered. This can be done by using **Figure 6.10a**, where the *MDR* is around 1.4 and therefore the modified maximum displacement is 1.4 × 200 = 280 mm, which is 40% higher than that calculated by the engineer. To mitigate the ratcheting effect, more reinforcement needs to be added to the tension side of the column until the period ratio equals 1.0.

7. CONCLUSIONS AND FUTURE RESEARCH RECOMMENDATIONS

In this thesis, the effect of seismic ratcheting and the possible causes of it were explained, and evaluated against the current ratcheting provisions provided in NZS1170.5 (2016), where inconsistencies were identified and methods to overcome these issues were proposed. In addition, graphs and empirical equations were provided to estimate maximum and residual displacements when ratcheting was not accounted for, and solutions to mitigate ratcheting were presented that can be used by engineers in practice. It was also shown that the optimal strength increment ratio presented in the literature is not adequate when the stiffness–strength relationship is considered, and a more rational value was presented.

7.1 Conclusions

The major findings of this thesis are described according to the questions mentioned in the introduction. These are as follows:

1. *What are the issues with the new NZS1170.5 ratcheting provisions and are they adequate to estimate maximum displacements when ratcheting is considered?*

There are some issues with the current ratcheting provisions in NZS1170.5 (2016) which are not clear. These mainly relate to the wording used in the standards in defining (i) the design lateral strength, (ii) the forward and reverse directions, and (iii) the parameter S_g. Furthermore, methods to consider the P-delta effect in the calculation of the ratcheting index, r_i, is not clear. These issues were discussed and alternative definitions were proposed.

It was found that NZS1170.5 (2016) is not conservative in estimating the increase in maximum displacement for RC single-degree-of-freedom structures due to ratcheting for high values of force reduction factor ($R > 5$) and low values of axial load ratios ($P/P_o < 0.1$), while it was conservative for other cases. Furthermore, it was also found that the provisions underestimate the increase in maximum displacement for steel structures for all studied cases.

2. *How can the maximum and residual displacements of C-bent columns with eccentric gravity loads be estimated, and can ratcheting be mitigated?*

Graphs were provided to estimate displacement demands for different cases, and simplified equations were also provided as an easy and fast way for engineers, who ignored ratcheting effect in their calculations, to estimate both the maximum and the residual displacements. In addition, it was found that ratcheting in maximum displacement can be mitigated by adding more reinforcement on the tension side of the column so that its flexural strength increased as a ratio of the eccentric moment, which was defined by the

parameter β. It was found that when β is around 3.4 then there will be no ratcheting in maximum displacement due to the eccentric moment. This value was reported as the optimal strength increment ratio, β_o.

3. *Can simple design/assessment methods be developed for engineers in practice to estimate displacement demands and mitigate ratcheting effects for single-storey structures?*

Several different methods were presented as alternative approaches to estimate displacement demands and to mitigate ratcheting. These methods are based on the period ratio in each direction and the energy concept. The period-ratio method was chosen as the more suitable method because it provides accurate results and the engineers are familiar with its calculation.

7.2 Future Research Recommendations

- The model used in this research is a cantilever column that represents single-degree-of-freedom structures and other structures where the first mode of vibration is dominant. However, there is a need to use multi-degree-of-freedom models to represent different types of structures, such as multi-storey structures, and to take the effect of frames into account.

- More structural configurations need to be studied, such as T-shaped walls and steel frames with lateral bracing, as the structural shape is one of the causes of ratcheting and may affect the results.

- The inelastic time history analyses only considered the horizontal component of ground motions. Therefore, it is recommended that the vertical component of ground motions be included in future studies.

- More in-depth studies need to be conducted on the energy concept and the period ratio methods to explain the observations in more detail.

8. REFERENCES

Abdolahirad, A., MacRae, GA., Yeow, T. and Bull, D. (2017) Dynamically Straightening of Low-Damage Steel Buildings After Earthquake. Santiago, Chile: 16th World Conference on Earthquake Engineering, 16WCEE 2017, 9-–13 Jan 2017.

Alavi, B., & Krawinkler, H. (2004). Behavior of moment-resisting frame structures subjected to near-fault ground motions. Earthquake engineering & structural dynamics, 33(6), 687-706.

Bauschinger, J. "Ueber die Veranderung der Elasticitatagrenze und dea Elasticitatamoduls verschiadener Metalle," Zivilingenieur, vol. 27, pp. 289–348, 1881.

Chang, Y. S., Li, Y. F., & Loh, C. H. (2004). Experimental study of seismic behaviors of as-built and carbon fiber reinforced plastics repaired reinforced concrete bridge columns. Journal of Bridge Engineering, ASCE 9(4), 391–402 doi:10.1061//ASCE/1084-0702/2004/9:4/391

Chen, L. K., Zhang, N., Jiang, L. Z., Zeng, Z. P., Chen, G. W., & Guo, W. (2014). Near-fault directivity pulse-like ground motion effect on high-speed railway bridge. Journal of Central South University, 21(6), 2425-2436.

Clark P. et al. Large-scale testing of steel unbonded braces for energy dissipation, advanced technology in structural engineering. Proceedings of the 2000 Structures Congress & Exposition, May 8–10, 2000, Philadelphia, PA, American Society of Civil Engineers, Reston, VA, 2000.

Dupuis, M. R., Best, T. D. D., Elwood, K. J., & Anderson, D. L. (2014). Seismic performance of shear wall buildings with gravity-induced lateral demands. Canadian Journal of Civil Engineering, 41(4), 323-332. doi:10.1139/cjce-2012-0482

Federal Emergency Management Agency (FEMA). (2009). Quantification of building seismic performance factors: FEMA P-695.

Fenwick, R. (2017). Personal correspondence.

Jamnani, H. H., Karbassi, A., & Lestuzzi, P. (2013). Fling-step effect on the seismic behaviour of high-rise RC buildings during the Christchurch earthquake. In 2013 NZSEE Conference.

Japan Road Association. (1990). Design Specifications for Road Bridges Part V Seismic Design.

Kam, W.Y., Pampanin, S. and Elwood, K. 2011. Seismic Performance of Reinforced Concrete Buildings in The22 February Christchurch (Lyttelton) Earthquake. Bulletin of the New Zealand Society for EarthquakeEngineering, 44(4), 239-278.

Kawashima, K., Seigi, N. and Watanabe, G. (2010). “Seismic performance of a bridge supported by C-bent columns,” Journal of Earthquake Engineering 14(8), 1172–1220.

Kawashima K., MacRae G. A., Hoshikuma J. and Nagaya K., "Residual Displacement Response Spectrum", ASCE Journal of Structural Engineering, ASCE, May 1998, pp. 523-530.

Kawashima, K., MacRae G. A. and Hasegawa K., “The Strength and Ductility of Steel Bridge Piers Based on Load Tests”, Journal of Research of the Public Work Research Institute, Vol.29, Tsukuba, March, 1992.

MacRae, G. A., & Kawashima, K. (1993). The seismic response of bilinear oscillators using Japanese earthquake records. Journal of Research of the Public Works Research Institute, 30.

MacRae G. A., "P-Δ Effects on Single-Degree-of-Freedom Structures in Earthquakes", Earthquake Spectra, Vol. 10, No. 3, August 1994, pp. 539-568.

McKenna, F., Fenves, G. L., Scott, M. H., & Jeremic, B. (2016). Open System for Earthquake Engineering Simulation (OpenSees). University of California, Berkeley: Pacific Earthquake Engineering Research Center.

Menegotto M, Pinto PE. Method of analysis of cyclically loaded RC plane frames including changes in geometry and nonelastic behavior of elements under normal force and bending. Preliminary report IABSE, vol. 13, Zurich;1973. p. 15–22.

National Building Code of Canada (NBCC), 2015. Issued by the Canadian Commission on Building and Fire Codes, National Research Council of Canada, Ottawa, ON, 2015.

Popovics, S. (1973). A numerical approach to the complete stress-strain curve of concrete. Cement and Concrete Research, 3(5), 583-599. doi:10.1016/0008-8846(73)90096-3

Priestley, M.J.N. (2003) Myths and Fallacies in Earthquake Engineering, Revisited. The Mallet Milne Lecture, 2003, IUSS Press, Pavia, 121 pp.

Priestley, M.J.N. and Grant, D.N. (2005) Viscous Damping in Seismic Design and Analysis Journal of Earthquake Engineering Vol 9 Special Issue pp 229-255

Priestley, M.J.N. (2006) Initial Stiffness or Secant Stiffness for Seismic Design – Which is More Appropriate? 1st European Conference on Earthquake Engineering and Seismology, paper 469.

Royal Commission (2011). Canterbury earthquakes Royal Commission interim report, Canterbury Earthquakes Royal Commissions Christchurch, N.Z.

Saif K.Z., Lee C.-L., MacRae G.A. and Yeow T.Z. (2017) Effect of Eccentric Moments on Seismic Ratcheting of Single-Degree-Of-Freedom Structures. Wellington: 2017 NZSEE Conference, 27-29 Apr 2017.

Standards New Zealand. (2016). NZS1170.5:2004 Structural Design Actions Part 5 Earthquake actions New Zealand. Incorporating Amendment 1, 2016.

Standards New Zealand. (2016). NZS1170.5:2016 Structural Design Actions Part 5 Earthquake actions New Zealand.

Standards New Zealand. (2006). NZS3101:2006 Concrete Structures Standard Part 1 The Design of Concrete Structures, New Zealand.

Takai, N., Shigefuji, M., Rajaure, S. et al. Earth Planets Space (2016) 68: 10. doi:10.1186/s40623-016-0383-7

Takeda, T., Sozen, M.A. and Nielsen, N. (1970). “Reinforced Concrete Response to Simulated Earthquakes.” Journal of Structural Engineering, ASCE, 96(ST 12), 2557-2573.

Yeow, T. Z., MacRae, G. A., Sadashiva, V. K., & Kawashima, K. (2013). Dynamic Stability and Design of C-Bent Columns. Journal of Earthquake Engineering, 17(5), 750-768. doi:10.1080/13632469.2013.771591

9. APPENDICES

9.1 Time Histories Graphs

The following sections show hysteresis loops for the different cases considered in this study.

9.1.1 Effect of Axial Load

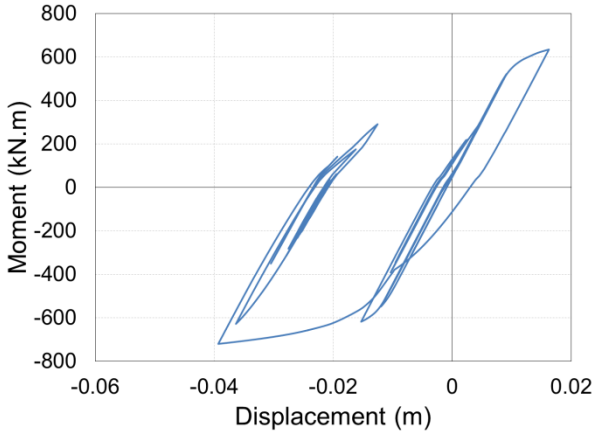

(a) Dynamic response for β = 0

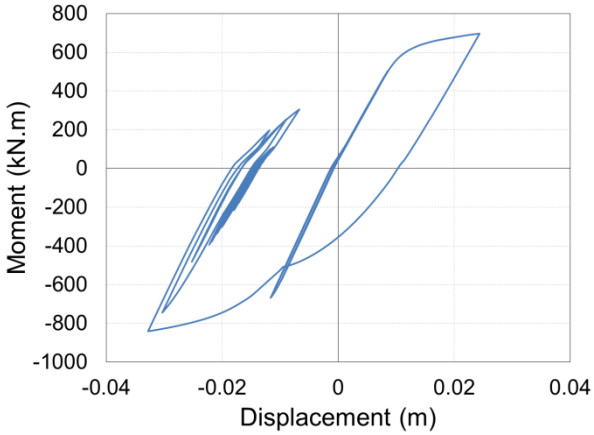

(b) Dynamic response for β = 1

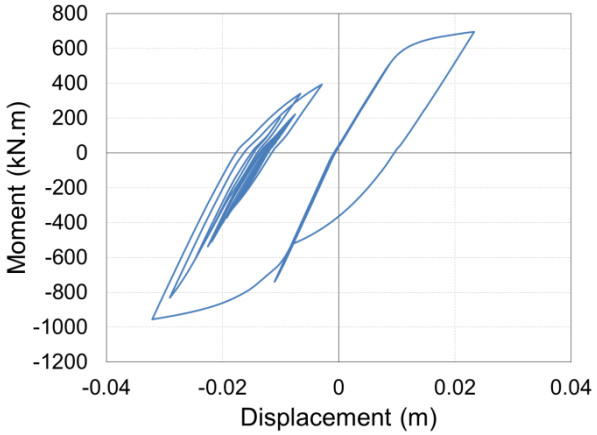

(c) Dynamic response for β = 2

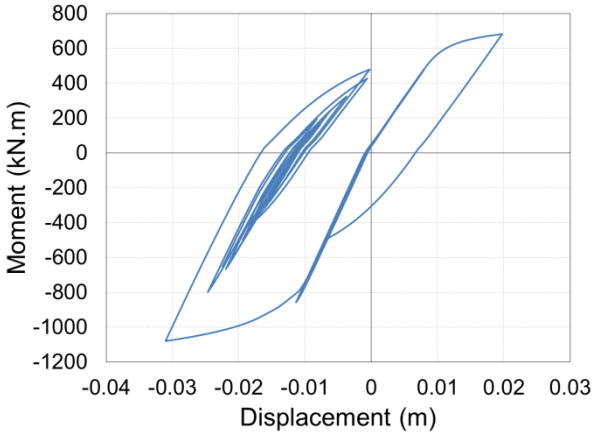

(d) Dynamic response for β = 3

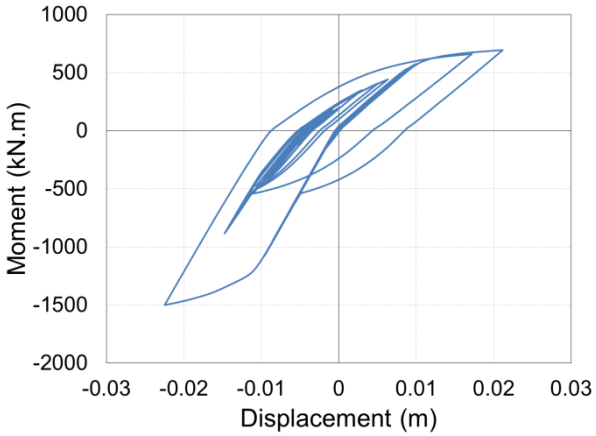

(e) Dynamic response for β = 4

Figure 9.1: Time histories for axial load ratio P/P_o = 0 with different values of strength increment ratio, β (α = 0.2, R = 4, and T = 1.0s)

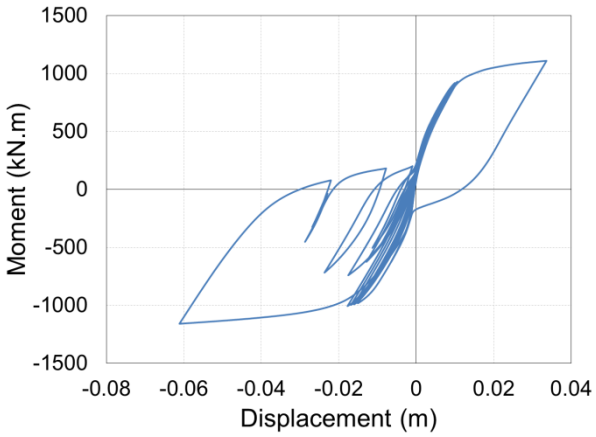

(a) Dynamic response for β = 0

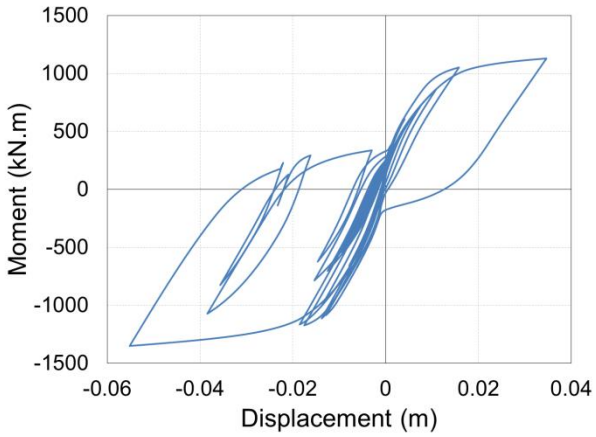

(b) Dynamic response for β = 1

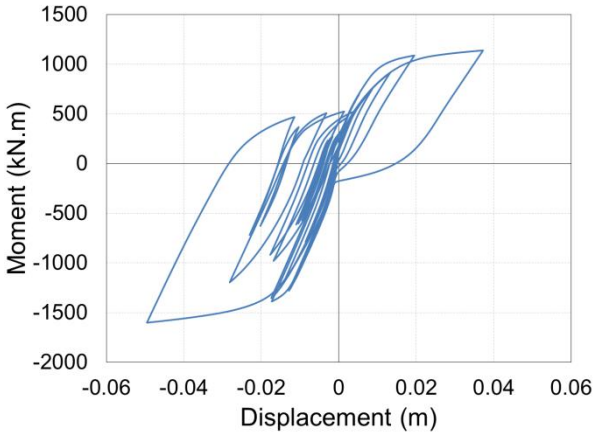

(c) Dynamic response for β = 2

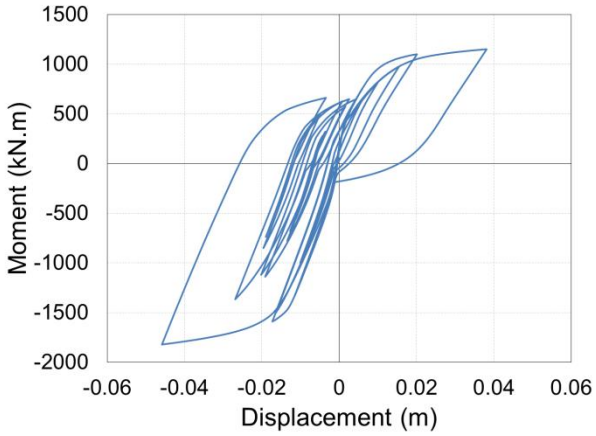

(d) Dynamic response for β = 3

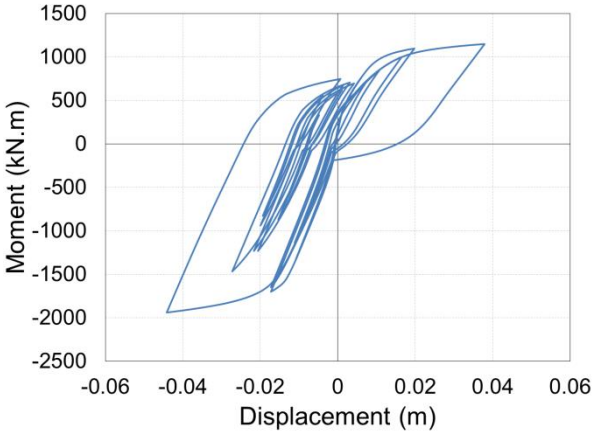

(e) Dynamic response for β = 4

Figure 9.2: Time histories for axial load ratio P/P_o = 0.1 with different values of strength increment ratio, β (α = 0.2, R = 4, and T = 1.0s)

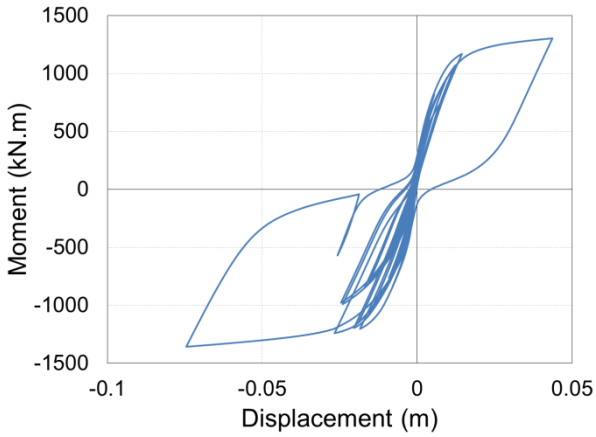

(a) Dynamic response for β = 0

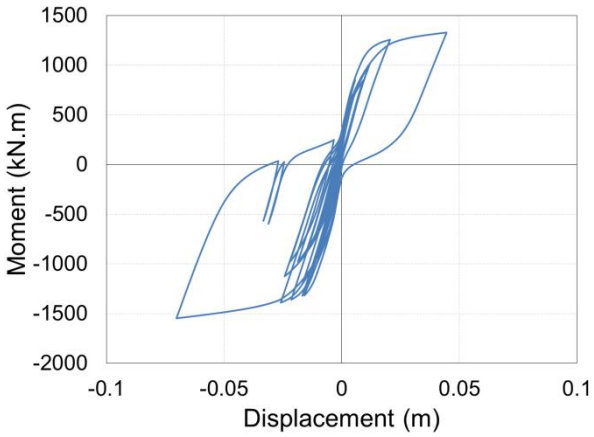

(b) Dynamic response for β = 1

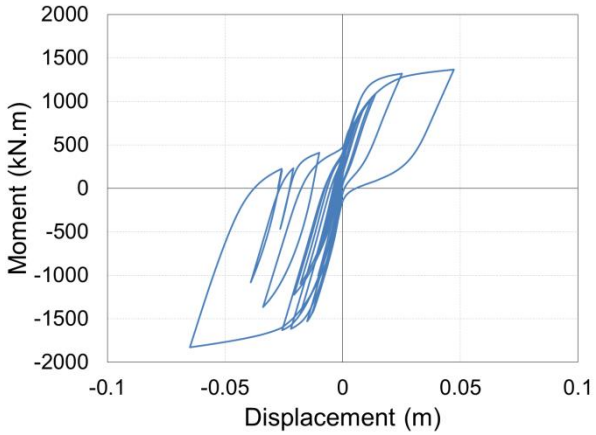

(c) Dynamic response for β = 2

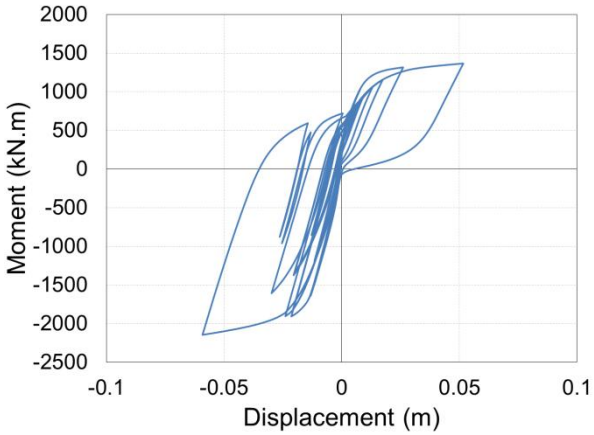

(d) Dynamic response for β = 3

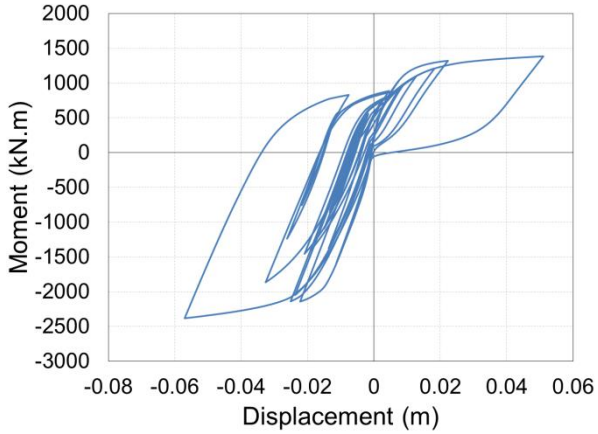

(e) Dynamic response for β = 4

Figure 9.3: Time histories for axial load ratio P/P_o = 0.15 with different values of strength increment ratio, β (α = 0.2, R = 4, and T = 1.0s)

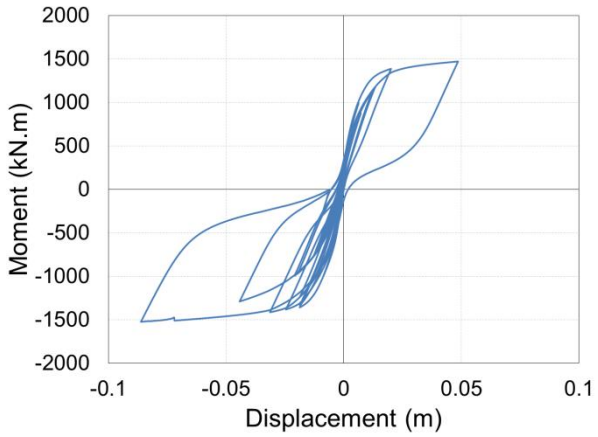

(a) Dynamic response for β = 0

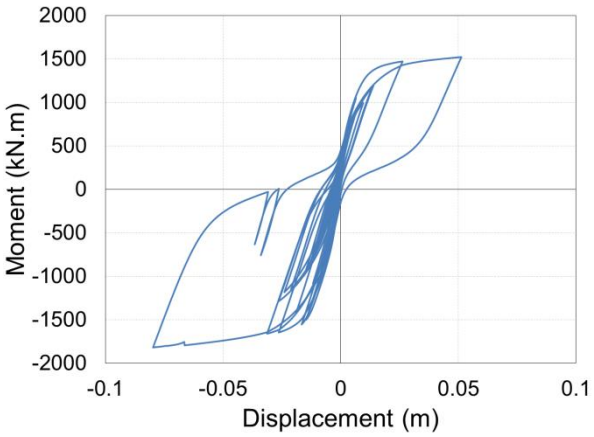

(b) Dynamic response for β = 1

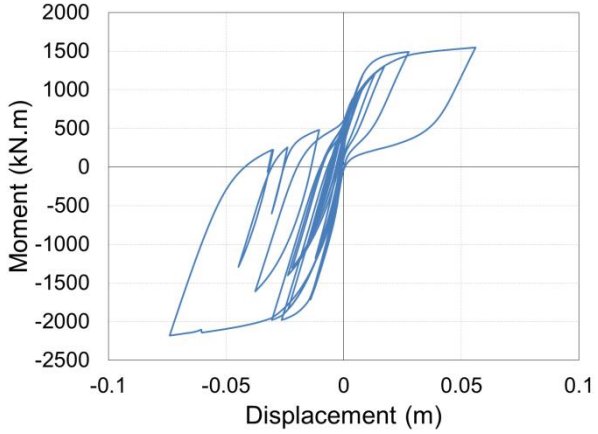

(c) Dynamic response for β = 2

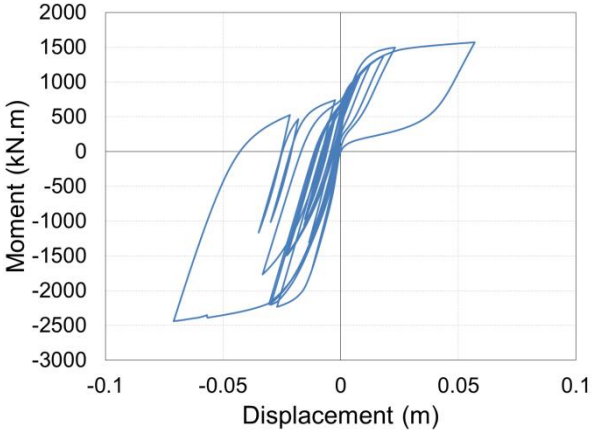

(d) Dynamic response for β = 3

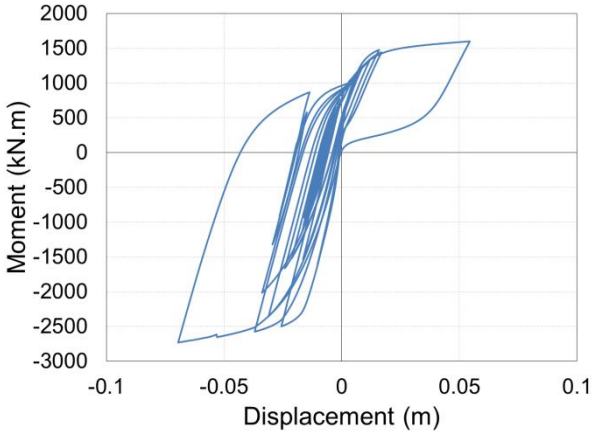

(e) Dynamic response for β = 4

Figure 9.4: Time histories for axial load ratio P/P_o = 0.2 with different values of strength increment ratio, β (α = 0.2, R = 4, and T = 1.0s)

9.1.2 Effect of Eccentric Moment

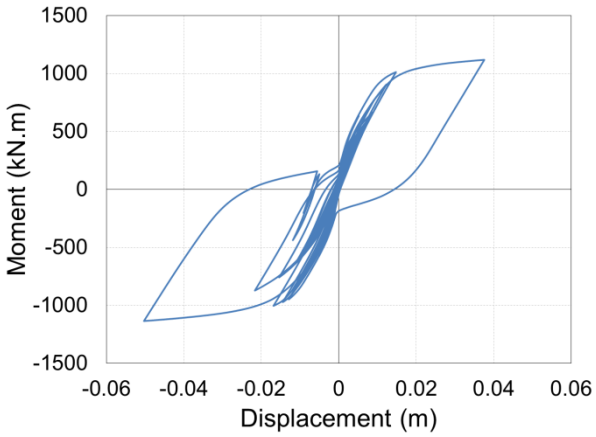

(a) Dynamic response for β = 0

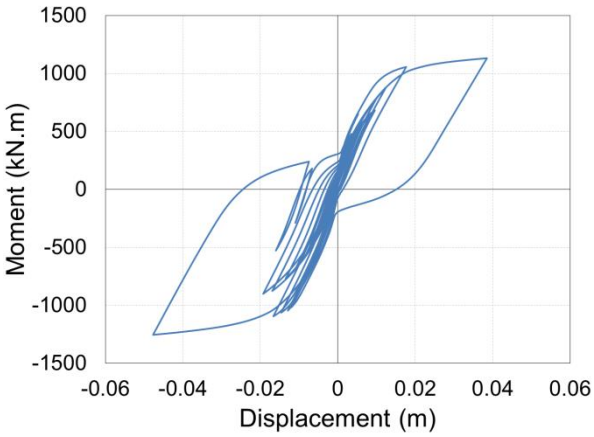

(b) Dynamic response for β = 1

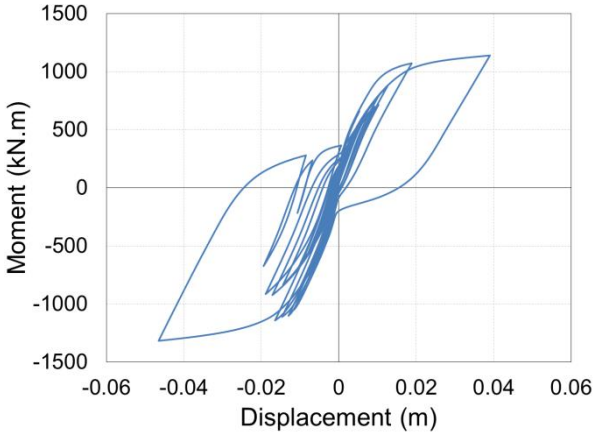

(c) Dynamic response for β = 2

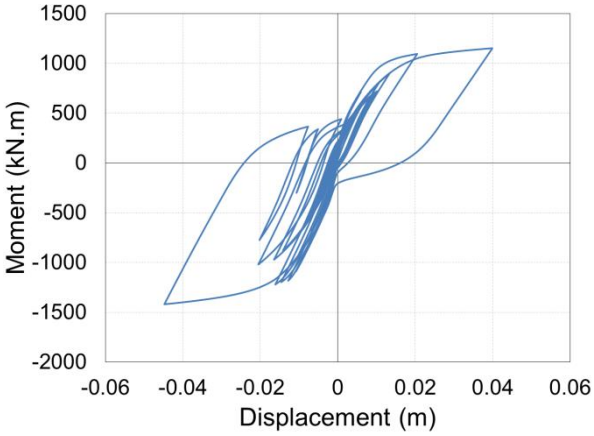

(d) Dynamic response for β = 3

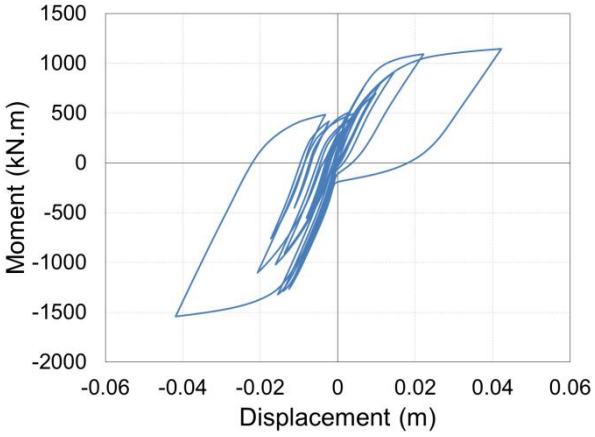

(e) Dynamic response for β = 4

Figure 9.5: Time histories for eccentric moment ratio α = 0.1 with different values of strength increment ratio, β (P/P_o = 0.1, R = 4, and T = 1.0s)

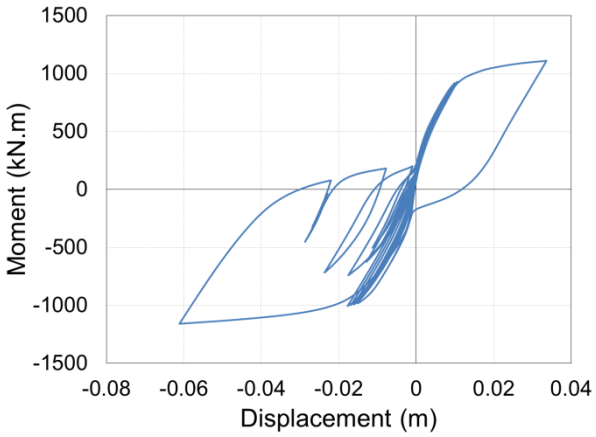

(a) Dynamic response for β = 0

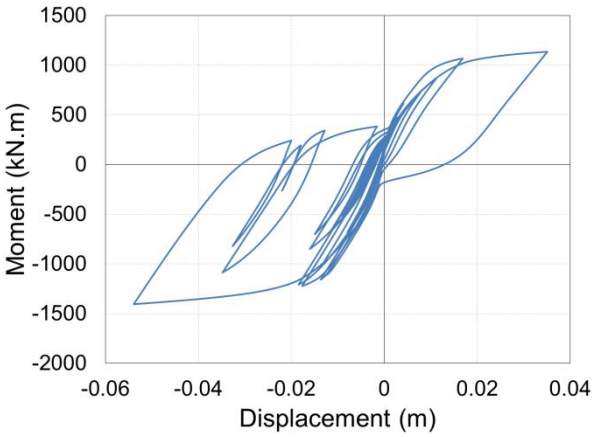

(b) Dynamic response for β = 1

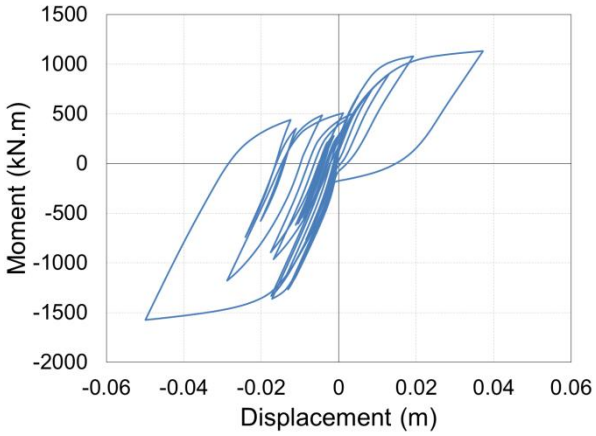

(c) Dynamic response for β = 2

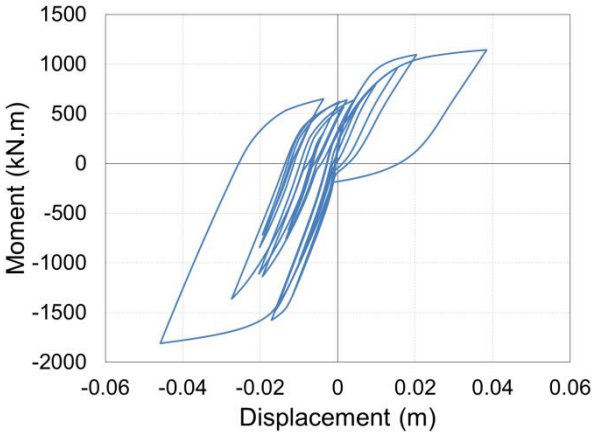

(d) Dynamic response for β = 3

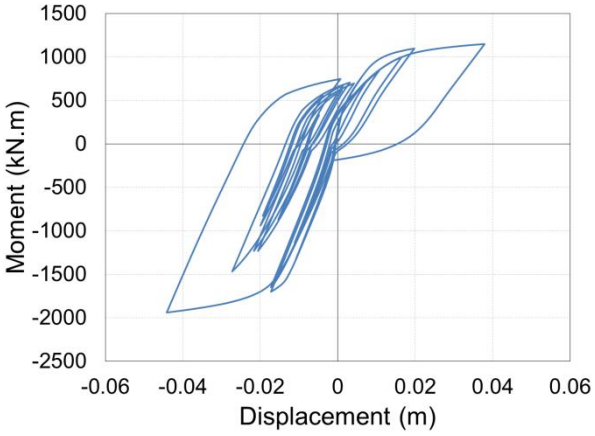

(e) Dynamic response for β = 4

Figure 9.6: Time histories for eccentric moment ratio α = 0.2 with different values of strength increment ratio, β (P/P_o = 0.1, R = 4, and T = 1.0s)

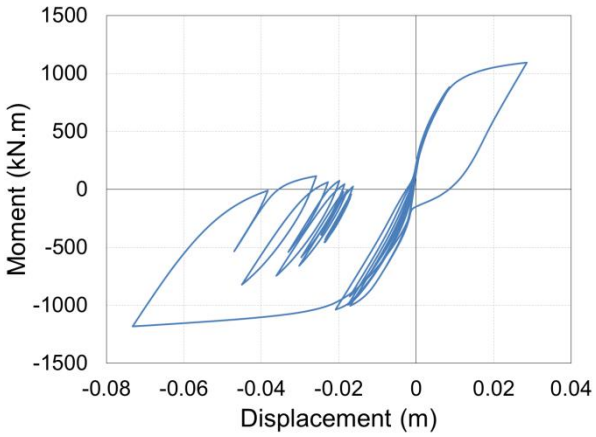

(a) Dynamic response for β = 0

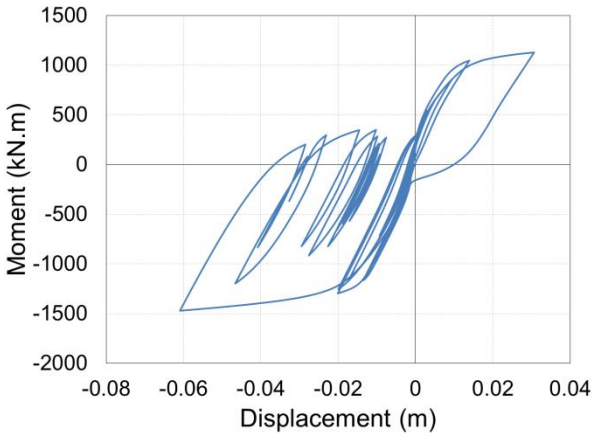

(b) Dynamic response for β = 1

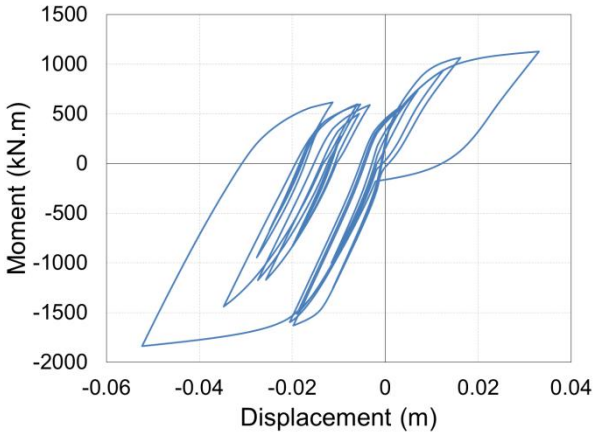

(c) Dynamic response for β = 2

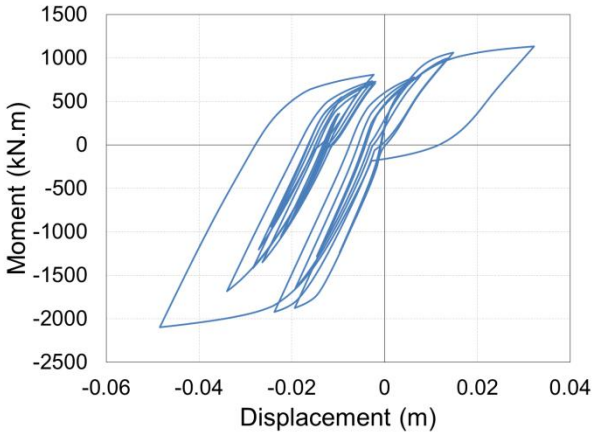

(d) Dynamic response for β = 3

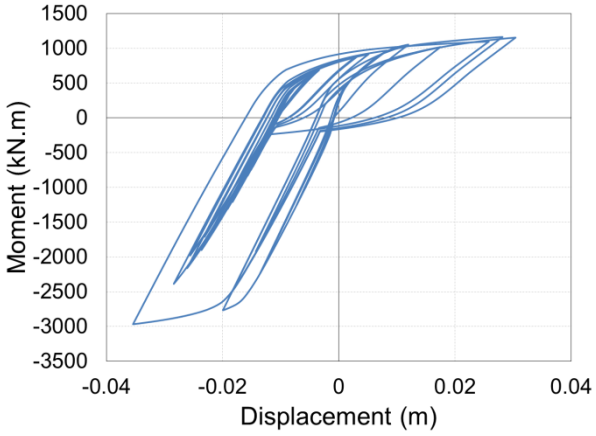

(e) Dynamic response for β = 4

Figure 9.7: Time histories for eccentric moment ratio α = 0.3 with different values of strength increment ratio, β (P/P_o = 0.1, R = 4, and T = 1.0s)

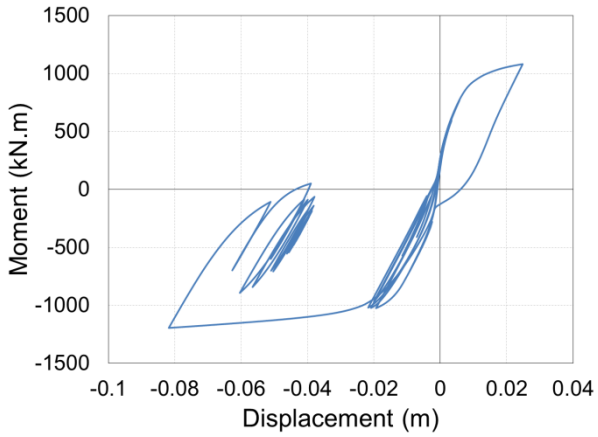

(a) Dynamic response for β = 0

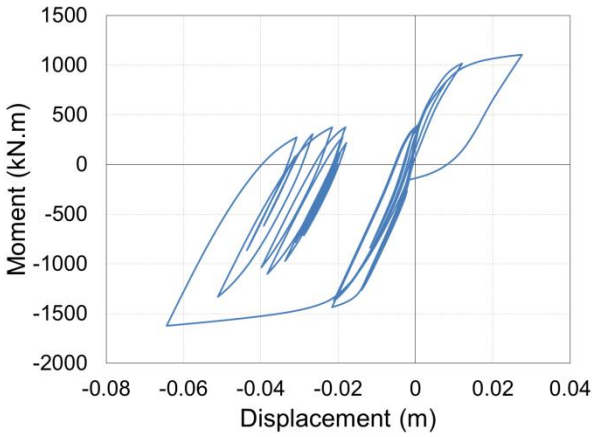

(b) Dynamic response for β = 1

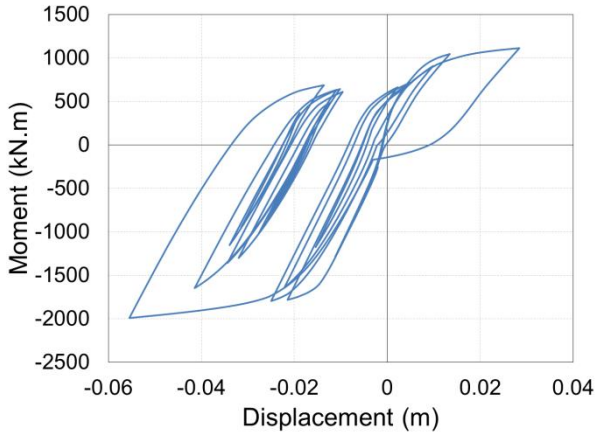

(c) Dynamic response for β = 2

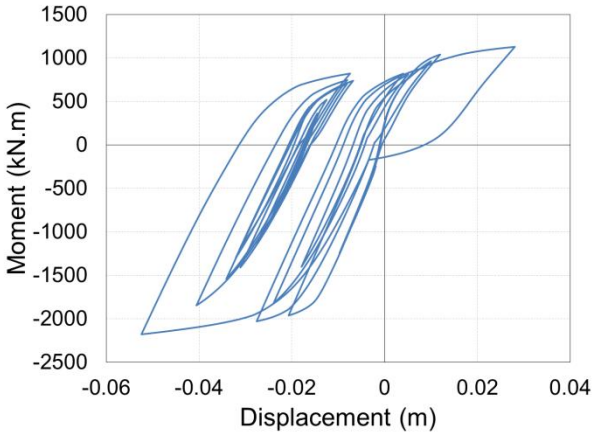

(d) Dynamic response for β = 3

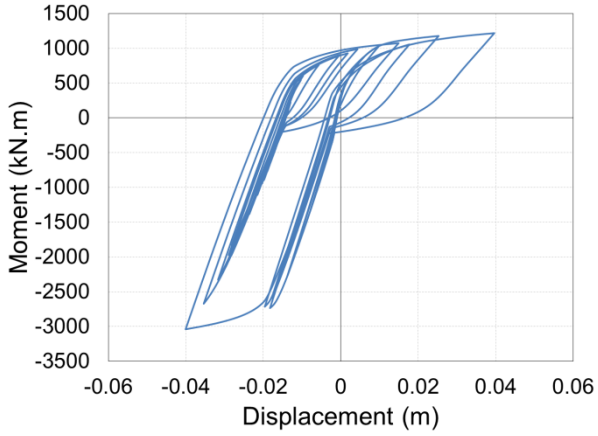

(e) Dynamic response for β = 4

Figure 9.8: Time histories for eccentric moment ratio α = 0.4 with different values of strength increment ratio, β (P/P_o = 0.1, R = 4, and T = 1.0s)

9.1.3 Effect of Force Reduction Factor

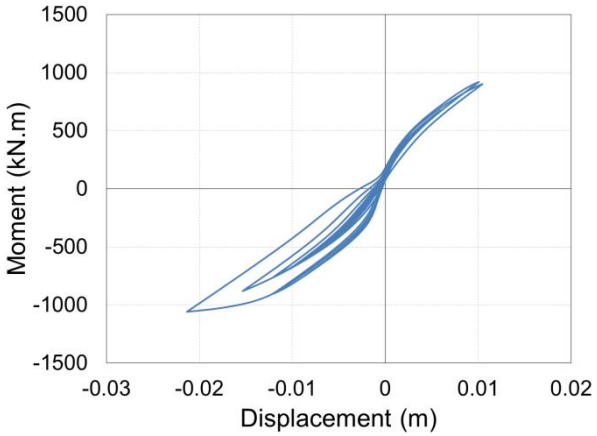

(a) Dynamic response for β = 0

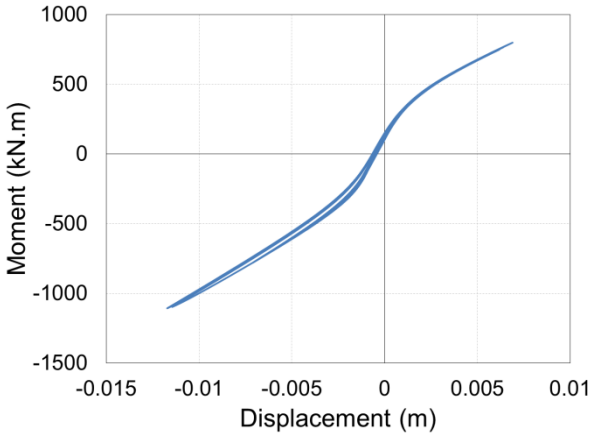

(b) Dynamic response for β = 1

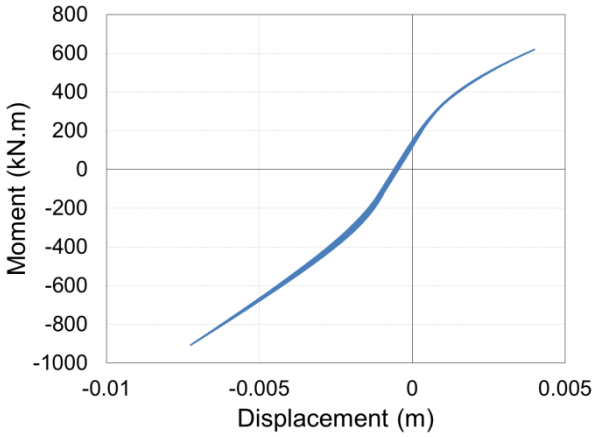

(c) Dynamic response for β = 2

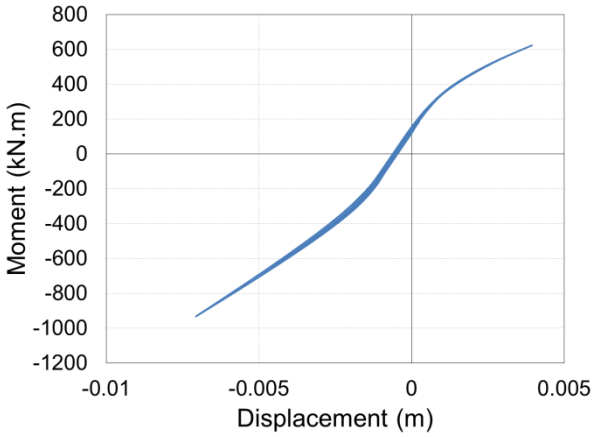

(d) Dynamic response for β = 3

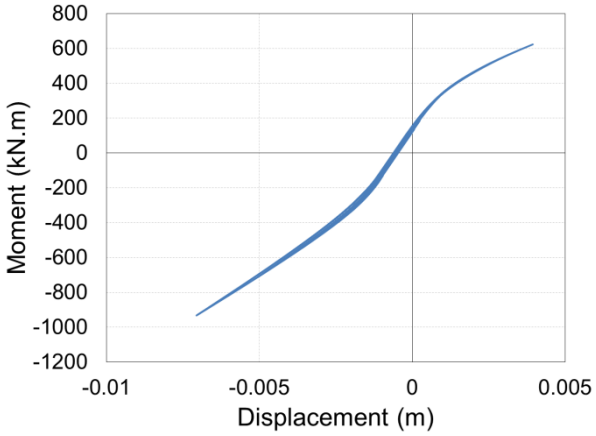

(e) Dynamic response for β = 4

Figure 9.9: Time histories for force reduction factor R = 1 with different values of strength increment ratio, β (P/P_o = 0.1, α = 0.2, and T = 1.0s)

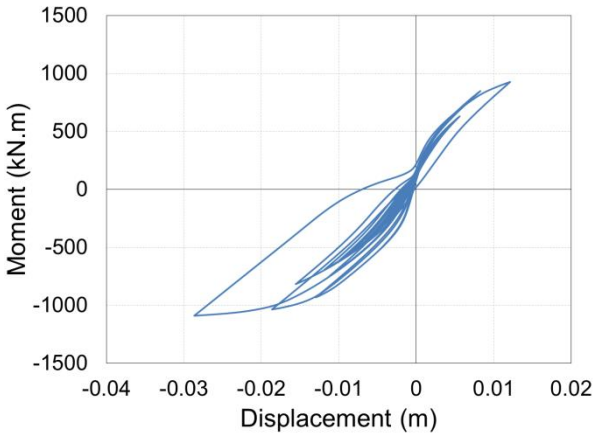

(a) Dynamic response for β = 0

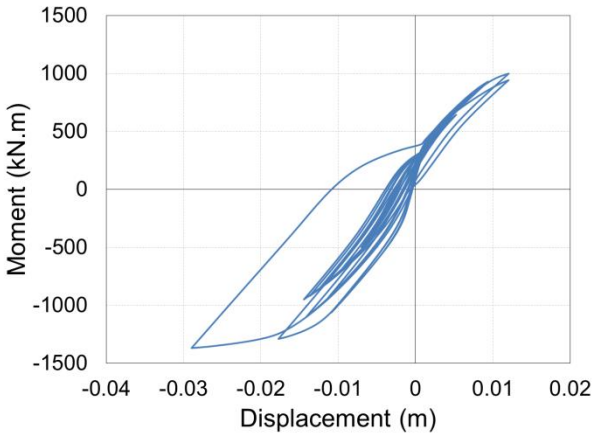

(b) Dynamic response for β = 1

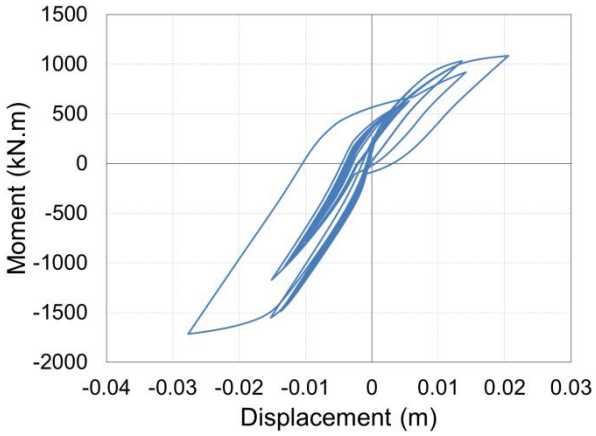

(c) Dynamic response for β = 2

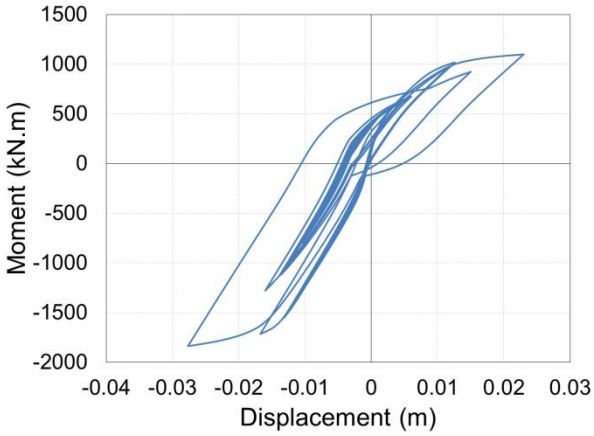

(d) Dynamic response for β = 3

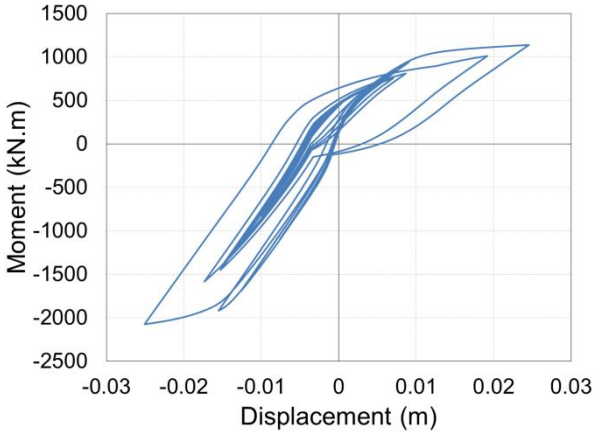

(e) Dynamic response for β = 4

Figure 9.10: Time histories for force reduction factor *R* = 2 with different values of strength increment ratio, β (*P*/*P*$_o$ = 0.1, *α* = 0.2, and *T* = 1.0s)

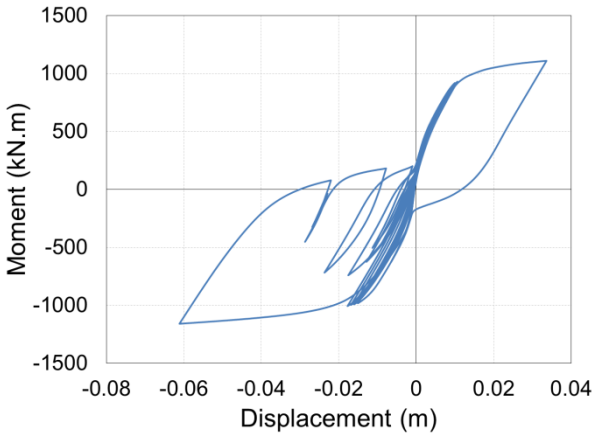

(a) Dynamic response for β = 0

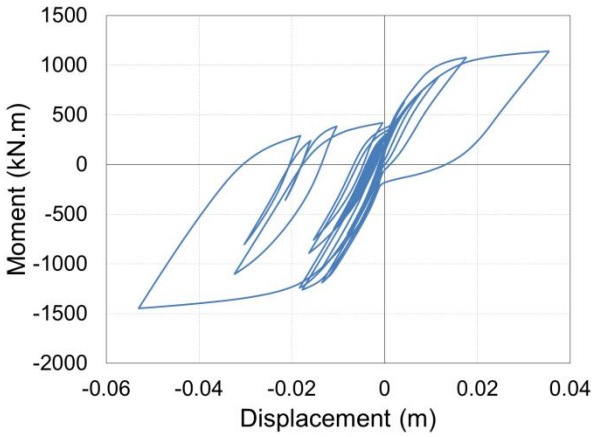

(b) Dynamic response for β = 1

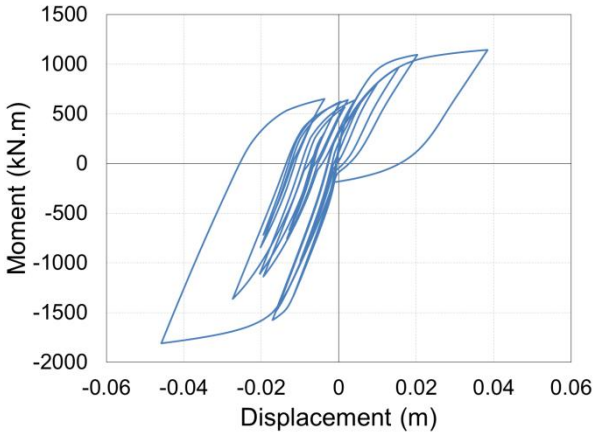

(c) Dynamic response for β = 2

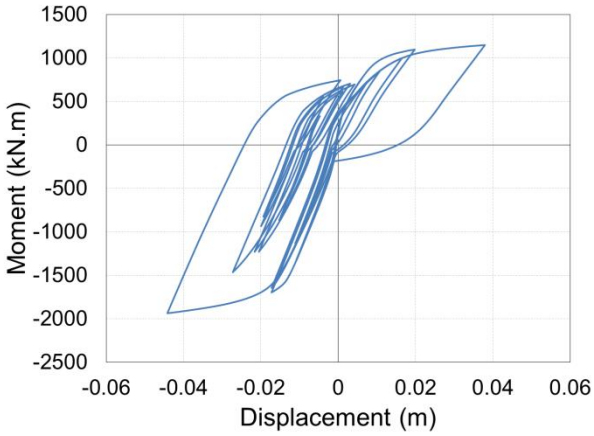

(d) Dynamic response for β = 3

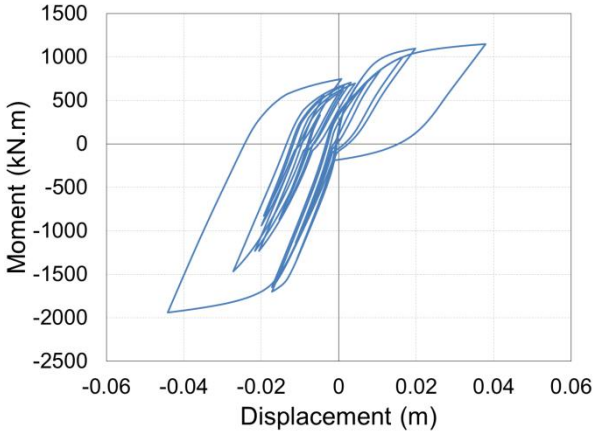

(e) Dynamic response for β = 4

Figure 9.11: Time histories for force reduction factor *R* = 4 with different values of strength increment ratio, β (*P*/*P*$_o$ = 0.1, *α* = 0.2, and *T* = 1.0s)

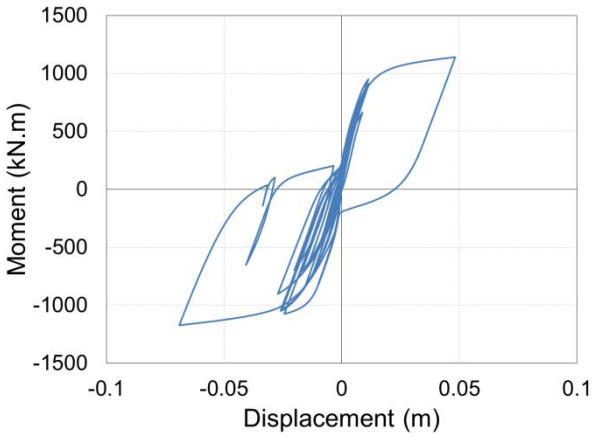

(a) Dynamic response for β = 0

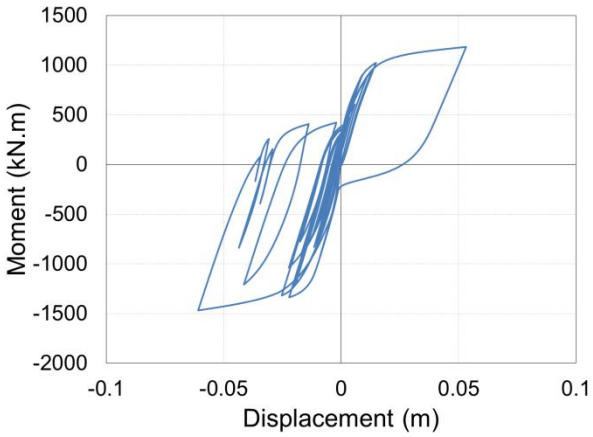

(b) Dynamic response for β = 1

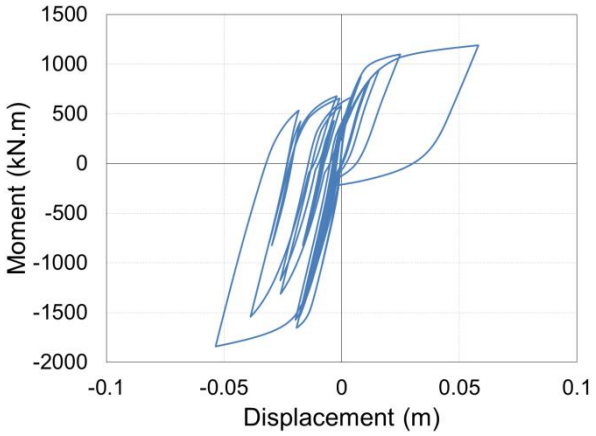

(c) Dynamic response for β = 2

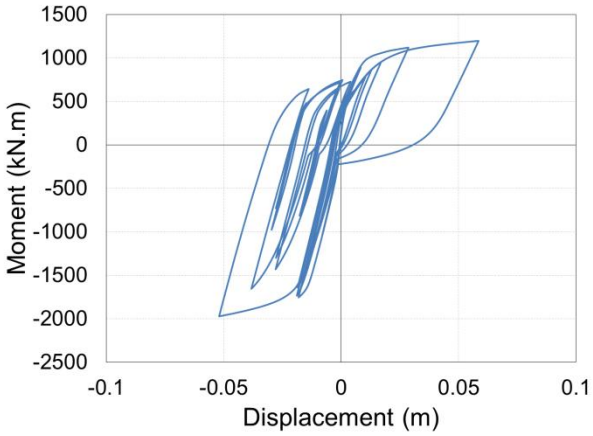

(d) Dynamic response for β = 3

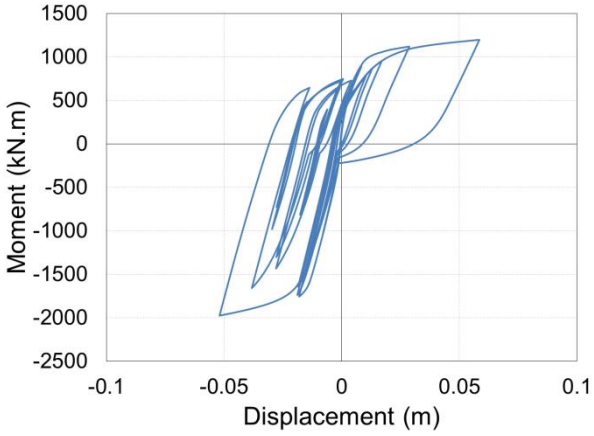

(e) Dynamic response for β = 4

Figure 9.12: Time histories for force reduction factor *R* = 6 with different values of strength increment ratio, β (*P*/*P*$_o$ = 0.1, *α* = 0.2, and *T* = 1.0s)

9.1.4 Effect of Period

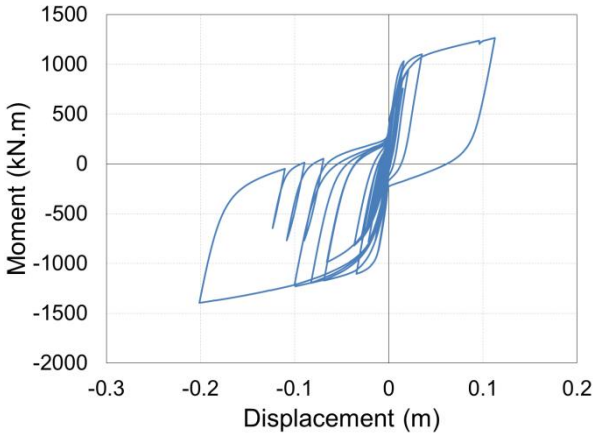

(a) Dynamic response for β = 0

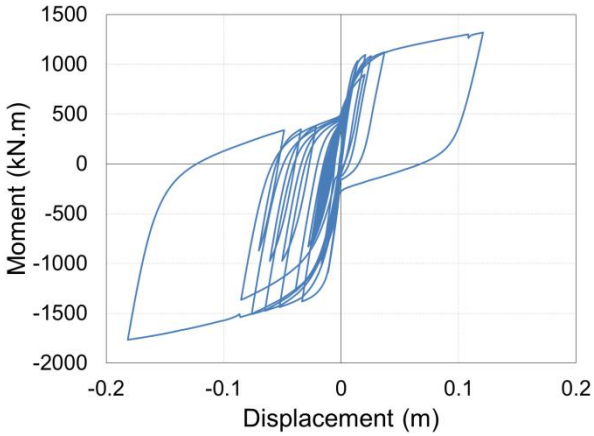

(b) Dynamic response for β = 1

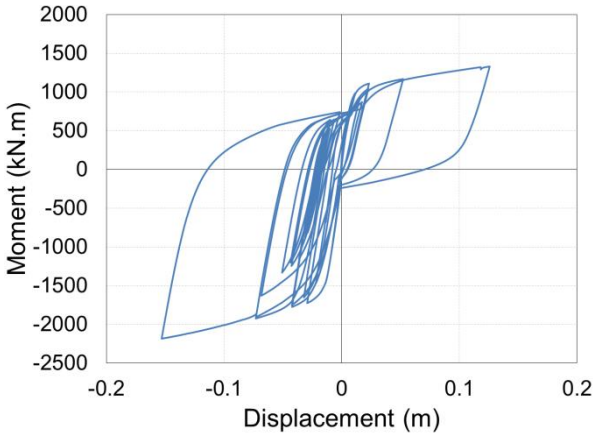

(c) Dynamic response for β = 2

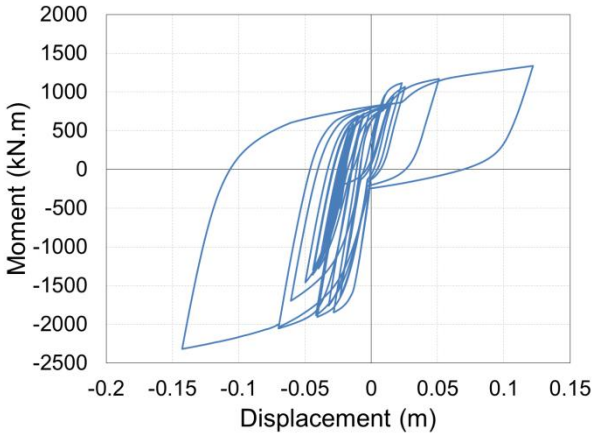

(d) Dynamic response for β = 3

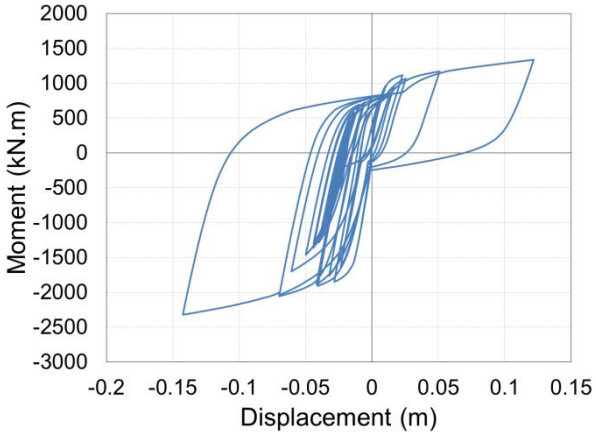

(e) Dynamic response for β = 4

Figure 9.13: Time histories for structural period T = 0.5s with different values of strength increment ratio, β (P/P_o = 0.1, α = 0.2, and R = 4)

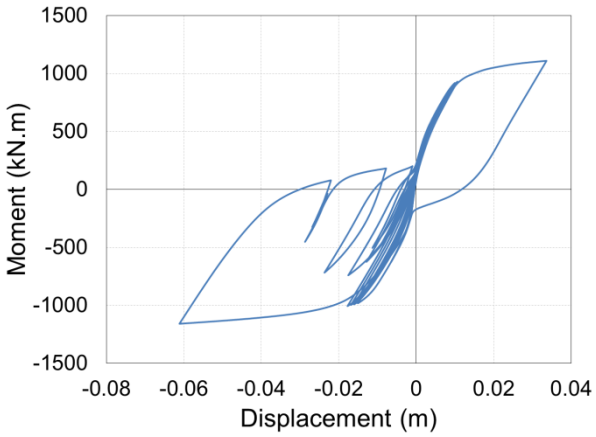

(a) Dynamic response for β = 0

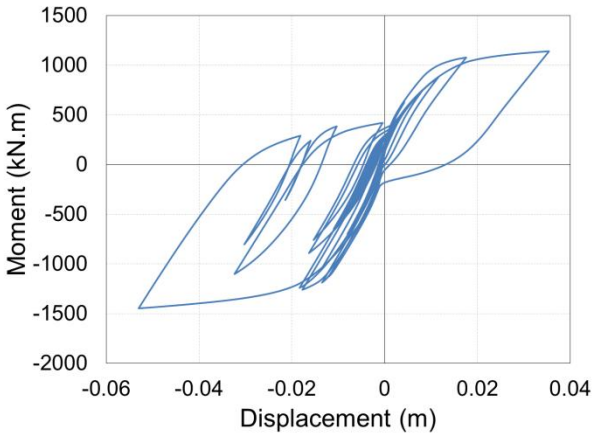

(b) Dynamic response for β = 1

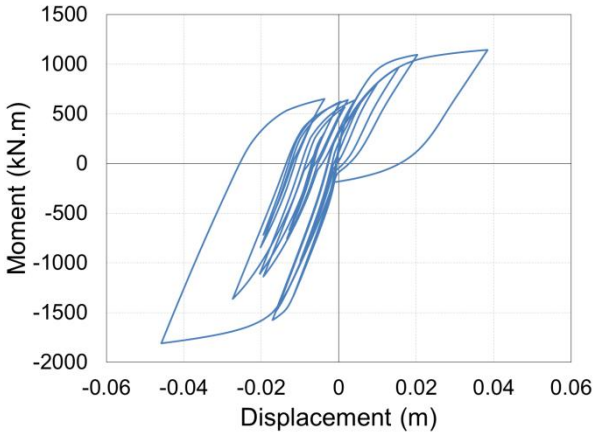

(c) Dynamic response for β = 2

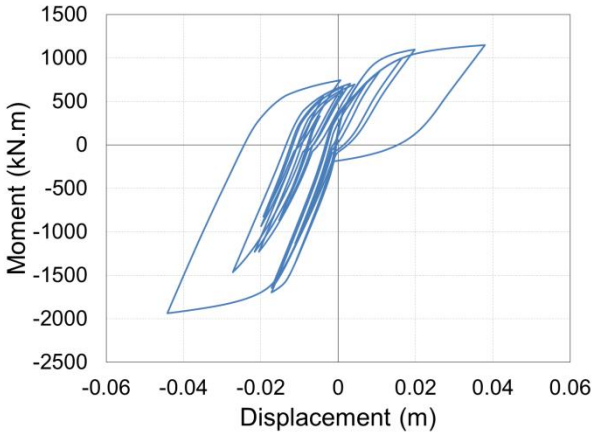

(d) Dynamic response for β = 3

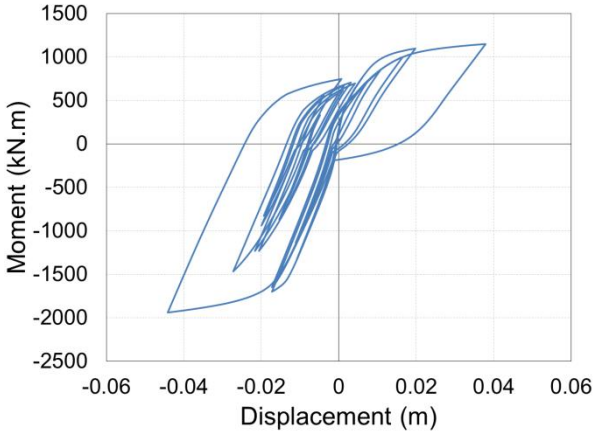

(e) Dynamic response for β = 4

Figure 9.14: Time histories for structural period T = 1.0s with different values of strength increment ratio, β (P/P_o = 0.1, α = 0.2, and R = 4)

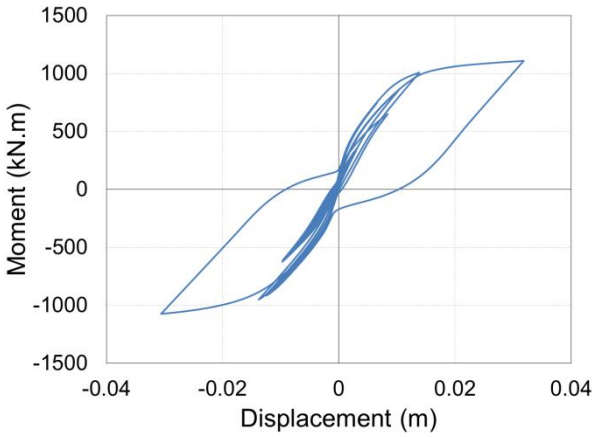

(a) Dynamic response for β = 0

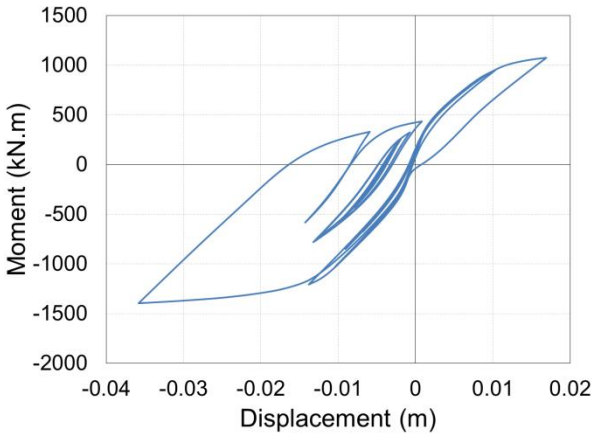

(b) Dynamic response for β = 1

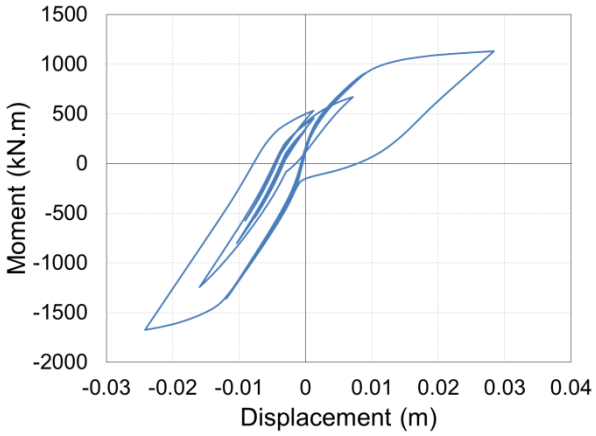

(c) Dynamic response for β = 2

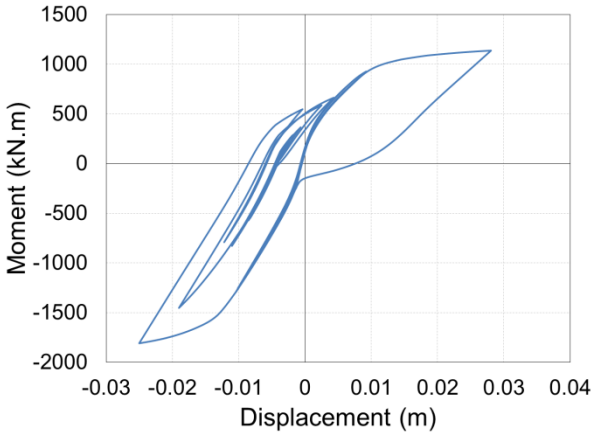

(d) Dynamic response for β = 3

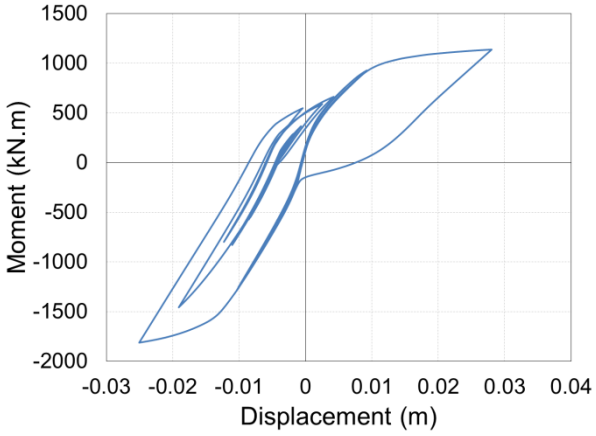

(e) Dynamic response for β = 4

Figure 9.15: Time histories for structural period T = 1.5s with different values of strength increment ratio, β (P/P_o = 0.1, α = 0.2, and R = 4)

9.2 Energy Method and Period Ratio Results

The following tables show the detailed results of energy and period ratio methods. The ratio was changed by adding more reinforcement in one side of the column (changing β).

9.2.1 Method 1: Energy Method of the Yielding Point – Linear Approximation

Table 9-1: Energy ratios using method 1 for different eccentric moment values

α	β	A1	A2	A1/A2
0.40	0.00	1.87	0.83	2.25
0.40	1.00	1.83	1.63	1.12
0.40	2.00	1.80	2.47	0.73
0.40	3.00	1.80	3.00	0.60
0.40	4.00	1.75	4.57	0.38
0.30	0.00	1.75	0.97	1.81
0.30	1.00	1.74	1.50	1.16
0.30	2.00	1.70	2.29	0.74
0.30	3.00	1.67	2.94	0.57
0.30	4.00	1.66	3.61	0.46
0.20	0.00	1.62	1.09	1.48
0.20	1.00	1.61	1.64	0.98
0.20	2.00	1.57	2.46	0.64
0.20	3.00	1.56	2.79	0.56
0.20	4.00	1.55	3.12	0.50
0.10	0.00	1.49	1.22	1.22
0.10	1.00	1.61	1.45	1.11
0.10	2.00	1.49	1.57	0.95
0.10	3.00	1.49	1.78	0.84
0.10	4.00	1.46	2.08	0.70

Table 9-2: Energy ratios using method 1 for different axial load values

P/P_o	β	A1	A2	A1/A2
0.00	0.00	0.98	0.68	1.45
0.00	1.00	0.99	0.91	1.09
0.00	2.00	0.99	1.58	0.62
0.00	3.00	0.99	1.89	0.53
0.00	4.00	0.99	2.17	0.45
0.10	0.00	1.62	1.09	1.48
0.10	1.00	1.61	1.64	0.98
0.10	2.00	1.57	2.46	0.64
0.10	3.00	1.56	2.79	0.56
0.10	4.00	1.55	3.12	0.50
0.20	0.00	2.36	1.59	1.48
0.20	1.00	2.32	2.20	1.06
0.20	2.00	2.26	3.07	0.73
0.20	3.00	2.23	3.74	0.59
0.20	4.00	2.21	4.56	0.48

9.2.2 Method 2: Energy Method of the Yielding Point – Full Area under the Curve

Table 9-3: Energy ratios using method 2 for different eccentric moment values

α	β	B1	B2	B1/B2
0.40	0.00	2.81	0.84	3.36
0.40	1.00	2.84	1.51	1.88
0.40	2.00	2.89	2.32	1.24
0.40	3.00	2.92	4.54	0.64
0.40	4.00	2.99	5.81	0.51
0.30	0.00	2.55	1.00	2.55
0.30	1.00	2.58	1.54	1.68
0.30	2.00	2.61	2.33	1.12
0.30	3.00	2.65	2.96	0.89
0.30	4.00	2.68	3.58	0.75
0.20	0.00	2.29	1.25	1.83
0.20	1.00	2.29	1.81	1.26
0.20	2.00	2.26	2.64	0.86
0.20	3.00	2.24	2.97	0.76
0.20	4.00	2.23	3.31	0.67
0.10	0.00	2.04	1.50	1.36
0.10	1.00	2.03	1.76	1.16
0.10	2.00	2.05	1.88	1.09
0.10	3.00	2.07	2.09	0.99
0.10	4.00	2.07	2.40	0.86

Table 9-4: Energy ratios using method 2 for different axial load values

P/P_o	β	B1	B2	B1/B2
0.00	0.00	1.17	0.56	2.09
0.00	1.00	1.19	0.81	1.46
0.00	2.00	1.19	1.18	1.01
0.00	3.00	1.18	1.60	0.74
0.00	4.00	1.17	1.89	0.62
0.10	0.00	2.30	1.27	1.81
0.10	1.00	2.30	1.81	1.27
0.10	2.00	2.30	2.63	0.87
0.10	3.00	2.28	2.96	0.77
0.10	4.00	2.24	3.30	0.68
0.20	0.00	3.37	1.85	1.82
0.20	1.00	3.35	2.46	1.36
0.20	2.00	3.33	3.33	1.00
0.20	3.00	3.27	4.00	0.82
0.20	4.00	3.31	4.83	0.69

9.2.3 Method 3: Total Hysteresis Energy Ratio

Table 9-5: Energy ratios using method 3 for different eccentric moment values

α	β	C1	C2	C1/C2
0.40	0.00	17.14	6.91	2.48
0.40	1.00	19.02	10.91	1.74
0.40	2.00	20.11	14.48	1.39
0.40	3.00	20.72	19.37	1.07
0.40	4.00	21.20	22.34	0.95
0.30	0.00	15.59	7.91	1.97
0.30	1.00	17.17	10.73	1.60
0.30	2.00	18.21	14.22	1.28
0.30	3.00	18.88	16.76	1.13
0.30	4.00	19.29	19.32	1.00
0.20	0.00	14.08	8.94	1.57
0.20	1.00	15.42	11.36	1.36
0.20	2.00	15.94	12.96	1.23
0.20	3.00	16.70	15.26	1.09
0.20	4.00	17.04	16.53	1.03
0.10	0.00	12.61	10.13	1.25
0.10	1.00	13.26	11.32	1.17
0.10	2.00	13.58	11.94	1.14
0.10	3.00	14.13	12.98	1.09
0.10	4.00	14.44	14.16	1.02

Table 9-6: Energy ratios using method 3 for different axial load values

P/P_o	β	C1	C2	C1/C2
0.00	0.00	10.08	6.82	1.48
0.00	1.00	10.40	8.63	1.21
0.00	2.00	10.60	10.01	1.06
0.00	3.00	10.78	11.51	0.94
0.00	4.00	10.90	12.68	0.86
0.10	0.00	14.08	8.94	1.57
0.10	1.00	15.42	11.36	1.36
0.10	2.00	15.94	12.96	1.23
0.10	3.00	16.70	15.26	1.09
0.10	4.00	17.04	16.53	1.03
0.20	0.00	16.31	10.34	1.58
0.20	1.00	17.33	12.07	1.44
0.20	2.00	18.86	14.67	1.29
0.20	3.00	20.05	17.46	1.15
0.20	4.00	20.71	19.64	1.05

9.2.4 Method 4: Loading-Unloading Energy Ratio

Table 9-7: Energy ratios using method 4 for different eccentric moment values

α	β	X1	X2	X1/X2
0.40	0.00	0.08	0.03	2.60
0.40	1.00	0.07	0.03	2.16
0.40	2.00	0.06	0.03	1.85
0.40	3.00	0.06	0.03	1.76
0.40	4.00	0.06	0.04	1.46
0.30	0.00	0.07	0.04	1.89
0.30	1.00	0.06	0.03	1.88
0.30	2.00	0.06	0.04	1.69
0.30	3.00	0.06	0.04	1.58
0.30	4.00	0.06	0.04	1.47
0.20	0.00	0.06	0.04	1.43
0.20	1.00	0.06	0.04	1.48
0.20	2.00	0.06	0.04	1.49
0.20	3.00	0.06	0.04	1.51
0.20	4.00	0.06	0.04	1.53
0.10	0.00	0.06	0.05	1.16
0.10	1.00	0.06	0.05	1.17
0.10	2.00	0.06	0.05	1.17
0.10	3.00	0.06	0.05	1.22
0.10	4.00	0.05	0.04	1.23

Table 9-8: Energy ratios using method 4 for different axial load values

P/P_o	β	X1	X2	X1/X2
0.00	0.00	0.05	0.03	1.55
0.00	1.00	0.04	0.03	1.39
0.00	2.00	0.04	0.03	1.28
0.00	3.00	0.04	0.03	1.21
0.00	4.00	0.04	0.03	1.18
0.10	0.00	0.06	0.04	1.43
0.10	1.00	0.06	0.04	1.48
0.10	2.00	0.06	0.04	1.41
0.10	3.00	0.06	0.04	1.36
0.10	4.00	0.06	0.04	1.33
0.20	0.00	0.07	0.05	1.37
0.20	1.00	0.07	0.05	1.35
0.20	2.00	0.06	0.05	1.35
0.20	3.00	0.06	0.05	1.36
0.20	4.00	0.06	0.04	1.34

9.2.5 Optimal Strength Increment Ratio Using Effective Period Method

Table 9-9: Period ratios for different eccentric moment values

α	β	T1	T2	T2/T1
0.40	0.00	0.88	1.31	1.48
0.40	1.00	0.86	1.09	1.26
0.40	2.00	0.85	0.98	1.15
0.40	3.00	0.84	0.92	1.08
0.40	4.00	0.82	0.82	1.00
0.30	0.00	0.92	1.22	1.33
0.30	1.00	0.90	1.08	1.21
0.30	2.00	0.89	0.98	1.11
0.30	3.00	0.87	0.92	1.05
0.30	4.00	0.86	0.87	1.00
0.20	0.00	0.94	1.13	1.20
0.20	1.00	0.92	1.05	1.13
0.20	2.00	0.90	0.99	1.06
0.20	3.00	0.90	0.93	1.03
0.20	4.00	0.89	0.90	1.00
0.10	0.00	0.99	1.09	1.09
0.10	1.00	0.96	1.05	1.06
0.10	2.00	0.98	1.02	1.05
0.10	3.00	0.97	0.99	1.02
0.10	4.00	0.97	0.97	1.00

Table 9-10: Period ratios for different axial load values

P/P_o	β	T1	T2	T2/T1
0.00	0.00	1.15	1.67	1.18
0.00	1.00	1.15	1.43	1.12
0.00	2.00	1.14	1.31	1.05
0.00	3.00	1.14	1.21	1.02
0.00	4.00	1.13	1.15	1.00
0.10	0.00	0.94	1.13	1.20
0.10	1.00	0.92	1.05	1.14
0.10	2.00	0.90	0.99	1.07
0.10	3.00	0.90	0.93	1.03
0.10	4.00	0.89	0.90	1.00
0.20	0.00	0.89	0.97	1.22
0.20	1.00	0.87	0.92	1.17
0.20	2.00	0.85	0.88	1.11
0.20	3.00	0.83	0.84	1.07
0.20	4.00	0.81	0.81	1.00

9.3 MATLAB Code

The following code was used in MATLAB to process the displacement results obtained by using OpenSees.

```
clear;
clc;

for MeRatio = 1:3
    if MeRatio == 1; MeStr = '01';
    elseif MeRatio == 2; MeStr = '02';
    elseif MeRatio == 3; MeStr = '03';
    end
 for B = 1:4
    Filename1 = ['EQ1_Alpha_+\dA',MeStr,'B',num2str(B-1),'.out']
    Filename2 = ['EQ1_Alpha_+\rdA',MeStr,'B',num2str(B-1),'.out']
    Temp1 = importdata(Filename1);
    Temp2 = importdata(Filename2);
    Final_Output = ['Forward',' ','Alpha=',' ',MeStr,' ','Beta=','
',num2str(B-1),' ',num2str([Temp1(1), Temp1(2), Temp2])]
    dlmwrite('Final_Output.txt',Final_Output,'-
append','delimiter','','newline','pc');
end
end


for MeRatio = 1:3
    if MeRatio == 1; MeStr = '01';
    elseif MeRatio == 2; MeStr = '02';
    elseif MeRatio == 3; MeStr = '03';
    end
 for B = 1:4
    Filename1 = ['EQ1_Alpha_-\dA',MeStr,'B',num2str(B-1),'.out']
    Filename2 = ['EQ1_Alpha_-\rdA',MeStr,'B',num2str(B-1),'.out']
    Temp1 = importdata(Filename1);
    Temp2 = importdata(Filename2);
    Final_Output = ['Reverse',' ','Alpha=',' ',MeStr,' ','Beta=','
',num2str(B-1),' ',num2str([Temp1(1), Temp1(2), Temp2])]
    dlmwrite('Final_Output.txt',Final_Output,'-
append','delimiter','','newline','pc');
end
end



for Paxial = 1:6
    if Paxial == 1; PStr = '0';
    elseif Paxial == 2; PStr = '0025'
    elseif Paxial == 3; PStr = '005'
    elseif Paxial == 4; PStr = '01';
    elseif Paxial == 5; PStr = '015';
    else PStr = '02';
    end
 for B = 1:4
    Filename1 = ['EQ1_P_+\dP',PStr,'B',num2str(B-1),'.out']
    Filename2 = ['EQ1_P_+\rdP',PStr,'B',num2str(B-1),'.out']
    Temp1 = importdata(Filename1);
    Temp2 = importdata(Filename2);
```

```
    Final_Output = ['Forward',' ','Pratio=',' ',PStr,' ','Beta=','
',num2str(B-1),' ',num2str([Temp1(1), Temp1(2), Temp2])]
    dlmwrite('Final_Output.txt',Final_Output,'-
append','delimiter','','newline','pc');
end
end


for Paxial = 1:6
    if Paxial == 1; PStr = '0';
    elseif Paxial == 2; PStr = '0025'
    elseif Paxial == 3; PStr = '005'
    elseif Paxial == 4; PStr = '01';
    elseif Paxial == 5; PStr = '015';
    else PStr = '02';
    end
 for B = 1:4
    Filename1 = ['EQ1_P_-\dP',PStr,'B',num2str(B-1),'.out']
    Filename2 = ['EQ1_P_-\rdP',PStr,'B',num2str(B-1),'.out']
    Temp1 = importdata(Filename1);
    Temp2 = importdata(Filename2);
    Final_Output = ['Revarse',' ','Pratio=',' ',PStr,' ','Beta=','
',num2str(B-1),' ',num2str([Temp1(1), Temp1(2), Temp2])]
    dlmwrite('Final_Output.txt',Final_Output,'-
append','delimiter','','newline','pc');
end
end

for R = 1:4
    if R==1; RStr = '1';
    else RStr = num2str((R-1)*2);
    end
 for B = 1:4
    Filename1 = ['EQ1_R_+\dR',RStr,'B',num2str(B-1),'.out']
    Filename2 = ['EQ1_R_+\rdR',RStr,'B',num2str(B-1),'.out']
    Temp1 = importdata(Filename1);
    Temp2 = importdata(Filename2);
    Final_Output = ['Forward',' ','R=',' ',RStr,' ','Beta=','
',num2str(B-1),' ',num2str([Temp1(1), Temp1(2), Temp2])]
    dlmwrite('Final_Output.txt',Final_Output,'-
append','delimiter','','newline','pc');
end
end

for R = 1:4
    if R==1; RStr = '1';
    else RStr = num2str((R-1)*2);
    end
 for B = 1:4
    Filename1 = ['EQ1_R_-\dR',RStr,'B',num2str(B-1),'.out']
    Filename2 = ['EQ1_R_-\rdR',RStr,'B',num2str(B-1),'.out']
    Temp1 = importdata(Filename1);
    Temp2 = importdata(Filename2);
    Final_Output = ['Reverse',' ','R=',' ',RStr,' ','Beta=','
',num2str(B-1),' ',num2str([Temp1(1), Temp1(2), Temp2])]
    dlmwrite('Final_Output.txt',Final_Output,'-
append','delimiter','','newline','pc');
end
```

```
end

for T = 1:6
    if T == 1; TStr = '025';
    elseif T == 2; TStr = '05';
    elseif T == 3; TStr = '075';
    elseif T == 4; TStr = '1';
    elseif T == 5; TStr = '125';
    else TStr = '15';
    end
 for B = 1:4
    Filename1 = ['EQ1_T_+\dT',TStr,'B',num2str(B-1),'.out']
    Filename2 = ['EQ1_T_+\rdT',TStr,'B',num2str(B-1),'.out']
    Temp1 = importdata(Filename1);
    Temp2 = importdata(Filename2);
    Final_Output = ['Forward',' ','T=',' ',TStr,' ','Beta=','
',num2str(B-1),' ',num2str([Temp1(1), Temp1(2), Temp2])]
    dlmwrite('Final_Output.txt',Final_Output,'-
append','delimiter','','newline','pc');
end
end

for T = 1:6
    if T == 1; TStr = '025';
    elseif T == 2; TStr = '05';
    elseif T == 3; TStr = '075';
    elseif T == 4; TStr = '1';
    elseif T == 5; TStr = '125';
    else TStr = '15';
    end
 for B = 1:4
    Filename1 = ['EQ1_T_-\dT',TStr,'B',num2str(B-1),'.out']
    Filename2 = ['EQ1_T_-\rdT',TStr,'B',num2str(B-1),'.out']
    Temp1 = importdata(Filename1);
    Temp2 = importdata(Filename2);
    Final_Output = ['Reverse',' ','T=',' ',TStr,' ','Beta=','
',num2str(B-1),' ',num2str([Temp1(1), Temp1(2), Temp2])]
    dlmwrite('Final_Output.txt',Final_Output,'-
append','delimiter','','newline','pc');
end
end
```

9.4 OpenSees Script

The following script was used to run the inelastic time history analysis using FEMA P695 (2009) far field records.

```
# SET UP ---------------------------------------------------------------
-
wipe;                                   # clear memory of all past
model definitions

# N,mm,
# define UNITS
set mm 1.;                              # define basic units --
output units length
set N 1.;                               # define basic units --
output units force
set sec 1.;                             # define basic units --
output units time
set LunitTXT "mm";                      # define basic-unit text for
output
set FunitTXT "N";                       # define basic-unit text for
output
set TunitTXT "sec";                     # define basic-unit text for
output
set m [expr 1000.*$mm];                 # define engineering units
set kN [expr 1000.*$N];                 # define engineering units
set m2 [expr $m*$m];                    # m^2
set mm2 [expr $mm*$mm];                 # mm^2
set mm4 [expr $mm*$mm*$mm*$mm];         # mm^4
set MPa [expr $N/$mm2];
set Pa [expr $N/$m2];
set cm [expr $mm*10.];                  # centimeter, needed for
displacement input
set PI [expr 2.*asin(1.0)];             # define constant PI
set g [expr 9.81*$m/pow($sec,2)];       # define constant
gravitational acceleration
#-------------------------------------------------------------------------
--------------

# Enter the parameters here:
# For Example;
set Folder "EQ1_Alpha_+";               # Folder name
set Axial 0.1;                          # Axial load
set Alpha 0.1;                          # Eccentric moment ratio
set dir 1;                              # EQ direction
set R 4;                                # Force reduction factor
set SF 0.714;                           # Scaling factor
set Ab1 201;                            # Bars area outer left
set Ab2 0;                              # Bars area inner left
set An1 8;                              # Bars number outer left
set An2 0;                              # Bars number inner left

set EQRec 1-a.tcl;                      # Ground motion file name
set Dt 0.01;                            # Ground motion time interval
set Steps 50000;                        # Ground motion steps
set Peak dA01B0;                        # Peak Displacement output
name
set Rsdl rdA01B0;                       # Residual Disp output name
```

```
#-------------------------------------------------------------------------
------------
model BasicBuilder -ndm 2 -ndf 3;           # Define the model builder,
ndm=#dimension, ndf=#dofs
file mkdir $Folder;                             # To create a folder

# define Global GEOMETRY ---------------------------------------------
-------------
set HCol [expr 3.25*$m];                     # Column Height (m)
set Weight [expr 13500*$kN];                 # section total compression
capacity(kN)

# define section geometry
set LCol [expr 0.75*$m];                     # Column Length  (m)- Y
Direction.
set BCol [expr 0.60*$m];                     # Column Breadth (m)- Z
Direction.


# nodal coordinates:
node 1 0 0;                                 # node#, X, Y (m).
node 2 0 $HCol;

# Single point constraints -- Boundary Conditions
fix 1 1 1 1;                                # node DX DY RZ - node 1
fixed, node 2 free.


# nodal masses:
mass 2 $Mass 0 0 ;                          # node#, Mx My Mz, neglect
rotational inertia at nodes



# MATERIAL parameters
# confinded concrete
set fpc    [expr 37*$MPa];                    # Concrete compressive
strength at 28 days
set Epsc0  0.01;                            # concrete strain at maximum
strength
set fpcu   [expr 55.2*$MPa];                 # concrete crushing
strength. MPa
set Epsu   0.028;                           # concrete strain at
crushing strength
set Ec [expr 5000*($fpc**0.5)*$MPa];

# unconfinded concrete
set fupc   [expr 30*$MPa];                   # Concrete compressive
strength at 28 days
set Eupsc0  0.002;                          # concrete strain at maximum
strength
set fupcu  [expr 0.0*$fupc];                 # concrete crushing
strength. MPa
set Eupsu   0.0097;                         # concrete strain at crushing
strength
set Euc [expr 5000*($fupc**0.5)*$MPa];
```

```
# Steel
set fy   [expr 300*$MPa];                    # yield strength
set Es   [expr 200000*$MPa];                 # reinforcement steel
modulus of elasticity
set Bs   0.01;                              # ratio of post-yield tangent
stiffness to elastic modulus



# Stress-Strain properties

#uniaxialMaterial Concrete04 $matTag $fc $ec $ecu $Ec <$fct $et> <$beta>
uniaxialMaterial Concrete04    1     -$fpc -$Epsc0 -$Epsu $Ec; #Confined
uniaxialMaterial Concrete04    2     -$fupc -$Eupsc0 -$Eupsu $Euc;
#Unconfined

uniaxialMaterial Steel02  3  $fy  $Es $Bs 20 0.925 0.15;#Reinforcement
steel

section Fiber 100 {

# Create the concrete core fibers (confined conc - material tag 1)
patch rect 1 30 24 [expr -0.35*$m] [expr -0.275*$m] [expr 0.35*$m] [expr
0.275*$m];

# Create the concrete cover fibers (Order:top, bottom, left, right.
Unconfined conc - material tag 2)
patch rect 2 30 1  [expr -0.375*$m] [expr  0.275*$m] [expr 0.375*$m]
[expr  0.300*$m]; #Top
patch rect 2 30 1  [expr -0.375*$m] [expr  -0.30*$m] [expr 0.375*$m]
[expr -0.275*$m]; #Bottom
patch rect 2  1 22 [expr -0.375*$m] [expr -0.275*$m] [expr -0.35*$m]
[expr  0.275*$m]; #Left
patch rect 2  1 22 [expr 0.350*$m] [expr -0.275*$m] [expr 0.375*$m] [expr
0.275*$m]; #Right

# Create the reinforcing fibers (Order:top, bottom, left, right. -
material tag 3)
layer straight 3 8  [expr 201*$mm2] [expr -0.272*$m] [expr  0.275*$m]
[expr 0.272*$m] [expr 0.275*$m];
layer straight 3 8  [expr 201*$mm2] [expr -0.272*$m] [expr -0.275*$m]
[expr 0.272*$m] [expr -0.275*$m];

layer straight 3 $An1     [expr $Ab1*$mm2] [expr -0.35*$m] [expr -
0.275*$m] [expr -0.35*$m] [expr 0.275*$m];

layer straight 3 $An2  [expr $Ab2*$mm2] [expr -0.272*$m] [expr -0.197*$m]
[expr -0.272*$m] [expr 0.197*$m];

layer straight 3 8  [expr 201*$mm2] [expr  0.35*$m] [expr -0.275*$m]
[expr  0.35*$m] [expr 0.275*$m];

}
```

```
# define geometric transformation:which performs a linear geometric
transformation of beam stiffness and resisting force from the basic
system to the global coordinate system, considering second-order P-Delta
effects.

geomTransf PDelta 1;                          # To Consider second-order P-
Delta effects


# element connectivity:

#element nonlinearBeamColumn $eleTag $iNode $jNode $numIntgrPts $secTag
$transfTag
element nonlinearBeamColumn     1      1      2         4        100
1;
#element elasticBeamColumn   1     1     2   [exp $BCol*$LCol]  $Es [exp
$BCol*$LCol*$LCol*$LCol/12] 1;




# define GRAVITY -------------------------------------------------------
-----


pattern Plain 1 Linear {
   load 2 0 [expr -$Axial*$Weight] [expr $Alpha*820*$kN*$m]
};


# Gravity-analysis parameters -- load-controlled static analysis

set Tol 1.0e-12;                               # convergence tolerance for
test
test NormDispIncr $Tol 10;                     # determine if convergence
has been achieved
constraints Plain;                            # how it handles boundary
conditions
numberer Plain;                               # renumber dof's to minimize
band-width (optimization)
system BandGeneral;                           # how to store and solve the
system of equations

algorithm Newton;                             # use Newton's solution
algorithm

integrator LoadControl 0.1;                   # determine the next time
step for an analysis
analysis Static;                              # define type of analysis
static or transient

set gok [analyze 10];                         # apply gravity in 10 steps
(0.1*10= 1 load factor)

if {$gok == 0} {
  puts "Gravity analysis completed SUCCESSFULLY";
} else {
  puts "Gravity analysis FAILED";
```

```
}

puts "Model Built";
loadConst -time 0.0;                          # Maintain constant gravity
loads and reset time to zero


# DEFINE NLTH ANALYSIS-------------------------------------------------
----------

recorder Node -file $Folder/disp_$Alpha$Peak.out -time -node 2 -dof 1
disp;#Record the displacement at node 2.

recorder Node -file $Folder/reac_$Alpha$Peak.out -time -node 1 -dof 1 3
reaction;#Record the reaction at node 1.

recorder EnvelopeNode -file $Folder/$Peak.out -node 2 -dof 1 disp;#Record
the displacement at node 2.

timeSeries Path 2 -dt $Dt -filePath $EQRec -factor [expr
$dir*$R*$SF*9810];
pattern UniformExcitation 2 1 -accel 2;
set freq [expr [eigen -fullGenLapack 1]**0.5]
set dampRatio 0.05
rayleigh 0. 0. 0. [expr 2*$dampRatio/$freq]
set PERIOD [expr (2*$PI/$freq)];

wipeAnalysis;

set Tol 1.0e-12;                               # convergence tolerance for
test
constraints Plain;                            # how it handles boundary
conditions
numberer Plain;                               # renumber dof's to minimize
band-width (optimization)
system BandGeneral;                           # how to store and solve the
system of equations
test NormDispIncr $Tol 10;                     # determine if convergence
has been achieved
algorithm Newton;                             # use Newton's solution
algorithm

integrator Newmark 0.5 0.25 ;                 # determine the next time
step for an analysis
analysis Transient;                           # define type of analysis
static or transient
set ok [analyze $Steps 0.001];                   # apply 3995 0.01-sec time
steps in analysis


if {$ok == 0} {
  puts "analysis is fine till now";
} else {
  puts "!Convergence failure!";
}
                # ---------------- --if convergence failure-----------
---
                # if analysis fails, we try some other stuff
```

```
                    if {$ok != 0} {
                         puts "Trying Newton with Initial Tangent ..";
                         test NormDispIncr   $Tol 2000 0;
                         algorithm Newton -initial;
                         set ok [analyze 1816 0.02];
                         if {$ok == 0} {puts "that worked .. back to
regular newton"}
                                        test NormDispIncr   $Tol  10;
                         algorithm Newton;
                                 }

                    if {$ok != 0} {
                         puts "Trying Broyden ..";
                         algorithm Broyden 8;
                         set ok [analyze 1816 0.02];
                                       if {$ok == 0} {puts "that
worked .. back to regular newton"}
                                        test NormDispIncr   $Tol  10;
                         algorithm Newton;

                                 }
                    if {$ok != 0} {
                         puts "Trying NewtonWithLineSearch ..";
                         algorithm NewtonLineSearch 0.8 ;
                         set ok [analyze 1816 0.02];
                                        if {$ok == 0} {puts "that
worked .. back to regular newton"}
                                        test NormDispIncr   $Tol  10;
                         algorithm Newton;
                                  }

                                if {$ok != 0} {
                         puts "This step failed in convergence...";

                                  }

# --------------------------------------------------------------------------
------------------------------
if {$ok == 0} {
  puts ">>>>>>>>>>>>>>>> NLTH analysis completed
SUCCESSFULLY<<<<<<<<<<<<<<<<<";
} else {
  puts ">>>>>>>>>>>>>>>> NLTH analysis FAILED<<<<<<<<<<<<<<<<<<<<<<<";
}
#--------------------------------------------------------------------------
------------------------------

set RSDL [open $Folder/$Rsdl.out "w"]
puts $RSDL "[nodeDisp 2 1]"
close $RSDL


wipe;
```